

# Spatial Spectral Analysis of Elastic Waves in a Three-Dimensional Truss Structure

Jeongho Park

B.S., Oceanography, Seoul National University, Korea (1993)

Submitted to the Department of Ocean Engineering  
in partial fulfillment of the requirements for the degree of

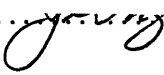
Master of Science in Ocean Engineering


at the


Massachusetts Institute of Technology

June 1996

© Massachusetts Institute of Technology 1996. All rights reserved.

Author .....  .....  
Department of Ocean Engineering  
May 10, 1995

Certified by .....  .....  
Professor Ira Dyer  
Weber-Shaughness Professor of Ocean Engineering  
Thesis Supervisor

Accepted by .....  .....  
Professor A. Douglas Carmichael  
Chairman, Departmental Graduate Committee

MASSACHUSETTS INSTITUTE  
OF TECHNOLOGY

JUL 26 1996

ENG

LIBRARIES

# Spatial Spectral Analysis of Elastic Waves in a Three-Dimensional Truss Structure

Jeongho Park

Submitted to the Department of Ocean Engineering on May 10, 1995,  
in partial fulfillment of the requirements for the degree of  
Master of Science in Ocean Engineering

## Abstract

The MIT Truss Damping group has been studying the application of truss-like structures to support the internal components of underwater vehicles. A truss structure is able to reduce the vibrational energy transmitted from internal noise sources to the hull by scattering and multi-paths. In a real application a truss will mount equipment at many points and this truss will be attached to the hull at various points.

Spatial spectral analysis of the total elastic wave field is conducted to find the phase relationship of the total elastic wave field at the joints of a three-dimensional truss. A single-input/multiple-output system is excited by broadband white noise at one base strut and measured by accelerometers at joints and on base struts along the axis of the truss. The phase of the cross-spectra shows an approximately linear phase relationship as a function of frequency. However, the frequency-wavenumber spectrum shows that the wavenumbers at the joints of the truss are evenly distributed in high inertance bands (approximately between  $-10dB$  and  $10dB$  re  $1/kg$ ). This is due to reverberation, and can be regarded as phase randomness.

A measurement of the major early arrival times is also conducted by measuring the impulse response at joints with a transient input. The results show that the total elastic wave field travels with approximately constant group delay in the high frequency bands and there is no preferential wave type distribution during propagation. Energy decay rates of the total elastic wave field depends upon position and frequency. The mean-free-paths of energy build up and energy decay are about 6 times the total shortest path in the truss.

The frequency domain results show that with a stationary input the wave propagates, as measured on the joints of the truss, both in positive and negative axial directions. The constant group delay of wave propagation at high frequency bands with a transient input in time domain will disappear after the truss becomes fully energized. The multi-paths on the truss causes phase randomness of the output at the joints over all frequency bands due to reverberation.

Thesis Supervisor: Ira Dyer

Title: Weber-Shaughness Professor of Ocean Engineering

# Acknowledgments

First of all, I would like to thank my adviser, Professor Ira Dyer, for his support and guidance in this study. He introduced me to the world of acoustics and taught me how to approach complex problems from a few basic theories in physics. He is one of the best scientists, engineers, and mentors I have ever met. It has been an honor to work with him.

I am also grateful to Dr. Joseph Bondaryk for his help in experiments, signal processing and steady encouragement to my work. You are a person who combines both a meticulous engineering mind and sense of humanity. You represent an exemplary model of a real engineer. I wish the best on your finding a position to teach and research in acoustics at a competitive environment. I would like to extend my sincere appreciation to your wife, Leslie, for her very helpful advice on improving my writing skills.

I would like to express my gratitude to Sabina Rataj, Taci Darnell, Isela Cordova, and Patrick Preston for taking care of everything so that students can concentrate on their work without disturbance. Sabina kindly arranged me to take a writing class at Harvard and encouraged me whenever I had hard time. I can hardly imagine the acoustics group without you.

The time I have spent at 5-435 with the buddies from all over the world is cherished in my memory. Thank you all to Matthew Conti, Peter Daly, Pierre Elisseeff, Mark Hayner, Tarun Kapoor, Michael Klausbruckner, Vince Lupien, Kai-Ulrich Machens, Brian Sperry, Brian Tracey, and the rest of folks at 5-435 and 5-007. Peter has all the answers for any computer problems and he did not mind sparing infinite amount of time for my computer questions. He finally installed Linux in my computer and a printer driver! Kai replied promptly to all the questions on truss experiments via the Internet from Berlin. Tarun was kind enough to answer my questions on reciprocity, and how to prepare cover letters and résumés. I had a great time discussing virtually everything with Vince and Michael. Jaiyong Lee helped me heartily from the beginning of my stay at MIT and I cannot forget his happy wedding where I was his best man. Best wishes to you and your family. Thanks to all others.

I am also grateful to my Korean colleagues for their help and encouragement during my stay at MIT. Pyongwon Yim and Daeyup Lee gave me a great deal of valuable advice about my career and they were always kind to me. Many thanks to Michalis Kilaras whose friendship made my two year stay in the Ashdown and Boston an exciting experience; such as visiting the museum of transportation on Sunday!

Finally, I would like to thank my parents for their love, encouragement and sacrifice. You always respected my opinion and left me to make right decisions by myself. Father even though you are not here any more you showed me again an exceptionally strong volition during your struggle against cancer. Every tiny bit of memory of you and mother's endless love toward me will be cherished in my heart through my life.

# Dedication

*To my parents*

*To study is to know,  
to know is to understand,  
to understand is to appreciate,  
to appreciate is to love.*

# Contents

- 1 Introduction 14**
  - 1.1 Previous Work at MIT . . . . . 14
  - 1.2 Motivation and Approach . . . . . 16
  - 1.3 MIT Truss Design . . . . . 16
  - 1.4 Experimental Setup . . . . . 17
  - 1.5 Overview of Thesis . . . . . 20
  
- 2 Spatial Cross-Spectrum of Elastic Waves 21**
  - 2.1 Spectral Analysis . . . . . 21
  - 2.2 Spatial Cross-Spectrum . . . . . 27
  
- 3 Early Arrival Times of Elastic Waves 59**
  - 3.1 Bandpass Filtering . . . . . 59
  - 3.2 Early Arrival Times . . . . . 60
  
- 4 Conclusions 93**
  - 4.1 Summary and Conclusions . . . . . 93
  - 4.2 Future Work . . . . . 95

<b>Appendix A: Timoshenko Beam Theory</b>	<b>96</b>
<b>Appendix B: MATLAB Codes</b>	<b>101</b>
<b>Bibliography</b>	<b>132</b>

# List of Figures

1-1	Application of a truss structure . . . . .	15
1-2	Typical joint design. . . . .	17
1-3	Label of joints and perspective view of truss . . . . .	17
1-4	Schematic of test setup. . . . .	19
1-5	Positions of shaker and accelerometers. . . . .	19
2-1	Schematic of single-input/multiple-output system. . . . .	23
2-2	Schematic of single-input/single-output system with multi-paths. . . . .	24
2-3	Spatial coherence of total elastic wave field between the input and the acceleration at the joints of the truss with frequency resolution of $\Delta f = 8Hz$ . . . . .	34
2-4	Spatial coherence of total elastic wave field between the input and the acceleration at the base struts of the truss with $\Delta f = 8Hz$ . . . . .	35
2-5	Spatial coherence of total elastic wave field between the input and the acceleration at the base struts of the truss with $\Delta f = 2Hz$ . . . . .	36
2-6	Multiple half-wave resonance frequencies of elastic waves. . . . .	37
2-7	Resonance frequencies of struts. . . . .	38
2-8	Resonance frequencies of truss. . . . .	39
2-9	Elastic wavelength as a function of frequency. . . . .	40



2-10	Magnitude of cross-spectra of total elastic wave field between the input and the acceleration at the joints of the truss with $\Delta f = 8Hz$ . . . . .	41
2-11	Phase angle of cross-spectra of total elastic wave field between the input and the acceleration at the joints of the truss with $\Delta f = 8Hz$ . . . . .	42
2-12	Unwrapped phase angle of cross-spectra of total elastic wave field between the input and the acceleration at the joints of the truss with $\Delta f = 8Hz$ . . . . .	43
2-13	Extracted wavenumber between two adjacent joints as a function of frequency with $\Delta f = 8Hz$ . . . . .	44
2-14	Extracted phase speed between two adjacent joints as a function of frequency with $\Delta f = 8Hz$ . . . . .	45
2-15	Extracted time delay between two adjacent joints as a function of frequency with $\Delta f = 8Hz$ . . . . .	46
2-16	Extracted group speed between two adjacent joints as a function of frequency with $\Delta f = 8Hz$ . . . . .	47
2-17	Extracted group delay between two adjacent joints as a function of frequency with $\Delta f = 8Hz$ . . . . .	48
2-18	Third octave band average of measured power of elastic waves for the strut <i>a6e6</i> ( <i>Z</i> excitation) with $\Delta f = 8Hz$ (Ref[20]). . . . .	49
2-19	Phase angle of cross-spectra of total elastic wave field between the input and the acceleration at the joints of the truss with $\Delta f = 0.5Hz$ . . . . .	50
2-20	Extracted wavenumber between two adjacent joints as a function of frequency with $\Delta f = 0.5Hz$ . . . . .	51
2-21	Extracted phase speed between two adjacent joints as a function of frequency with $\Delta f = 0.5Hz$ . . . . .	52
2-22	Extracted time delay between two adjacent joints as a function of frequency with $\Delta f = 0.5Hz$ . . . . .	53

2-23	Extracted group speed between two adjacent joints as a function of frequency with $\Delta f = 0.5Hz$ . . . . .	54
2-24	Extracted group delay between two adjacent joints as a function of frequency with $\Delta f = 0.5Hz$ . . . . .	55
2-25	Frequency-wavenumber (f-k) spectrum of inertance ( $Z$ excitation) at the $c$ joints with $\Delta f = 2Hz$ . . . . .	56
2-26	Cross section of inertance frequency-wavenumber spectrum at $k = 0.02m^{-1}$ . . . . .	57
2-27	Inertance wavenumber spectrum of high inertance bands. . . . .	58
3-1	Frequency response and impulse response functions of Gaussian band-pass filter. . . . .	66
3-2	Characteristics of the input signal. . . . .	67
3-3	Frequency response of FIR lowpass filter with cut-off frequency of $f_c = 25.6kHz$ . . . . .	68
3-4	Magnitude of lowpass filtered impulse response function from 0 to $0.125sec$ with $f_c = 25.6kHz$ . . . . .	69
3-5	Magnitude of lowpass filtered impulse response function from 0 to $5msec$ with $f_c = 25.6kHz$ . . . . .	70
3-6	Magnitude of Gaussian octave bandpass filtered impulse response function from 0 to $0.125sec$ with center frequency of $f_o = 16kHz$ . . . . .	71
3-7	Magnitude of Gaussian octave bandpass filtered impulse response function from 0 to $0.125sec$ with $f_o = 8kHz$ . . . . .	72
3-8	Magnitude of Gaussian octave bandpass filtered impulse response function from 0 to $0.125sec$ with $f_o = 4kHz$ . . . . .	73
3-9	Magnitude of Gaussian octave bandpass filtered impulse response function from 0 to $0.125sec$ with $f_o = 2kHz$ . . . . .	74

3-10	Magnitude of Gaussian octave bandpass filtered impulse response function from 0 to 0.125sec with $f_o = 1kHz$ . . . . .	75
3-11	Magnitude of Gaussian octave bandpass filtered impulse response function from 0 to 0.125sec with $f_o = 0.5kHz$ . . . . .	76
3-12	Magnitude of Gaussian octave bandpass filtered impulse response function from 0 to 0.125sec with $f_o = 0.25kHz$ . . . . .	77
3-13	Magnitude of Gaussian octave bandpass filtered impulse response function from 0 to 0.125sec with $f_o = 0.125kHz$ . . . . .	78
3-14	Magnitude of Gaussian octave bandpass filtered impulse response function from 0 to 5msec with $f_o = 16kHz$ and predicted major early arrival times. . . . .	79
3-15	Magnitude of Gaussian octave bandpass filtered impulse response function from 0 to 5msec with $f_o = 8kHz$ and predicted major early arrival times. . . . .	80
3-16	Magnitude of Gaussian octave bandpass filtered impulse response function from 0 to 5msec with $f_o = 4kHz$ and predicted major early arrival times. . . . .	81
3-17	Major early arrival times of octave bandpass filtered impulse response function with the shortest path as the $X$ axis. . . . .	82
3-18	Major early arrival times of octave bandpass filtered impulse response function with the axial distance as the $X$ axis. . . . .	83
3-19	Least square fitted curves of Gaussian octave bandpass filtered impulse response function with $f_o = 16kHz$ . . . . .	84
3-20	Least square fitted curves of Gaussian octave bandpass filtered impulse response function with $f_o = 8kHz$ . . . . .	85
3-21	Least square fitted curves of Gaussian octave bandpass filtered impulse response function with $f_o = 4kHz$ . . . . .	86

3-22	Decay rates of Gaussian octave bandpass filtered impulse response function. . . . .	87
3-23	Schematic of energy build up and decay processes in the truss . . . .	88
A-1	Dispersion relation of Timoshenko and Euler-Bernoulli beams. . . . .	98
A-2	Flexural wave speed of Timoshenko and Euler-Bernoulli beams. . . .	99

# List of Tables

2.1	Phase slope of cross-spectra at the $c$ joints of the MIT truss. . . . .	29
3.1	The first arrival time of elastic waves with single wave type propagation.	61
3.2	Early arrival times of Gaussian bandpass filtered elastic waves with $f_o = 16kHz$ . . . . .	89
3.3	Early arrival times of Gaussian bandpass filtered elastic waves with $f_o = 8kHz$ . . . . .	90
3.4	Early arrival times of Gaussian bandpass filtered elastic waves with $f_o = 4kHz$ . . . . .	91
3.5	Decay rates of Gaussian octave bandpass filtered elastic waves. . . . .	92
A.1	Elastic wave speeds in the MIT truss. . . . .	100

# Chapter 1

## Introduction

Truss structures have been used in many areas from civil structures to space structures, not only because of their low construction and maintenance cost, but also due to their structural advantage. Recently, the US Navy has been interested in truss-like structures as a new design concept for the internal component of marine vehicles, in an attempt to reduce the propagation of noise generated from machinery to the hull.

Truss structures are able to reduce the vibrational energy transmitted from internally mounted rotating and reciprocating noise sources to the hull by scattering and attenuation as a result of multi-paths. A truss mounting, contrary to the conventional marine vehicle mounting system, can simultaneously improve acoustic and structural performance, as well as lower construction and maintenance costs, and shorten refit times. It is believed that passive damping treatment applied to the truss could maximize attenuation of vibration, which is a crucial requirement for a marine vehicle operation. A schematic showing a truss as an internal structure to a marine vehicle is shown in Fig. 1-1.

### 1.1 Previous Work at MIT

The MIT truss program on machinery cradle damping began in early 1993 with support from the Office of Naval Research (ONR) and the Advanced Research Program

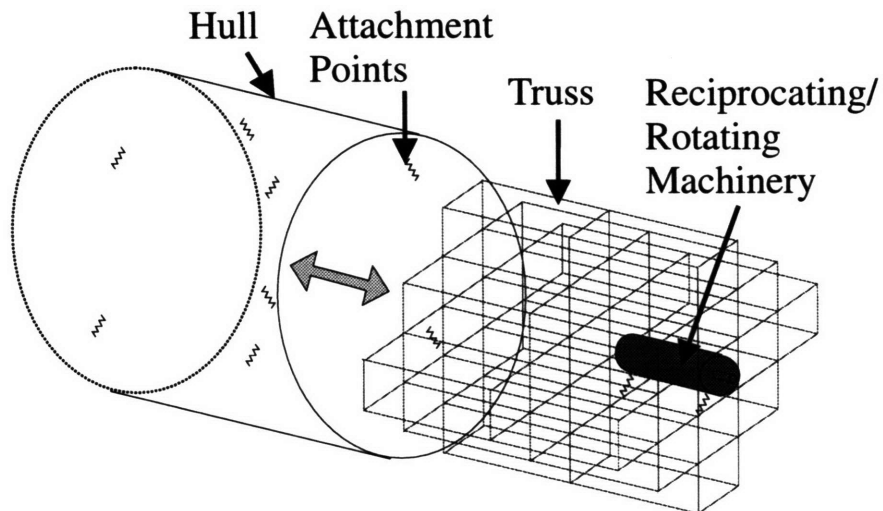


Figure 1-1: Application of a truss structure

Agency (ARPA). The MIT truss was designed and constructed by Heath[1]. He explored the dynamic behavior of the truss and showed that the major mechanisms of attenuation are scattering and strut radiation.

Branthonne[2] investigated the application of dynamic absorbers to the truss. His result shows that these treatments are very effective in attenuating the radiated noise from the truss, and he suggested that the assumption of equipartition of energy distribution might be incorrect. Energy partitioning in the truss was investigated by Machens and Dyer[3] and the result shows the existence of energy equilibrium in the truss instead of energy equipartition.

Research on optimized joint designs for a truss was conducted by Frink[4]. His result shows that pinned joints effectively maximize noise attenuation. Air borne noise radiation of the truss was studied by Chiasson[5] numerically and experimentally. His results show the ability to predict truss radiation from knowledge of its geometry.

Numerical wave propagation of the truss was studied by Guo[6] using a global-matrix method. He showed that it is possible to study large-scale complicated truss structures with numerical methods.

## 1.2 Motivation and Approach

In a real marine vehicle application, a truss could be mounted with machinery, equipment as well as compartments and will be attached to the hull at various points over the truss. The vibration can be coupled destructively or constructively through multi-paths and can propagate to the hull even though high attenuation is achieved by truss mounting isolators. Thus it becomes important to understand the characteristic response of the truss at these hull attachment points due to the forcing applied by the machinery at various points within the truss.

In this study I explore the spatial spectral analysis of the elastic waves in a truss structure. Spatial spectral analysis of the total elastic wave field, the sum of flexural, compressional, and torsional waves, measures the dynamic behavior of a truss with multiple attachment points and equipment loadings. With this approach I investigate the response characteristics of the truss by making measurement at the joints.

Multiple equipment loadings in a truss and its attachment points to a hull can be modeled as a multiple-input/multiple-output system. However, instead of using this complicated model, a simplified single-input/multiple-output model is used in this study for convenience. This model is equivalent to an ideal single machine mounting with many attachment points to the hull.

## 1.3 MIT Truss Design

The MIT truss is composed of eleven square-based pyramids made of aluminum 6061 T6 struts and joints. The nominal dimension of the structure is  $4.7 \times 0.84 \times 0.80m$  and its weight is approximately  $16kg$ . This configuration could be roughly a 1/15 scale of a marine vehicle internal structure. However, it is designed to investigate the dynamics of a fully three-dimensional truss and this is the reason it does not look like a practical internal structure.



The truss consists of 109 struts and 35 joints. There are three different strut lengths, 54 long diagonals (810mm), 11 horizontal diagonals (700mm) and 44 short base struts (484mm), made of 12.7mm outer diameter tubes with wall thickness of 1.65mm. The struts and joints are connected by epoxy to strengthen their connectivity, and the numbers of struts per joint vary from three to eight. A typical joint design schematic is shown Fig. 1-2. To facilitate reporting of experiments, these joints are labeled and a global coordinate system is assigned. Fig. 1-3 shows these labels and a perspective view of the MIT truss with the coordinate system. More detailed characteristics of the MIT truss are shown in Heath[1].

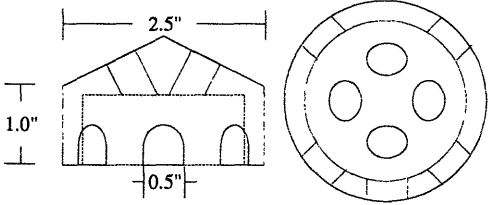


Figure 1-2: Typical joint design.

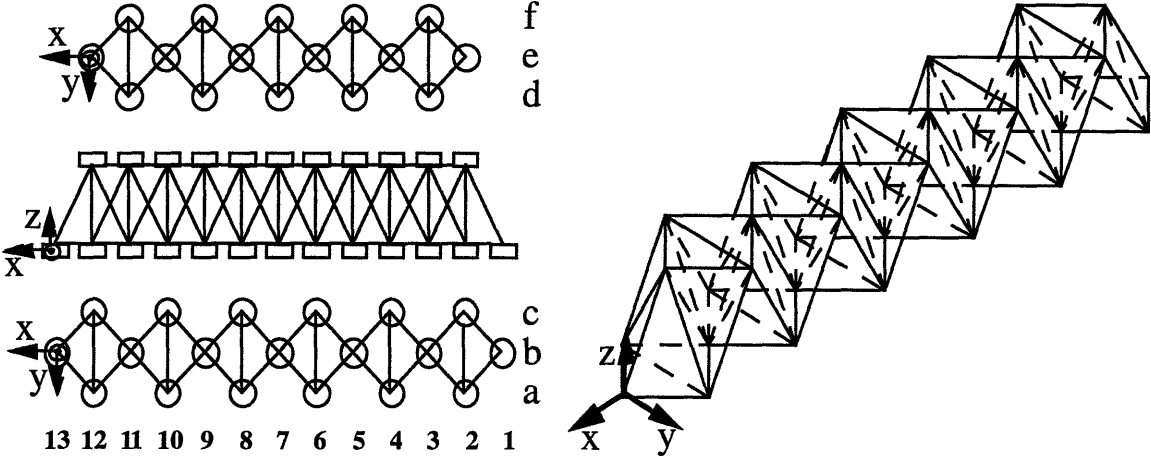


Figure 1-3: Label of joints and perspective view of truss

### 1.4 Experimental Setup

The following experimental setup is that commonly used for frequency spectrum measurement and early arrival time measurement, except for the way the input signal

is provided. A schematic of the test setup is shown in Fig. 1-4. The MIT truss is hung from a wooden support structure by bungee cords. This provides good isolation to model a free-free boundary condition above  $10Hz$ .

The truss is excited in the  $Z$  direction by a Brüel & Kjær (B&K) mini-shaker type 4810 at the base strut  $a4c4$   $16.5cm$  ( $6\frac{1}{2}$ "") from the joint  $a4$ . This  $a4c4$  strut is selected instead of the very end of the truss structure to avoid unfavorable boundary effects. The shaker position at the strut does not have any symmetry since the length of the  $a4c4$  strut is  $70.8cm$  ( $27\frac{7}{8}$ "") and the forcing location is closer to the joint  $a4$ .

A B&K impedance head type 8001 is used to measure the applied force and acceleration, and this is connected to a data acquisition system via two Piezotronics PCB MOD462A charge amplifiers. Twenty two  $0.5g$  Kistler Picotron type 8616 accelerometers are used to measure the accelerations at the  $b$  struts and  $c$  joints. The accelerometers at the  $b$  struts are located  $36.2cm$  ( $14\frac{1}{4}$ "") from the  $c$  joints, slightly off from the center of the  $b$  struts, to avoid lower mode's nodes and anti-nodes. The positions of the shaker and accelerometers are shown in Fig. 1-5.

For the frequency spectrum measurement, band limited white noise ( $0\sim 25kHz$ ) with  $30V_{pk}$  is provided to the shaker by a Hewlett Packard (HP) 3562A dynamic signal analyzer driven by a Wilcoxon Research (WR) PA7 power amplifier. For the early arrival time measurement, a periodic impulse-like signal is generated with a period of  $1Hz$  by using a HP3325A synthesizer/function generator and a WaveTek  $2MHz$  function generator model 20.

Data are acquired by a HP VXI acquisition system and processed by an I-DEAS signal processing software package. The frequency band from 0 to  $25.6kHz$  is sampled for the frequency spectrum measurement with 100 ensemble averages. For the early arrival time measurement, time frame length of  $0.125sec$  is used to avoid the overlap and reverberation of signal arrival. The sampling frequency is  $65,536Hz$  and 1.2207% pretrigger with 10% positive trigger is used to avoid unfavorable time delay effects which may contaminate the data. The time domain data are acquired with 100 ensemble averages to smooth the fluctuations inherent in any one test.

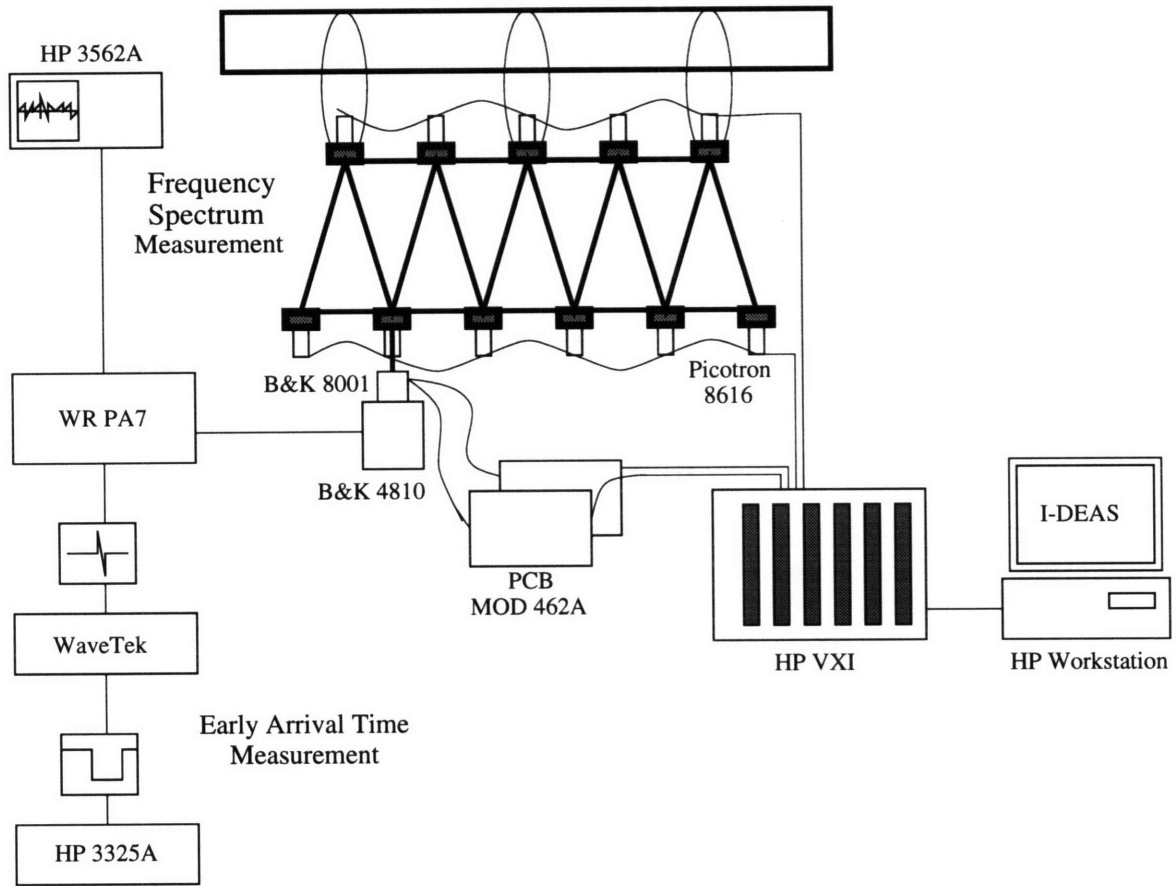


Figure 1-4: Schematic of test setup.

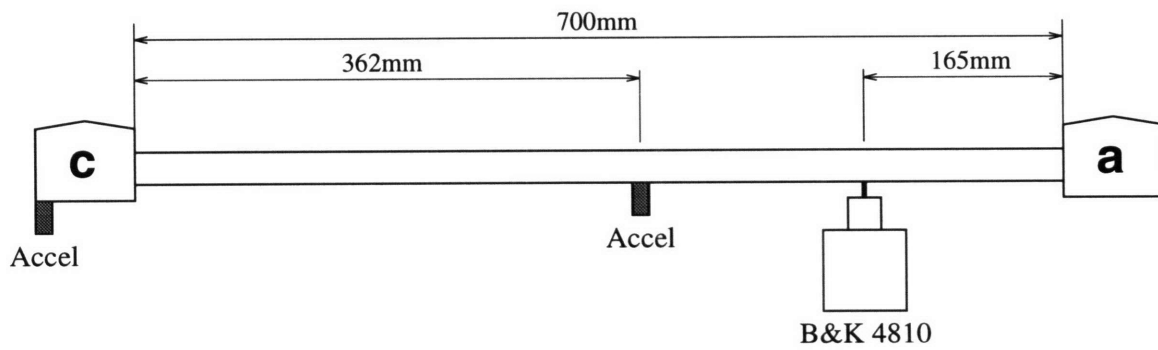


Figure 1-5: Positions of shaker and accelerometers.

## 1.5 Overview of Thesis

In Chapter 2, I investigate the spatial spectrum of the total elastic wave field at the joints of the MIT truss and analyze the result by an array signal processing method. The results show that spatial coherence at the joints is high except in stop bands caused by the periodicity of the truss, and an approximately linear phase relationship is observed at each joint from the phase of the cross-spectra. However, the frequency-wavenumber spectrum in high inertance spectrum bands show that there is no directional preference of the elastic wave propagation through the joints of the truss due to reverberation.

In Chapter 3, I analyze the early arrival times of the elastic waves using a transient input. To enhance data resolution, the Gaussian bandpass filtered impulse response function, rather than cross-correlation, is measured to find the major early arrival times. The results show that the elastic wave energy arrives with approximately constant group delay in high frequency bands with a transient input, but, the distribution of wave types becomes random. The decay rates of the elastic wave energy are not constant due to wave coupling properties of the truss.

In Chapter 4, I summarize the major results of this study and provide suggestions for future work. The wavenumber distribution of the truss is broad over all frequency bands in the frequency-wavenumber spectrum. This is due to the multi-paths of the truss structure which cause phase randomness of the cross-spectra by reverberation.

# Chapter 2

## Spatial Cross-Spectrum of Elastic Waves

### 2.1 Spectral Analysis

Previous research at MIT was confined to radiation, scattering and vibration of the truss. Moreover, much of the research in related fields was done on wave propagation in spatially periodic structures with multiple coupling of waves. Both theoretical and computational approaches were used and can be found in references such as [7], [8], [9], [10], [11], [12], [13], [14].

However, in a real application of the truss as an internal structure of a marine vehicle, equipment will be mounted at many points through the truss and eventually this truss structure will be attached to the hull at various points. Thus, it is important to understand the characteristic response of noise and vibration from these mounting points to the hull attachment points, since noise can propagate through multi-paths of a truss structure constructively or destructively.

The characteristic response at the joints of the truss and hull attachment points is hypothesized to be coherent in low frequency bands and more complicated with increasing frequency and distance due to the introduction of noise.

This hypothesis is based on the fact that the dynamic behavior of the MIT truss changes from global to local dynamics as suggested by Heath[1]. Heath postulated that the transition frequency occurs below  $1kHz$ . Below  $1kHz$  the MIT truss behaves as a single beam and above this frequency the truss behavior is more complicated and local. A numerical study of mode shape of the truss was conducted by Branthonne[15] and his result shows that even at the frequencies below  $100Hz$ , where the truss is fully energized, the mode shapes become very complicated.

To investigate the characteristic response of the joints of the truss I use spectral density functions defined below[16]. All the analysis in this study is done using the one-sided spectral density function. In practice we can extend measured positive frequency results to the negative domain due to symmetry. However, I use the two-sided spectra for analytical calculation since they are more convenient in the mathematics. The one-sided auto-spectral density and cross-spectral density functions are defined as

$$\begin{aligned} G_{xx}(f) &= 2S_{xx}(f) \\ &= 2 \int_{-\infty}^{\infty} R_{xx}(\tau) e^{-j2\pi f\tau} d\tau \quad f > 0, \end{aligned} \quad (2.1)$$

$$\begin{aligned} G_{xy}(f) &= 2S_{xy}(f) \\ &= 2 \int_{-\infty}^{\infty} R_{xy}(\tau) e^{-j2\pi f\tau} d\tau \quad f > 0. \end{aligned} \quad (2.2)$$

where  $R_{xx}(\tau)$  and  $R_{xy}(\tau)$  are auto-correlation function and cross-correlation function respectively and defined as

$$R_{xx}(\tau) = \lim_{T \rightarrow \infty} \frac{1}{T} \int_0^T x(t)x(t+\tau)dt, \quad (2.3)$$

$$R_{xy}(\tau) = \lim_{T \rightarrow \infty} \frac{1}{T} \int_0^T x(t)y(t+\tau)dt. \quad (2.4)$$

The coherence of total elastic wave field is defined as

$$\gamma_{xy}^2(f) = \frac{|G_{xy}(f)|^2}{G_{xx}(f)G_{yy}(f)} \quad 0 \leq \gamma_{xy}^2(f) \leq 1. \quad (2.5)$$

I use the  $Z$  component of acceleration from the truss. However, these data not only include the flexural component but also the compressional and torsional components of acceleration, since these different wave types couple to each other via interactions at the joints.

As mentioned in Chapter 1, the many equipment loadings in a truss and its attachment points to a hull can be modeled as a multiple-input/multiple-output system, but, I use a simplified single-input/multiple-output model for convenience. This model is equivalent to an ideal single machinery mounting with many attachment points through a hull and can be realized by exciting the truss with a single shaker and measuring at multiple accelerometers over the truss. A schematic of single-input/multiple-output system is shown in Fig. 2-1. Truss structures are characterized by their multiple paths connected by many joints to maintain their shape. If a forcing source is applied at an arbitrary position of a truss and a response is measured at another point, it can be modeled as a single-input/single-output with multi-paths. A schematic of this system is shown in Fig. 2-2.

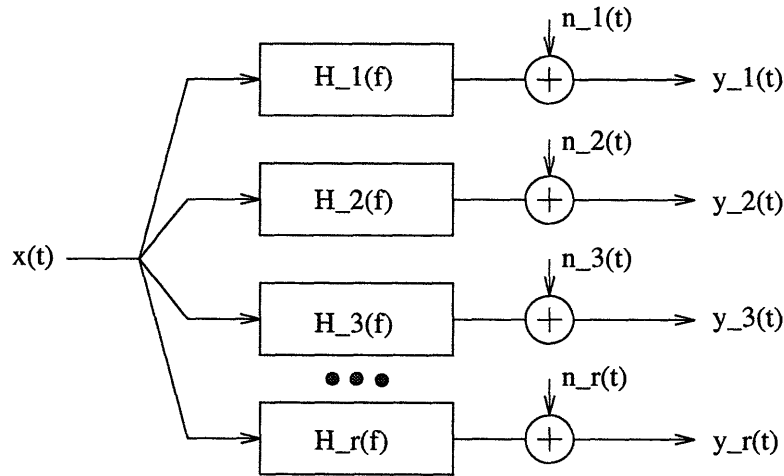


Figure 2-1: Schematic of single-input/multiple-output system.

For convenience, nondispersive propagation through multiple paths of an input  $x(t)$  from a stationary random process is considered first with an assumption of a

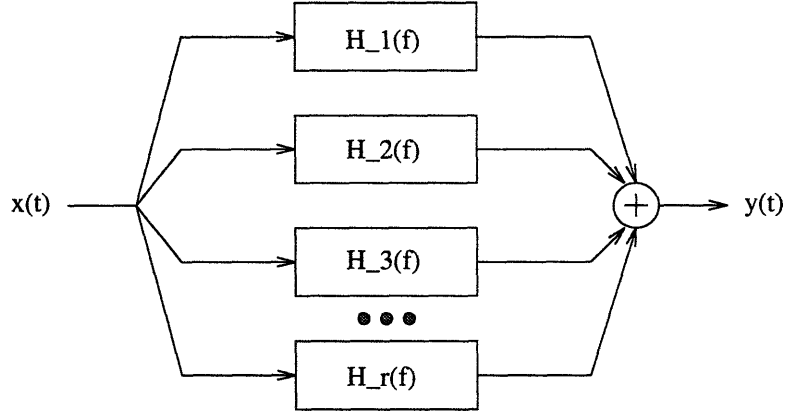


Figure 2-2: Schematic of single-input/single-output system with multi-paths.

uniform gain factor  $H_k$ ,  $k = 1, 2, 3, \dots, r$ . This will produce an output  $y(t)$  such that

$$\begin{aligned}
 y(t) &= H_1x(t - \tau_1) + H_2x(t - \tau_2) + \dots + H_rx(t - \tau_r) \\
 &= \sum_{k=1}^r H_kx(t - \tau_k)
 \end{aligned} \tag{2.6}$$

where  $\tau_k$  is time delay caused by each path. With use of equations Eq. (2.4) and Eq. (2.3), the cross-correlation function between the input  $x(t)$  and the output  $y(t)$  becomes

$$\begin{aligned}
 R_{xy}(\tau) &= \lim_{T \rightarrow \infty} \frac{1}{T} \int_0^T x(t) [H_1x(t - \tau_1 + \tau) + H_2x(t - \tau_2 + \tau) \\
 &\quad + \dots + H_rx(t - \tau_r + \tau)] dt \\
 &= \sum_{k=1}^r H_kR_{xx}(\tau - \tau_k).
 \end{aligned} \tag{2.7}$$

The above equation shows that the cross-correlation between  $x(t)$  and  $y(t)$  appears as a sum of autocorrelation functions of  $x(t)$  with offset by  $\tau_k$  with each  $H_k$ ,  $k = 1, 2, 3, \dots, r$ . However, since the truss is composed of multiple paths we cannot get clear resolution of cross-correlation in the time domain.

The Fourier transform of the cross-spectral density becomes

$$G_{xy}(f) = \sum_{k=1}^r H_kG_{xx}(f)e^{-j2\pi f\tau_k}. \tag{2.8}$$



This can be expressed in complex polar notation as

$$G_{xy}(f) = |G_{xy}(f)|e^{-j\theta_{xy}(f)} \quad (2.9)$$

where

$$|G_{xy}(f)| = G_{xx}(f) \left[ \sum_{i=1}^r \sum_{k=1}^r H_i H_k \cos 2\pi f(\tau_i - \tau_k) \right]^{1/2} \quad (2.10)$$

$$\theta_{xy}(f) = \tan^{-1} \left[ \frac{\sum_{k=1}^r H_k \sin 2\pi f \tau_k}{\sum_{k=1}^r H_k \cos 2\pi f \tau_k} \right]. \quad (2.11)$$

It can be shown from Eq. (2.10) that the magnitude of the cross-spectrum for multiple paths will produce destructive interference notches at frequency intervals of

$$\Delta f = \frac{1}{\tau_i - \tau_k}. \quad (2.12)$$

The coherence function between the input and output in multiple paths can be derived with the autospectrum of  $y(t)$ . These are expressed as

$$R_{yy}(\tau) = \sum_{i=1}^r \sum_{k=1}^r H_i H_k R_{xx}(\tau + \tau_i - \tau_k) \quad (2.13)$$

$$G_{yy}(f) = G_{xx}(f) \sum_{i=1}^r \sum_{k=1}^r H_i H_k \cos 2\pi f(\tau_i - \tau_k). \quad (2.14)$$

From the above results the coherence function,  $\gamma_{xy}^2(f)$ , should be always one at all frequencies for an ideal case where there is no noise;

$$\gamma_{xy}^2(f) = \frac{|G_{xy}(f)|^2}{G_{xx}(f)G_{yy}(f)} = 1. \quad (2.15)$$

However, introducing a non-uniform gain factor as a function of frequency,  $H_k(f)$ , and dispersive propagation will cause more complicated cross-spectrum phases.

The accelerations measured at the joints can be considered as a line array, and the spatial Fourier transform can be used to investigate the characteristic response of the truss at the joints in the frequency-wavenumber domain to determine the dispersion

relationship of traveling waves via these joints. The spatial Fourier transformation is defined as

$$A(\omega, k) = \frac{1}{N} \sum_{n=0}^{N-1} a(\omega, n\Delta x) e^{-in\Delta x}, \quad (2.16)$$

where  $\omega$  is angular frequency,  $k$  is wavenumber,  $N$  is the number of sensors and  $\Delta x$  is the interval between sensors.

In this array processing, I imagine the acceleration at joints as the response from a virtual beam which is attached to the joints. In a real application this virtual beam can be replaced by a hull. Thus if the frequency-wavenumber properties of the hull are known then the multiplication of the frequency-wavenumber properties of the truss and hull can give the frequency-wavenumber characteristic of the combined two systems because of the Fourier transform properties. Hence, it is important to look at the frequency-wavenumber characteristic of the truss at the joints, which will be attached to the hull.

The array used for the MIT truss has 6 accelerometers and the length of the array is  $3.917m$ , or 5 cells long. The spatial sampling rate is  $0.783m$  and the Nyquist wavenumber,  $k_s$ , becomes  $4.021/m$ . The resolution, half the main lobe width,  $k_x = 2\pi/L$ , of this array is  $1.604$ . If a continuous-variable signal is band limited to frequencies below  $k_s$ , then it can be periodically sampled without loss of information as long as the sampling period is less than  $\pi/k_s$ [17]. However, because of the sparse spatial sampling, aliasing occurs at high frequencies for flexural, torsional, and compressional waves approximately above  $52Hz$ ,  $1,986Hz$ , and  $3,259Hz$  respectively if the phase speeds of elastic wave propagation through the virtual beam are the same as that in the struts. This bad aliasing is what really happens in the truss, and we cannot avoid aliasing since the interval between the joints is fixed.

## 2.2 Spatial Cross-Spectrum

First, I measured the spatial coherence of the total elastic wave field at various locations on the truss to find the linear dependence between the input and outputs. It is assumed that the spatial coherence is unity,  $\gamma^2 = 1$ , over the entire frequency band except in destructive interference notches.

The spatial coherence measured at the  $c$  joints is shown in Fig. 2-3. As expected the coherence at each joint is nearly unity except in some wide notches at all frequencies, and irrespective of notches below  $5kHz$ . The coherence level decreases with increasing distance and this is due to the decrease of signal to noise ratio with increasing distance. Note that the coherence function can be expressed in terms of signal to noise ratio ( $SNR$ ) as

$$\gamma^2 = \frac{SNR}{1 + SNR}. \quad (2.17)$$

Notches become more dense with increasing distance and this is due to the wide spread of time delays caused by multiple paths of the truss. The low coherence below  $5kHz$  might be spurious since the frequency resolution in this measurement is  $\Delta f = 8Hz$  and this can cause contamination in low frequency bands. However, some of low coherence bands might be not spurious but caused by resonance frequencies of the struts.

Due to their location, the spatial coherence at the base struts of length  $700mm$ ,  $ac$ , might clearly show the contribution of these resonance frequencies rather than the coherence at the joints. Fig. 2-4 shows the spatial coherence at the base struts with the same frequency resolution of  $\Delta f = 8Hz$ . This figure shows more wide low coherence bands than the coherence of the joints, since the resonance is sensed more clearly on the struts than at the joints. The low coherence bands become deeper with increasing distance. At the farthest position shown,  $b12$ , three apparent low coherence bands are well developed, except below  $5kHz$ , approximately at  $5.5kHz$ ,  $10.5kHz$ , and  $14.5kHz$ .

Another measurement with the frequency resolution of  $\Delta f = 2Hz$  was conducted to examine whether this low coherence is spurious or caused by the stop bands of the truss. Fig. 2-5 shows the spatial coherence at the base struts with the frequency resolution of  $\Delta f = 2Hz$ . Coherence of unity is observed between the input and outputs at all locations and suggests that the low coherence below  $5kHz$  is spurious. Low coherence occurs below  $0.5kHz$  and this supports the frequency resolution error again. Thus the low coherence in the low frequency band is spurious and caused by resolution error. However, wide range notches at  $3kHz$  and  $5.5kHz$  are still observed regardless of the enhanced frequency resolution and these might not be spurious low coherence levels. These might be due to stop bands caused by resonance of the struts of the truss.

Stop band analysis was conducted with the assumption of struts as Euler-Bernoulli beams for convenience. Fig. 2-6 and Fig. 2-7 give the multiple half-wave resonance frequencies of the different elastic waves and struts respectively. Fig. 2-8 shows the total resonance frequencies in the truss. These resonance frequencies present a very large impedance to waves at the strut inputs, and thus cause stop bands in wave propagation, and therefore low spatial coherence. The major stop bands shown in Fig. 2-4 and Fig. 2-5, near  $3kHz$ ,  $5kHz$ ,  $10kHz$ , and  $14kHz$ , are well developed among the other resonance frequencies. It seems that these stop bands coincide with the frequencies where the strut lengths equal the integral multiple of half the elastic wavelengths such as  $\lambda/2$ ,  $\lambda$ ,  $3\lambda/2$ ,  $\dots$ .

The flexural wavelength equals twice the strut length below  $1kHz$  at the frequencies equivalent to the first few integral multiple of half the elastic wave lengths, and this frequency band is in the resolution error region; hence coherence becomes small regardless of strut resonance. Apart from these stop band frequency regions, coherence rises to unity again. The elastic wavelengths as a function of frequency are plotted in Fig. 2-9. The stop band near  $3kHz$  coincides with the frequencies where the strut lengths equal half of the torsional and compressional wavelengths. The next two major stop bands near  $5kHz$  and  $10kHz$  coincide with the frequencies where the

strut lengths equal these elastic wavelengths. The stop band near  $14kHz$  can also be explained in this manner.

The magnitude and phase of the cross-spectra at the joints are shown in Fig. 2-10 and Fig. 2-11 respectively. The resonance of struts and time delays through multi-paths in a stationary process cause dips and small oscillating peaks in the magnitude of the cross-spectra. If the elastic waves propagate with roughly constant group delay, the phase of the cross-spectra at the joints in Fig. 2-11 should be periodic. However, there is no such periodicity in the phase of the cross-spectra; thus the phase of the cross-spectra looks like a random process.

However, I unwrapped the phase to investigate more thoroughly the tendency of wave propagation to have constant group delay. The unwrapped phase of the cross-spectra at the joints is shown in Fig. 2-12. The unwrapped phase angle plot roughly shows a linear phase relationship with increasing frequency. These slopes are not constant and vary with frequency due to dispersion. Table 2.1 shows the slopes averaged over all measured frequencies and within octave bands.

Table 2.1: Phase slope of cross-spectra at the  $c$  joints of the MIT truss.

Joint	Phase slope ( $deg/kHz$ )			
	0~25.6kHz	16kHz octave band	8kHz octave band	4kHz octave band
c04	$-0.69 \times 10^3$	$-0.43 \times 10^3$	$-0.88 \times 10^3$	$-0.65 \times 10^3$
c06	$-1.72 \times 10^3$	$-1.06 \times 10^3$	$-2.14 \times 10^3$	$-2.15 \times 10^3$
c08	$-2.63 \times 10^3$	$-1.88 \times 10^3$	$-3.06 \times 10^3$	$-3.49 \times 10^3$
c10	$-2.99 \times 10^3$	$-2.37 \times 10^3$	$-2.99 \times 10^3$	$-3.31 \times 10^3$
c12	$-3.26 \times 10^3$	$-2.63 \times 10^3$	$-3.34 \times 10^3$	$-3.50 \times 10^3$

Both Fig. 2-12 and Table 2.1 show, with a few exceptions, that the magnitude of the phase slope increases with increasing distance from the input. From the octave band phase slopes, it seems that the magnitude of the phase slope decreases with increasing frequency. As mentioned above, this phase slope variation is due to dispersive propagation.

The exponential part of a harmonic traveling wave can be expressed as

$$e^{i(kx-\omega t)}, \quad (2.18)$$

and its phase is  $\varphi$ ,

$$\varphi = kx - \omega t. \quad (2.19)$$

Wavenumber, phase speed, time delay, group speed and group speed can be extracted from two adjacent joints, which are regarded as measuring points at the virtual beam, and become as follows

$$k = \frac{\Delta\varphi}{\Delta x}, \quad (2.20)$$

$$c_{phase} = \frac{\omega}{k}, \quad (2.21)$$

$$\tau = \frac{\Delta x}{c_p}, \quad (2.22)$$

$$c_{group} = \frac{\partial\omega}{\partial k}, \quad (2.23)$$

$$g_\tau = \frac{\Delta x}{c_g}, \quad (2.24)$$

where  $\Delta\varphi$  is the phase difference between two adjacent joints,  $\Delta x$  is the axial interval between two adjacent joints,  $0.783m$  (taken as positive),  $\tau$  is time delay, and  $g_\tau$  is group delay.

Fig. 2-13 shows the extracted wavenumber by the above method. It shows that negative wavenumbers are developed over all pairs of the adjacent joints, (c04,c06), (c06,c08), (c08,c10), and (c10,c12), except for the frequencies approximately below  $1kHz$  at (c04,c06) and (c10,c12). This is contrary to the positive wave propagation direction ( $k$  is positive for waves propagating in the direction away from the source), and needs to be interpreted (see page 31).

Fig. 2-14 shows the extracted phase speed of propagating waves via this virtual beam. Two different trends of phase speed magnitude are observed. For the first two pair of the two adjacent joints, (c04,c06) and (c06,c08), the fluctuation of phase

speed is large at frequencies below  $1kHz$ , and the phase speeds become approximately  $300m/sec$  at the highest frequency,  $25.6kHz$ . For the next two pair of the adjacent joints,  $(c08,c10)$  and  $(c10,c12)$ , the phase speeds increase with increasing frequency and become approximately  $800m/sec$  and  $1050m/sec$  respectively at the highest frequency. These two phase speeds also show that the wave propagates with different propagation signs below approximately  $11kHz$ .

Fig. 2-15 shows the extracted time delay of wave propagation. The time delays also are partly negative (mostly at low frequencies). However, the results above the order of  $10kHz$  (for some above  $3kHz$ ) are positive.

Fig. 2-16 shows the group speed of propagating waves via this virtual beam. All of the group speeds extracted show high fluctuation of propagation direction above approximately  $1kHz$ . This high fluctuation of propagation direction in the group speed is different from the relatively simple change of propagation signs in the phase speed as shown in Fig. 2-14 and this shows that the wave energy travels with more complications than the phase of waves, as measured on the joints at the truss.

Fig. 2-17 shows the extracted group delay. The group delay also shows high fluctuation in sign above  $1kHz$  due to the extracted group speed results. It must be emphasized, however, that the group speed and group delay plots shown in Fig. 2-16 and Fig. 2-17 are not accurate, since the frequency resolution of these results ( $\Delta f = 8Hz$ ) and this might cause under sampling which is crucial in differentiating angular frequency with wavenumber.

The reversals in propagation direction of waves in the truss are due to the phase data of the cross-spectra measured at the joints. Difficulties often arise in interpreting the phase data when obstructions or discontinuities lie in the path between the input and output locations. The obstructions or discontinuities cause scattering of the propagation energy; concerning scattering, obstructions or a lack of homogeneity along a propagation path can cause wide-angle reflections or an effective bending of the propagating energy flow[16]. Since the fully energized truss for a stationary input creates a highly reverberant environment, the phase between two points tends

to indicate the direction of power flow out of the reverberant region, independent of the direction from the source to the sensor position[18].

Moreover, absorption in a restricted location causes flow of power to that location; hence it can influence the phase data if the location of the absorption is to the side of the outputs rather than aft of them[16]. But Dyer[19] believes that the absorption is uniformly distributed in the truss, except at the source location. This uniformly distributed absorption causes more complicated phase data and hence both wave propagation directions in the truss. For the truss, reverberation cannot be avoided due to its characteristic configuration. Thus the phase data incorporate the complicated reverberation and scattering effects.

Bondaryk[20] showed that in some frequency bands the total power of the compressional wave is approximately  $10dB$  higher than the power of the other elastic waves; those bands can be found from Fig. 2-18 and they are  $0.2\sim 0.4kHz$ ,  $1\sim 1.1kHz$ , etc. There is a possibility of extracting more readily interpretable wavenumber, phase speed, time delay, group speed and group delay from the phase data, if these extraction methods are applied to these bands with a higher frequency resolution.

Fig. 2-19 shows the phase of the cross-spectra at the joints with the enhanced frequency resolution  $\Delta f = 0.5Hz$ . Simple phase relationships are found near the frequency bands  $0.3\sim 0.4kHz$  and  $0.8\sim 1.1kHz$  as expected. I chose the  $0.3\sim 0.4kHz$  frequency band to extract wavenumber, phase speed, time delay, group speed and group delay from the phase data and the results are shown in Fig. 2-20, Fig. 2-21, Fig. 2-22, Fig. 2-23 and Fig. 2-24 respectively. The results still show negative values and this is due to the reverberation and scattering of the truss as mentioned previously regardless of the enhanced frequency resolution. Moreover, the relatively wide interval between two adjacent joints and the inherent limitation of the phase unwrap algorithm also hinder extracting accurate results from the phase data.

These results show that the wave propagates in both positive and negative axial directions via these virtual attachment points. Fig. 2-25 shows a frequency-wavenumber spectrum of the inertance of the truss from the cross-spectra with the frequency res-



olution of  $\Delta f = 2Hz$ . If there is any elastic wave propagation with the same wave speed of the elastic wave propagation in the struts within the array, aliasing occurs at high frequencies for flexural, torsional, and compressional waves approximately above  $52Hz$ ,  $1,986Hz$ , and  $3,259Hz$  respectively, because of the sparse spatial sampling. Except for stop bands of the inertance spectrum and some other spots, it is hard to see any trend in the dispersion relationship.

Fig. 2-26 shows the cross section of this frequency-wavenumber plot with  $k = 0.02m^{-1}$ . The major stop bands are developed approximately at  $1kHz$ ,  $2.3kHz$ ,  $2.8kHz$ ,  $3.1kHz$ ,  $6kHz$ , etc. I plot in Fig. 2-27, the inertance wavenumber spectrum at some peak inertance bands at  $1,471Hz$ ,  $2,829Hz$ ,  $3,774Hz$ , and  $5,374Hz$ , to investigate wavenumber distribution. In the  $1,471Hz$  inertance band, some inertance wavenumber packets are developed either in positive and negative wavenumber regions and these packets resemble each other. However, with increasing frequency, the wavenumber spectrum spreads and becomes flatter and converges to the magnitude between  $-10$  and  $10 dB$  re  $1/kg$  except for the  $3,774Hz$  inertance band which is about  $20dB$  lower than other inertance bands. Thus it seems that for high inertance frequency bands no specific wavenumber packet is found.

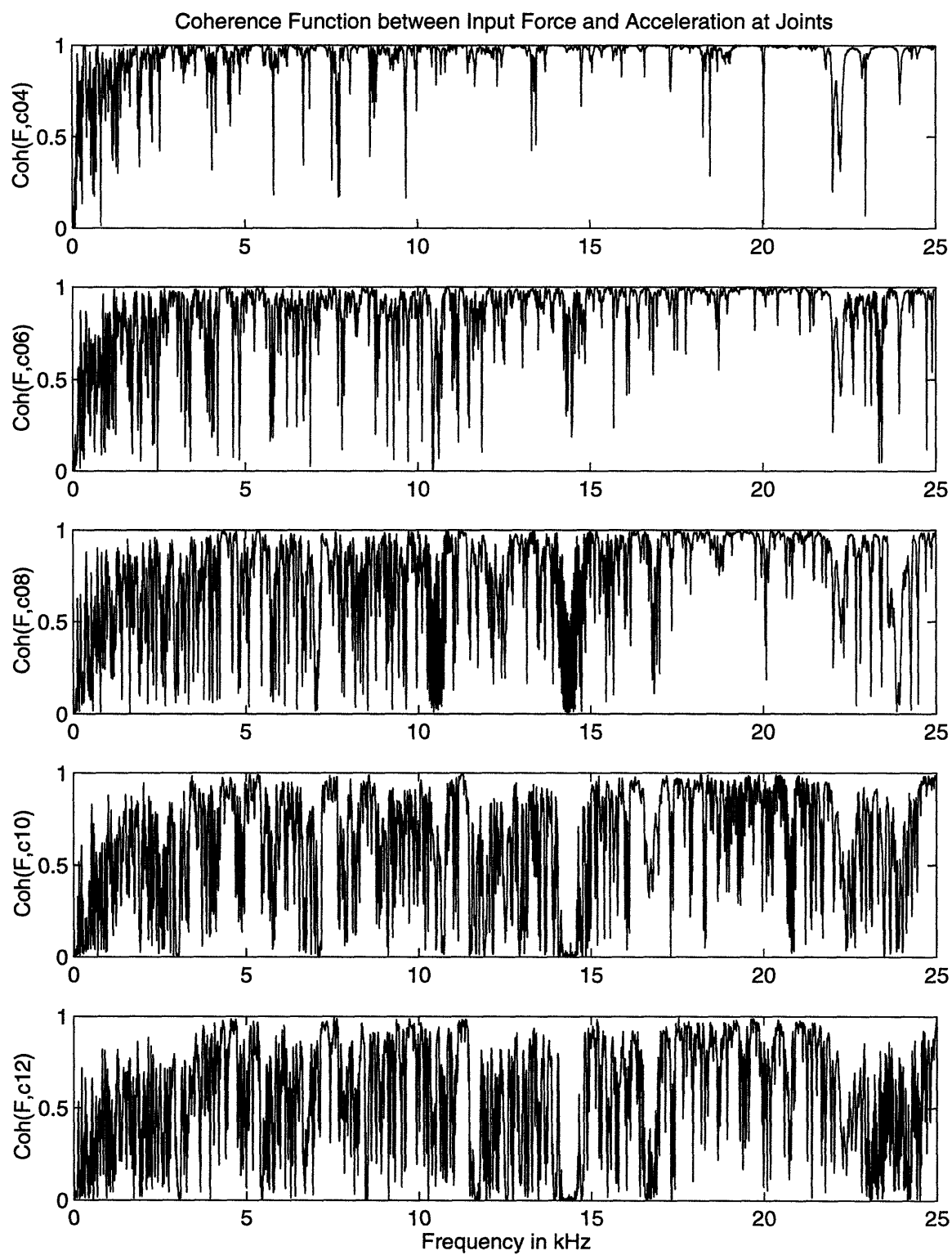


Figure 2-3: Spatial coherence of total elastic wave field between the input and the acceleration at the joints of the truss with frequency resolution of  $\Delta f = 8Hz$ .

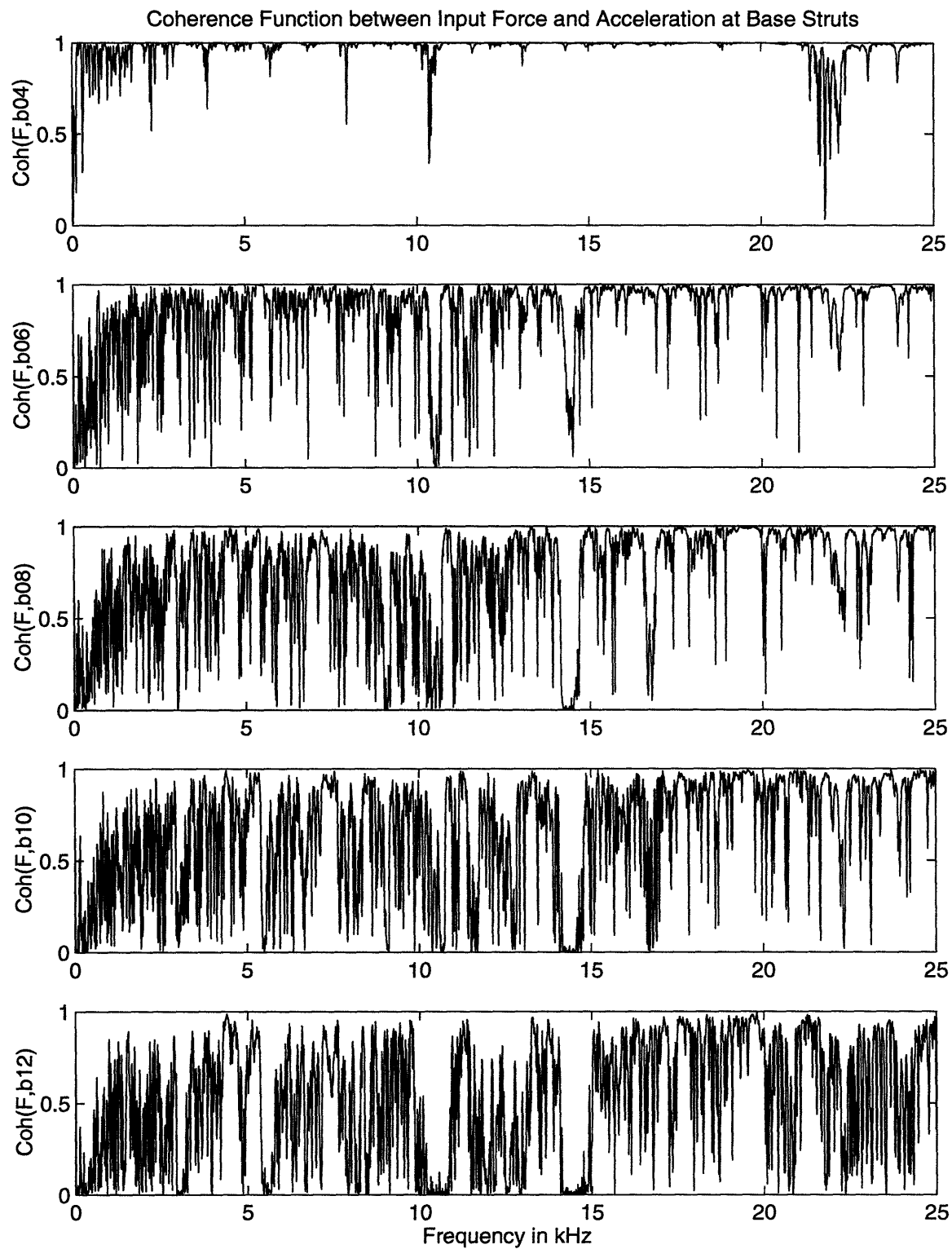


Figure 2-4: Spatial coherence of total elastic wave field between the input and the acceleration at the base struts of the truss with  $\Delta f = 8Hz$ .

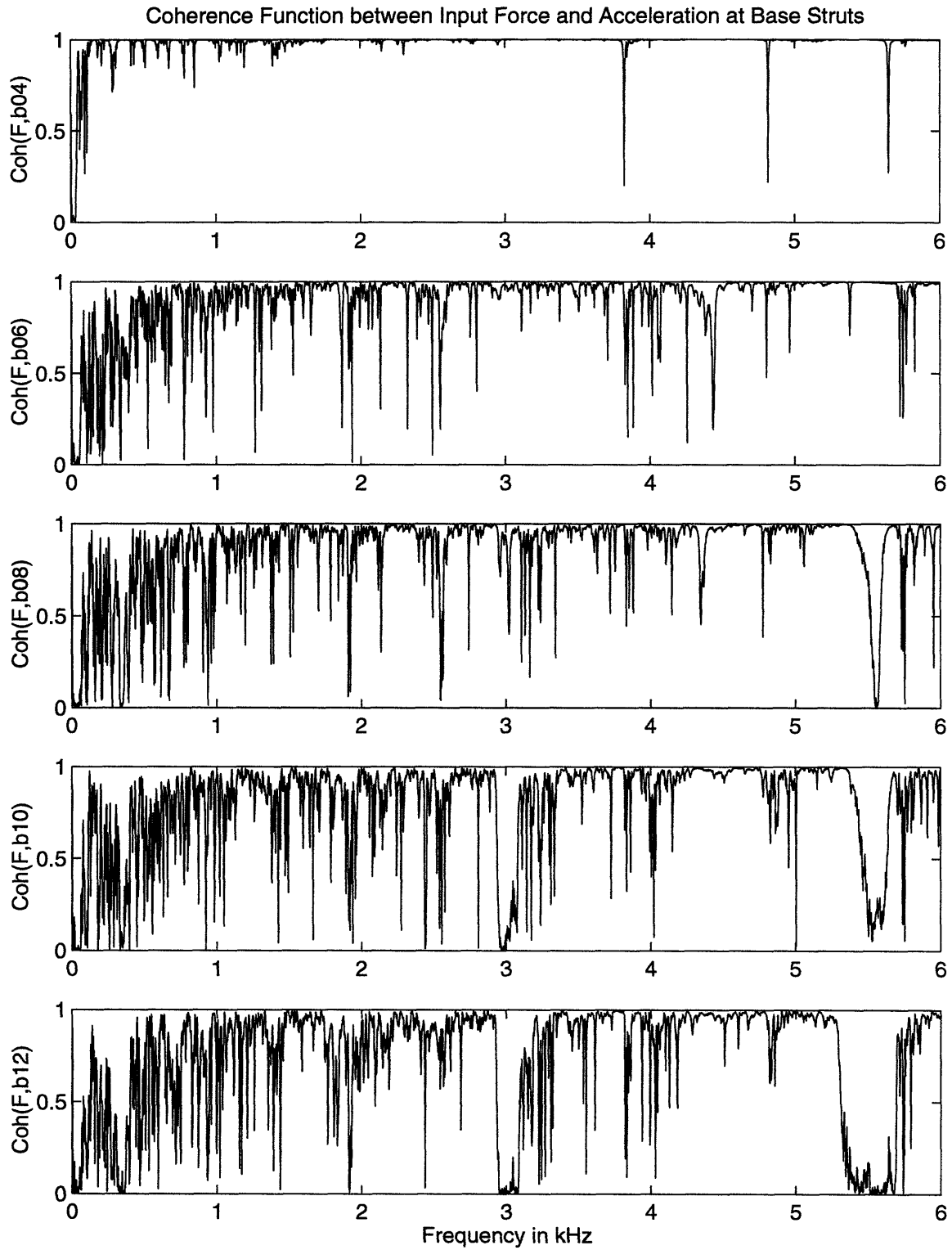


Figure 2-5: Spatial coherence of total elastic wave field between the input and the acceleration at the base struts of the truss with  $\Delta f = 2Hz$ .

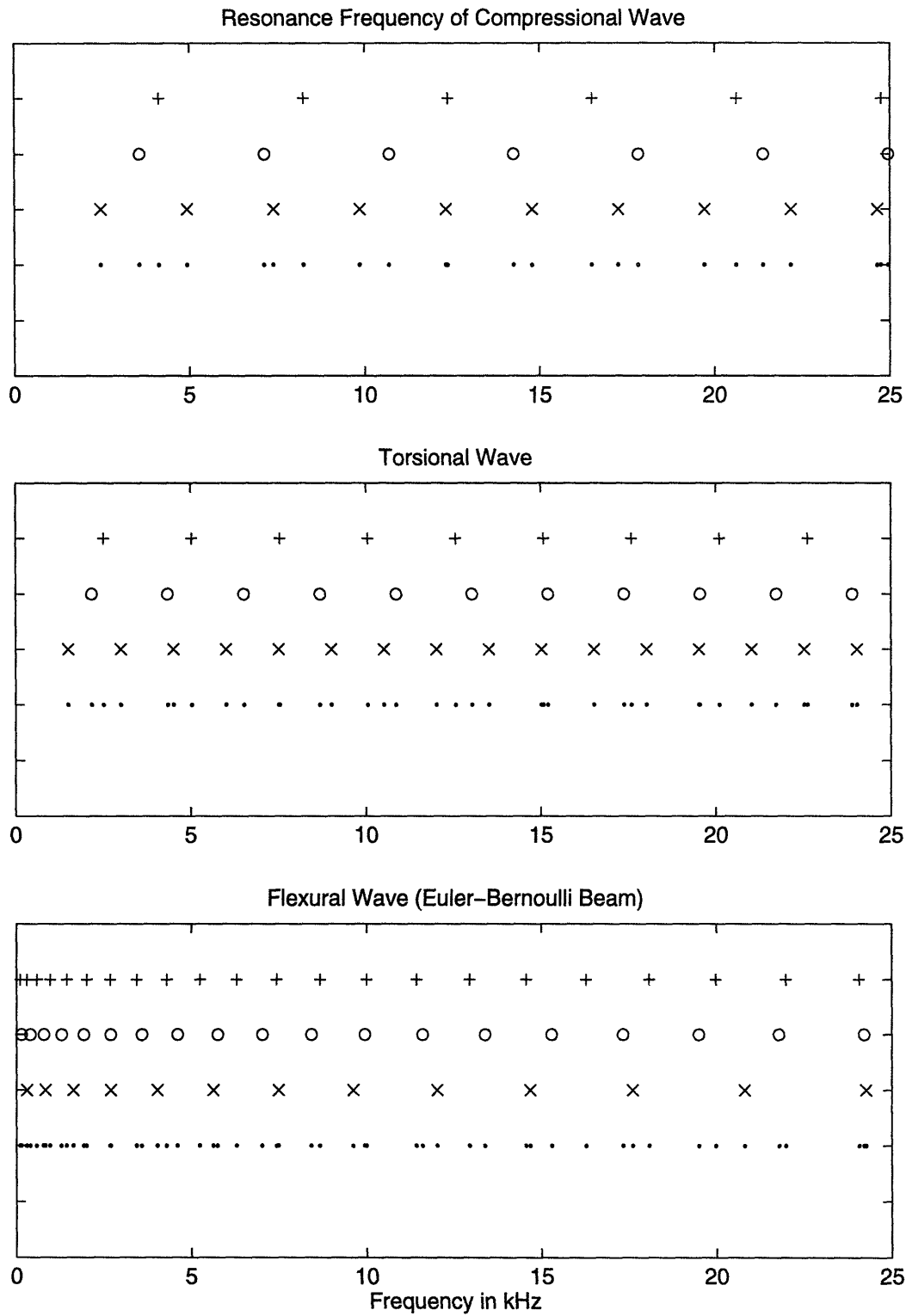


Figure 2-6: Multiple half-wave resonance frequencies of elastic waves, strut length=810mm (+), 700mm (o), 484mm (x), and total (·).

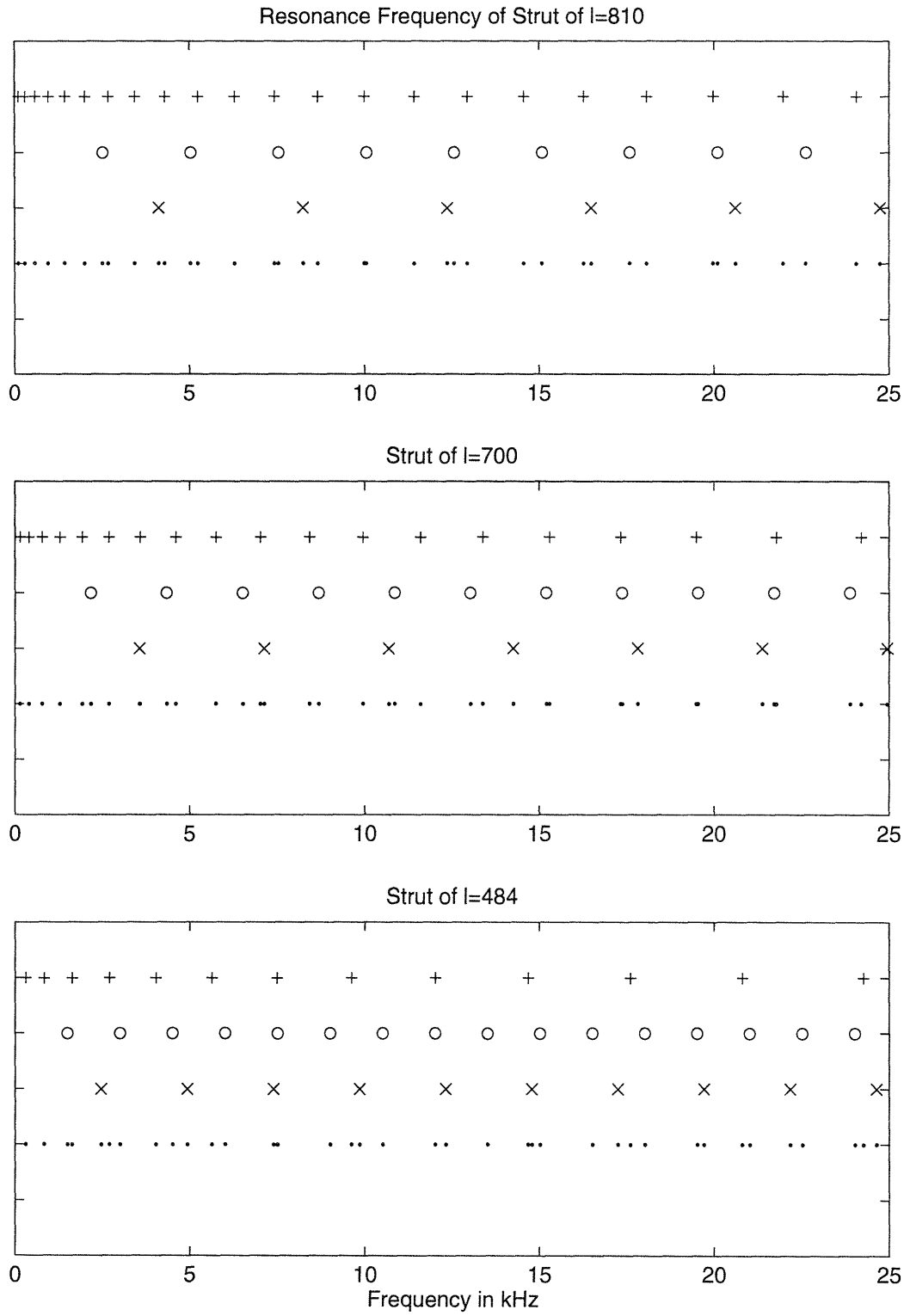


Figure 2-7: Resonance frequencies of struts, flexural (+), torsional (o), compressional (x), and total (·).

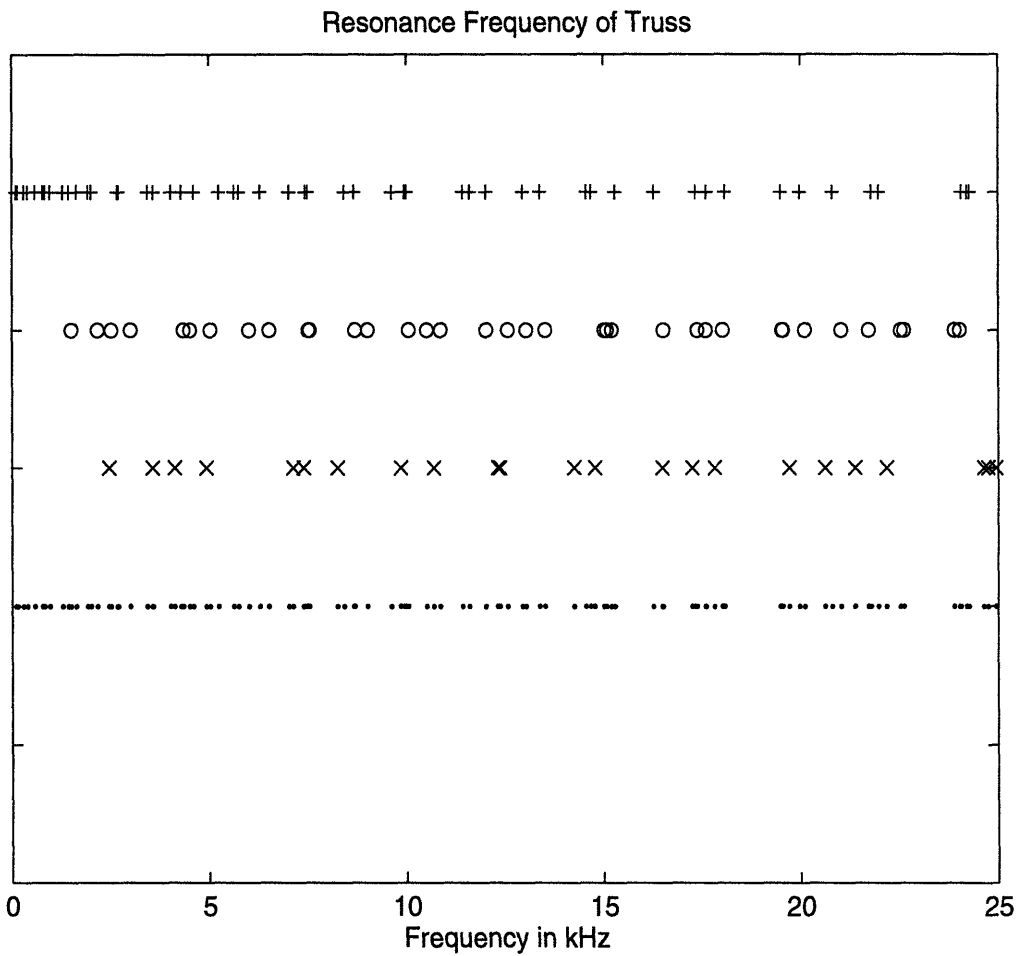


Figure 2-8: Resonance frequencies of truss, flexural (+), torsional (o), compressional (x), and total (.).

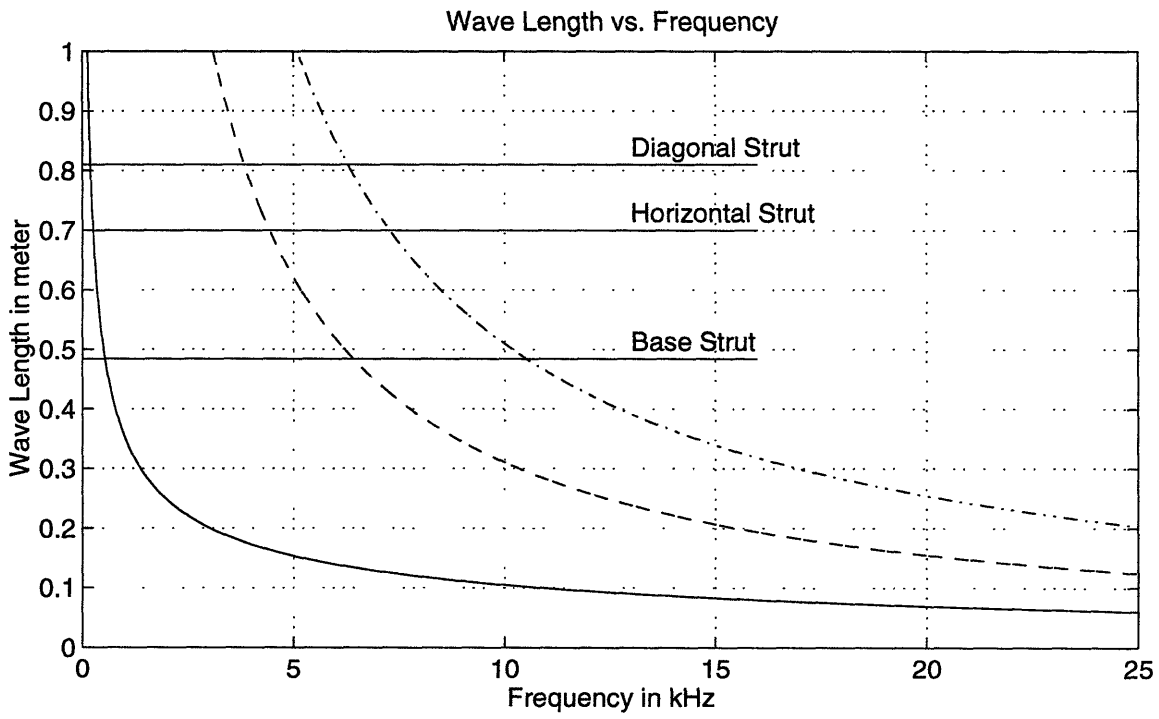
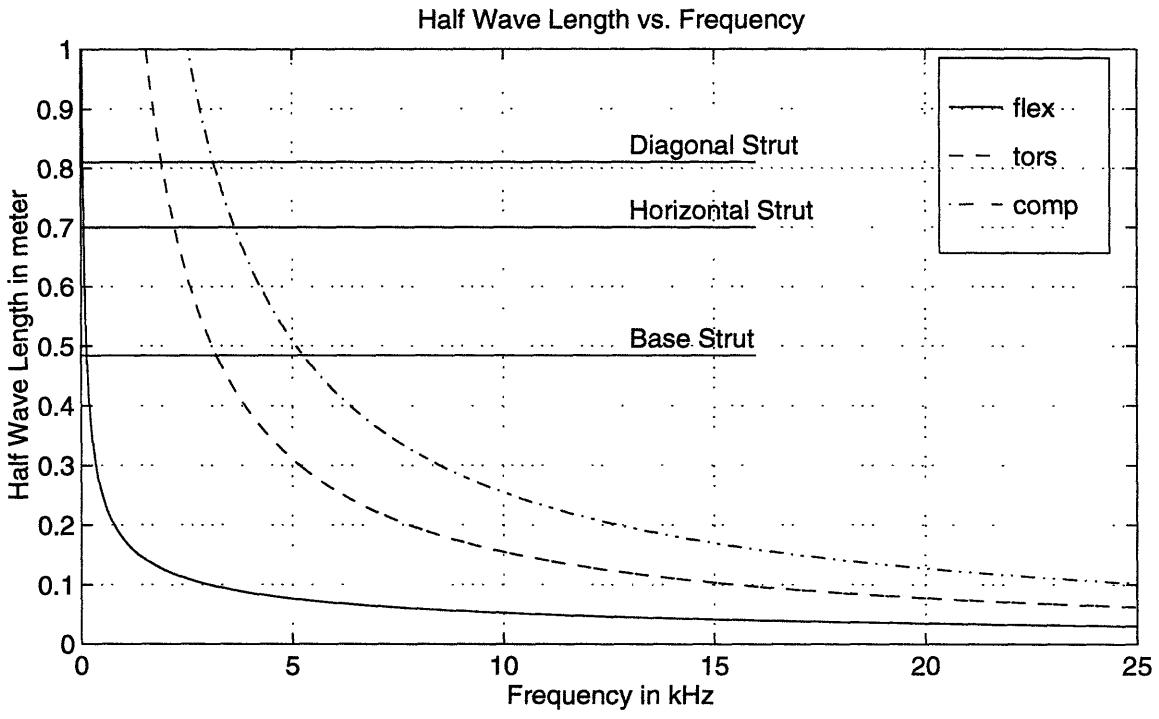


Figure 2-9: Elastic wavelength as a function of frequency.



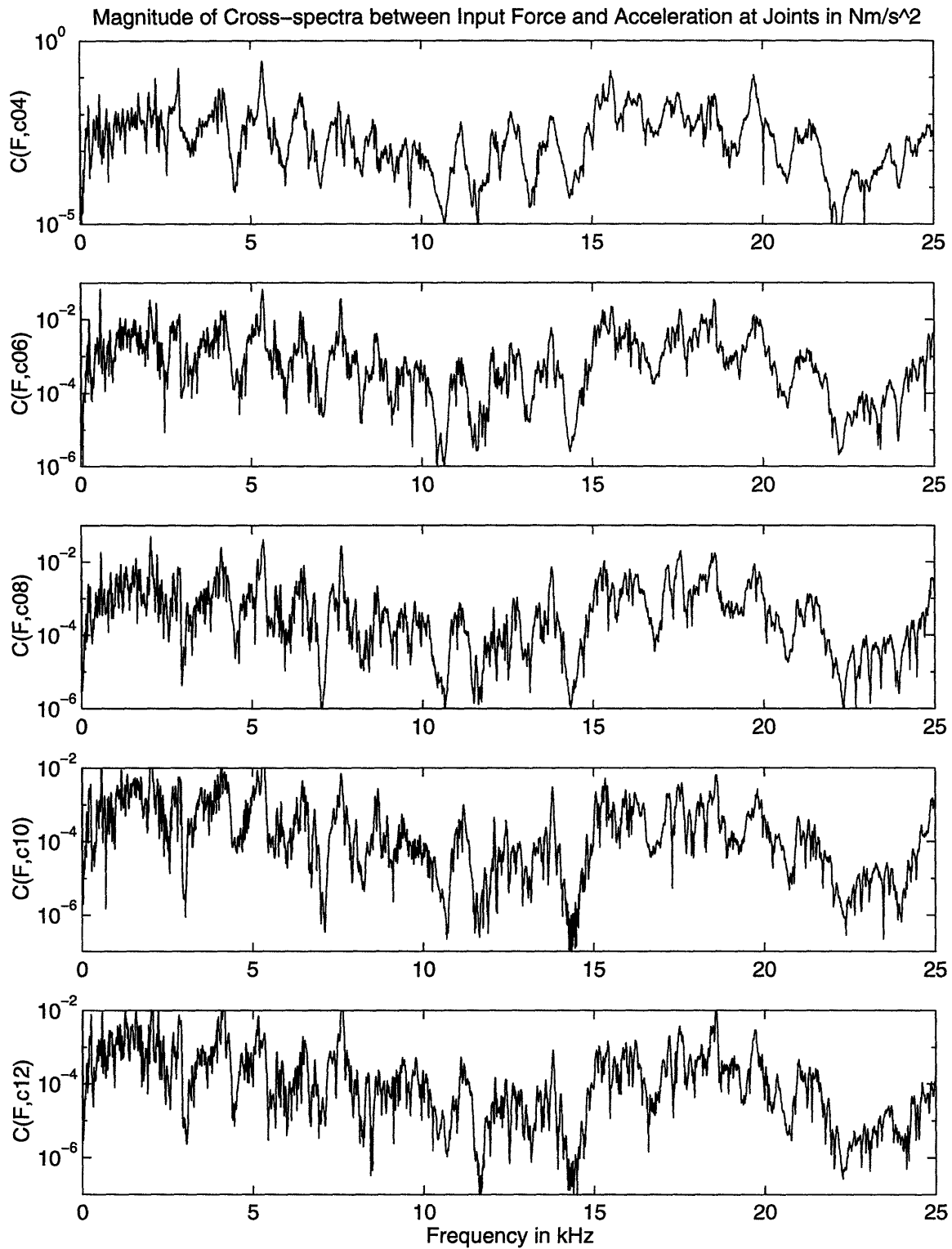


Figure 2-10: Magnitude of cross-spectra of total elastic wave field between the input and the acceleration at the joints of the truss with  $\Delta f = 8Hz$ .

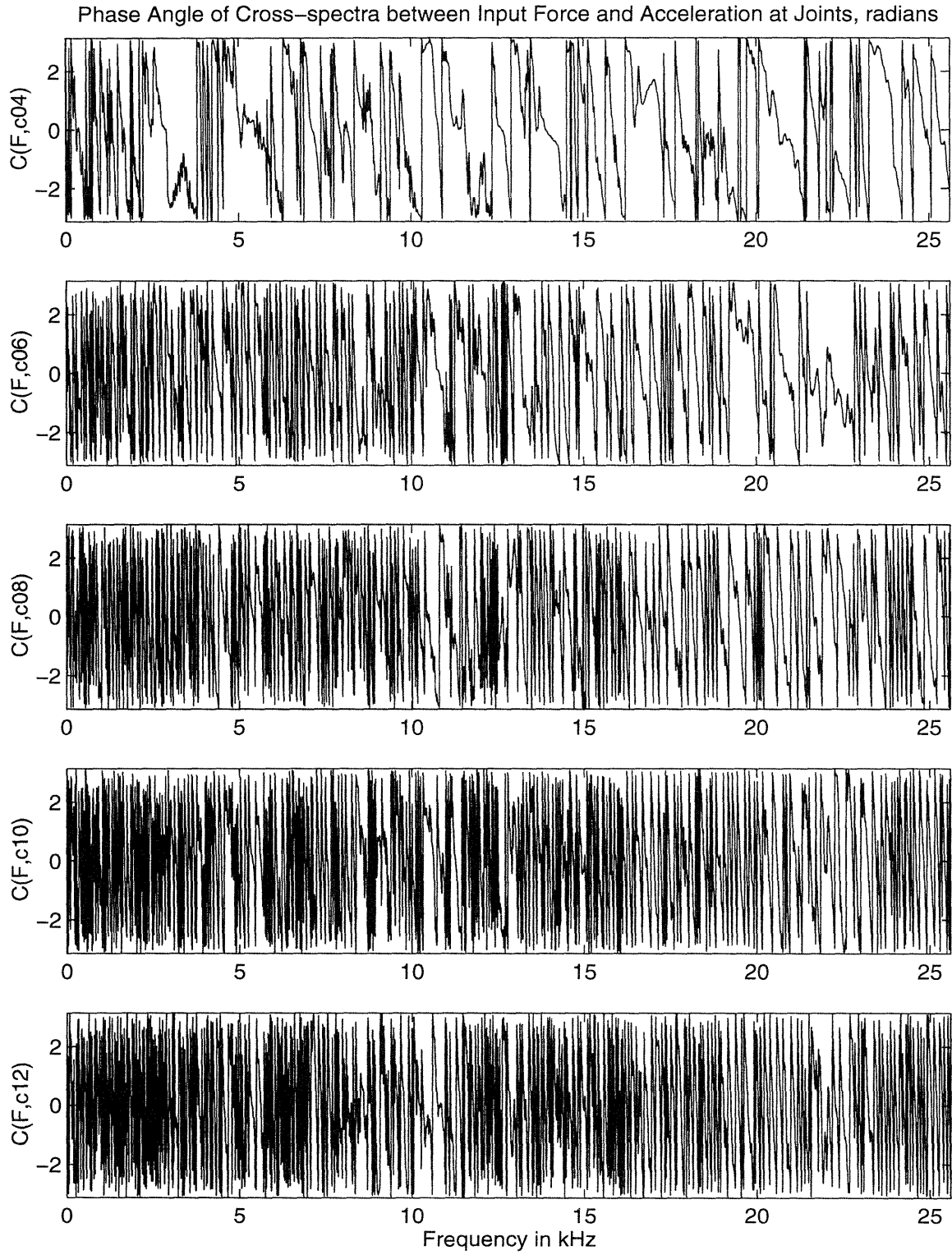


Figure 2-11: Phase angle of cross-spectra of total elastic wave field between the input and the acceleration at the joints of the truss with  $\Delta f = 8Hz$ .

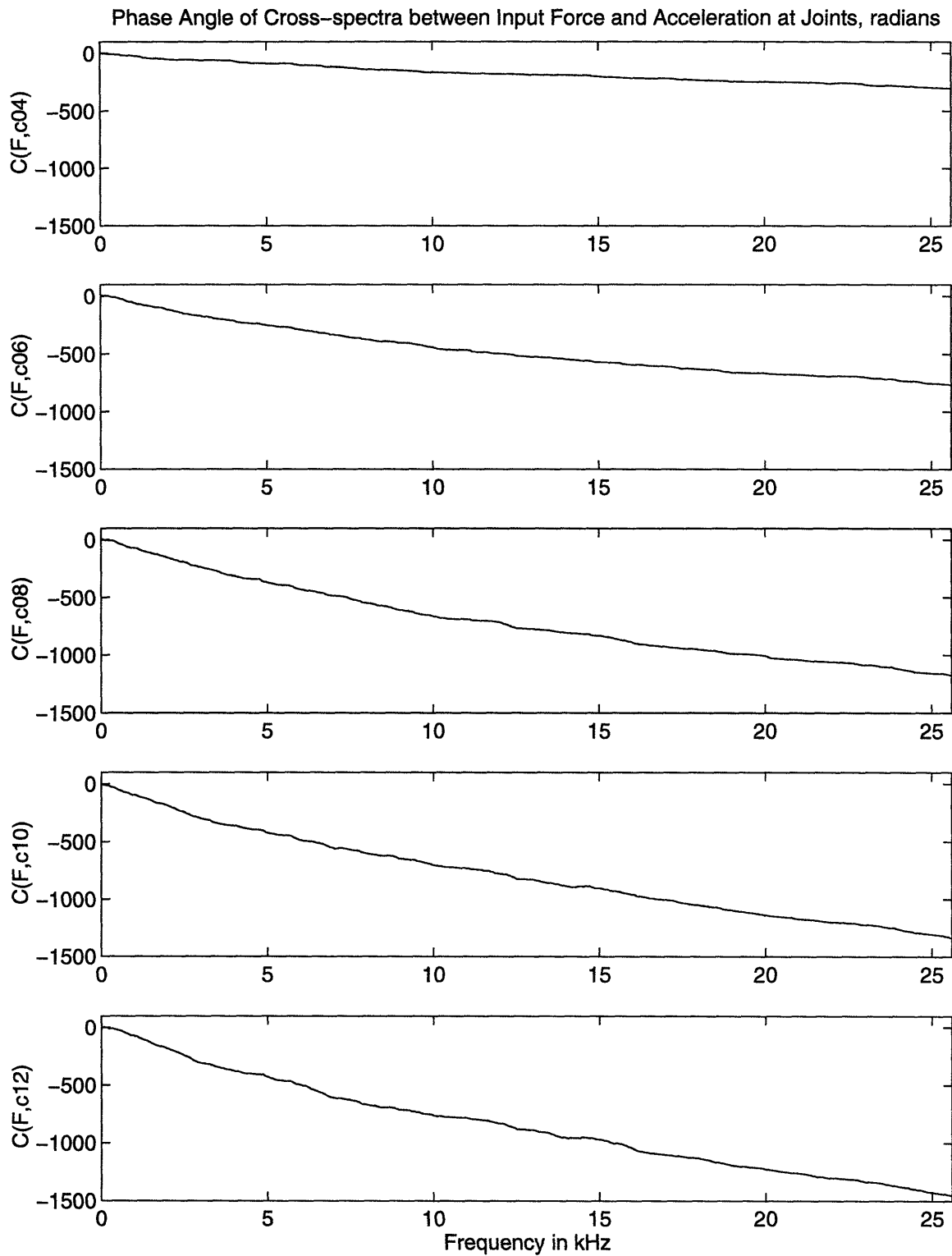


Figure 2-12: Unwrapped phase angle of cross-spectra of total elastic wave field between the input and the acceleration at the joints of the truss with  $\Delta f = 8Hz$ .

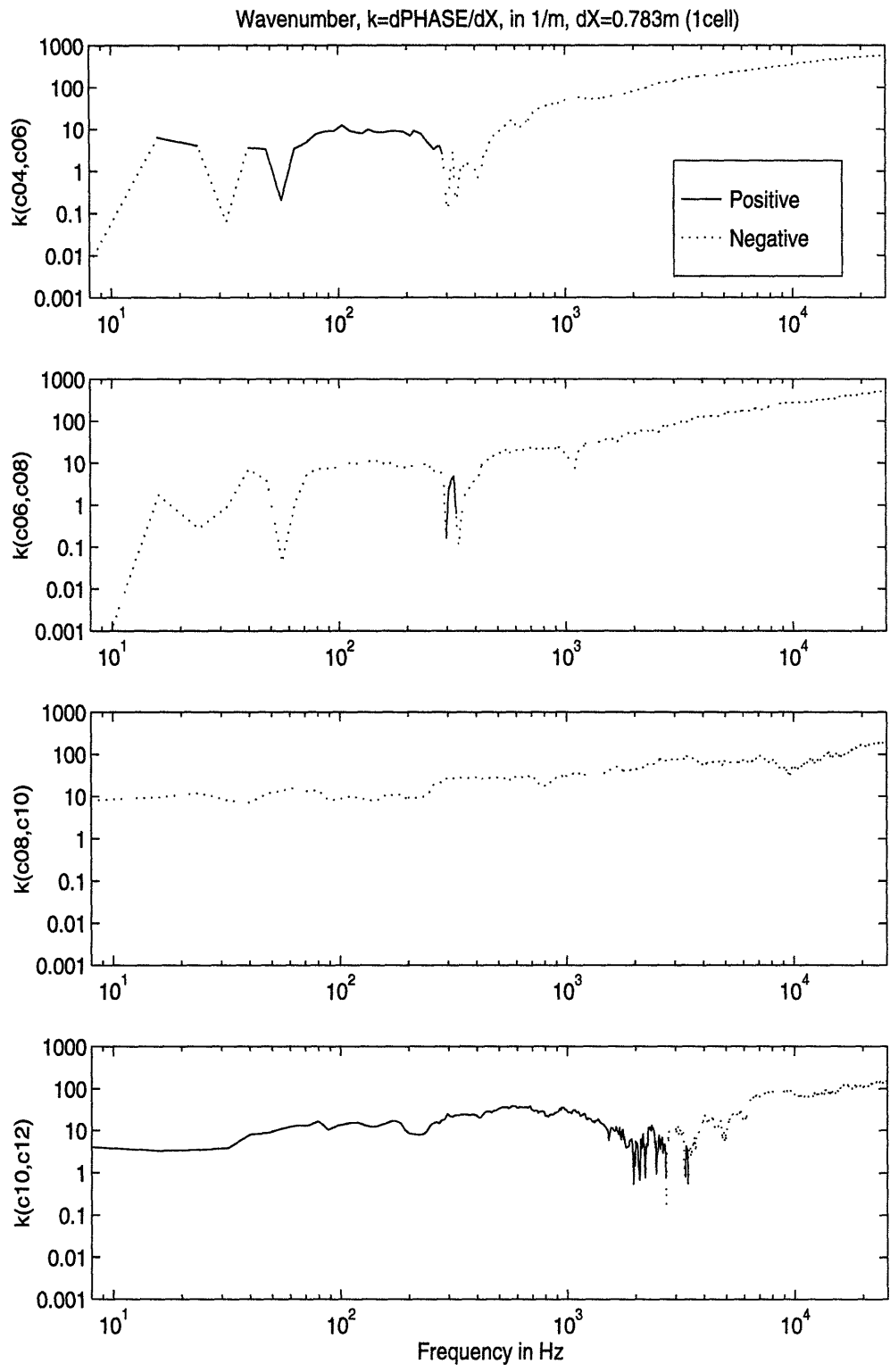


Figure 2-13: Extracted wavenumber between two adjacent joints as a function of frequency with  $\Delta f = 8\text{Hz}$ .

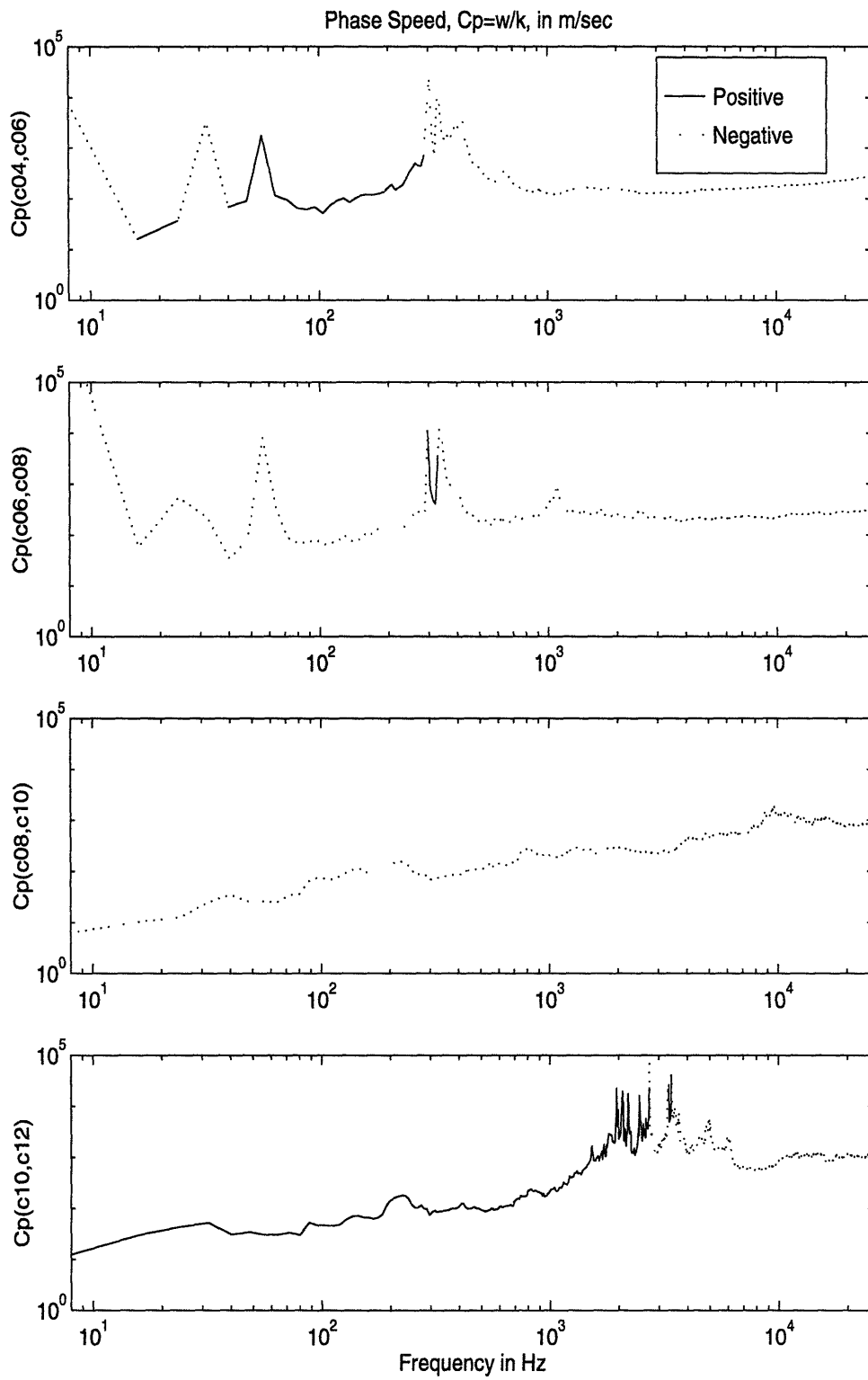


Figure 2-14: Extracted phase speed between two adjacent joints as a function of frequency with  $\Delta f = 8Hz$ .

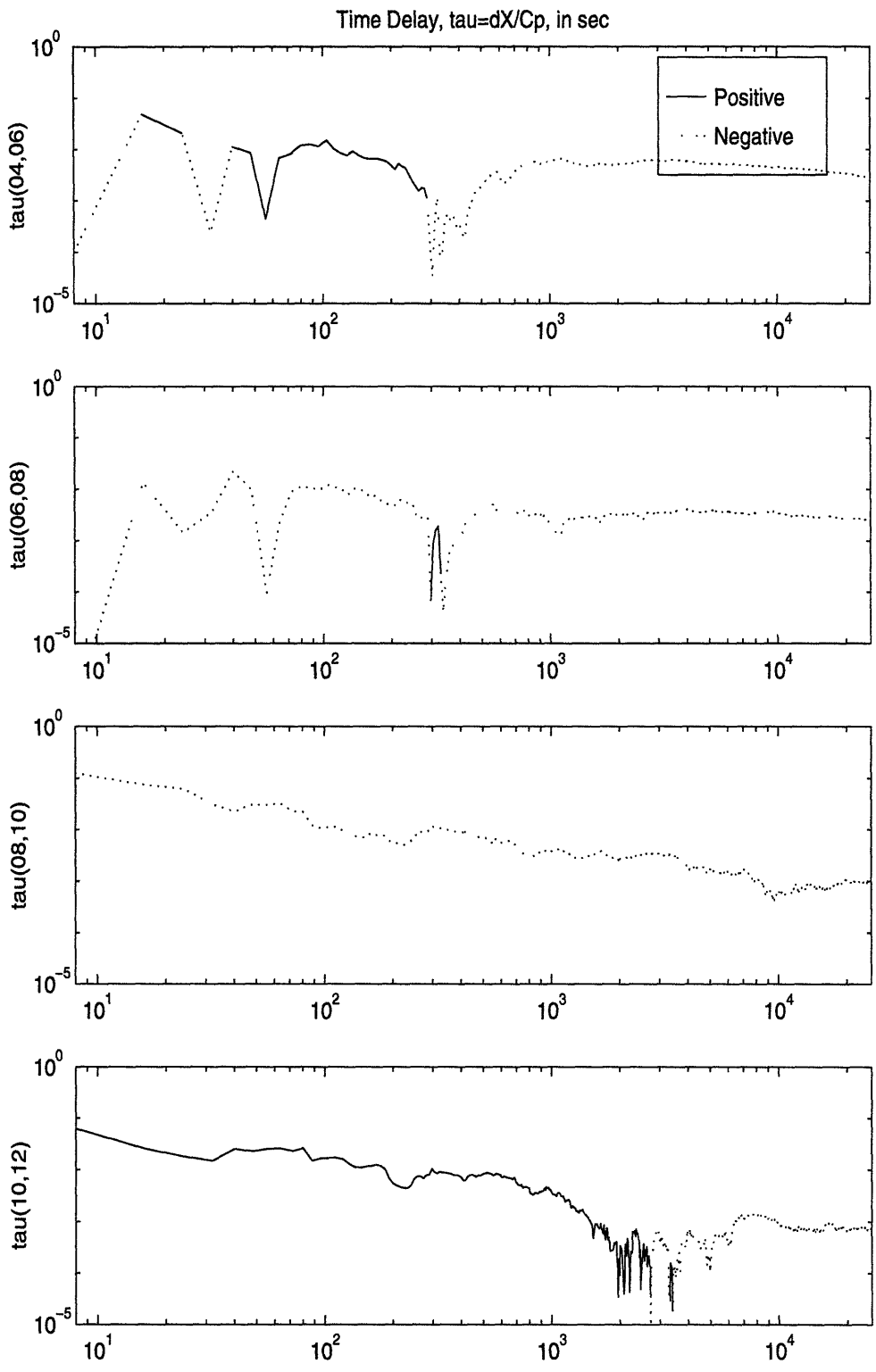


Figure 2-15: Extracted time delay between two adjacent joints as a function of frequency with  $\Delta f = 8Hz$ .

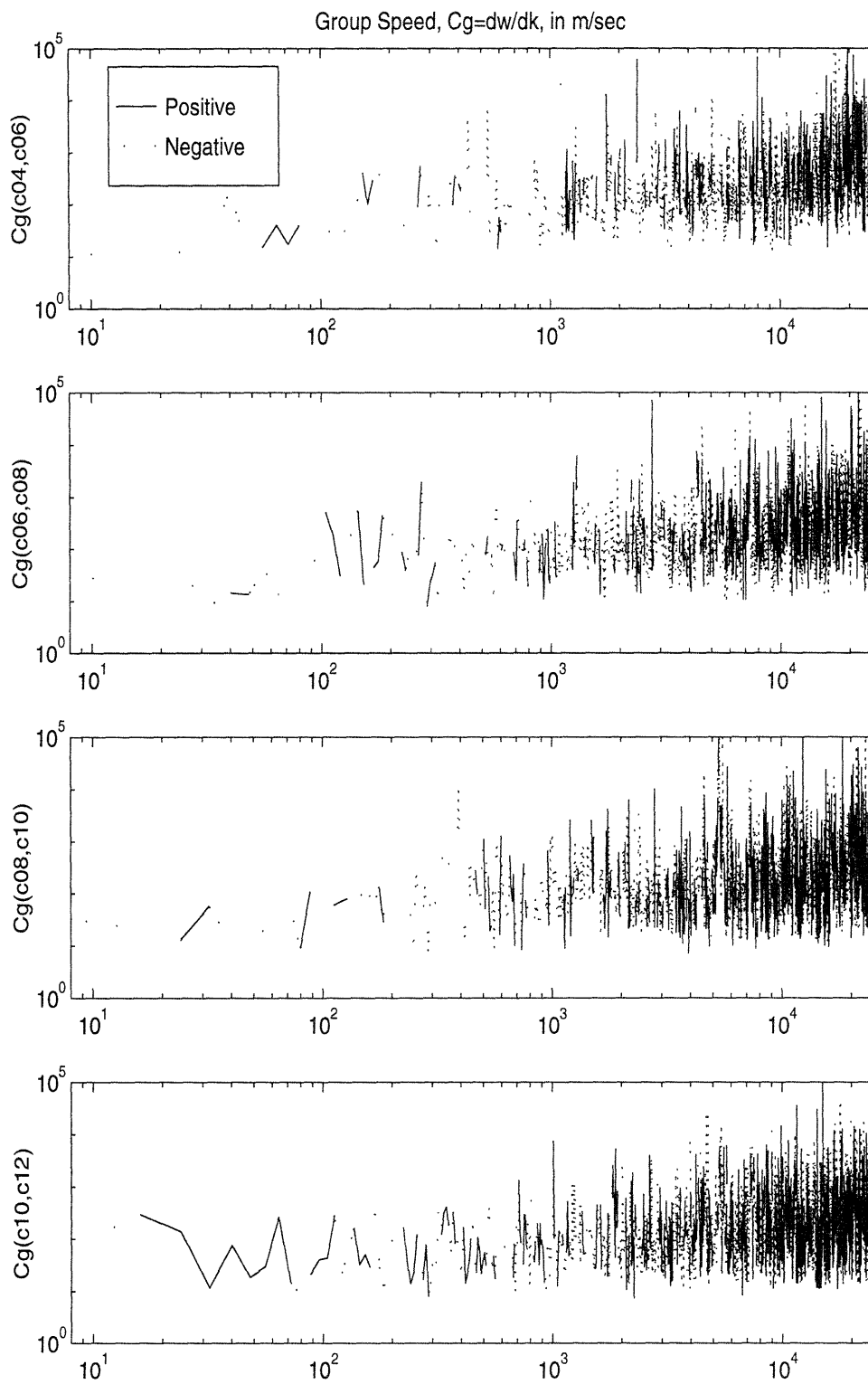


Figure 2-16: Extracted group speed between two adjacent joints as a function of frequency with  $\Delta f = 8Hz$ .

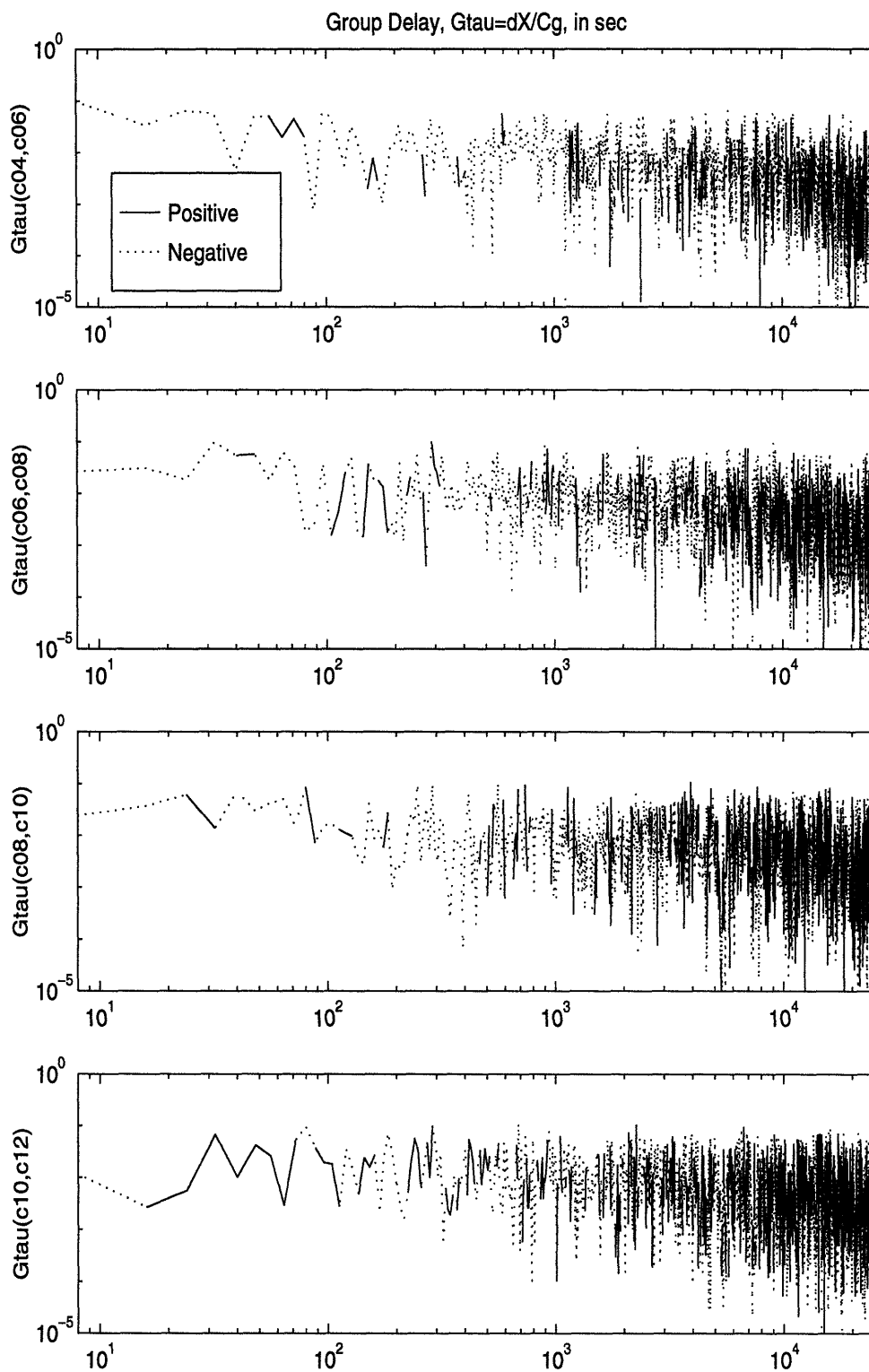


Figure 2-17: Extracted group delay between two adjacent joints as a function of frequency with  $\Delta f = 8Hz$ .



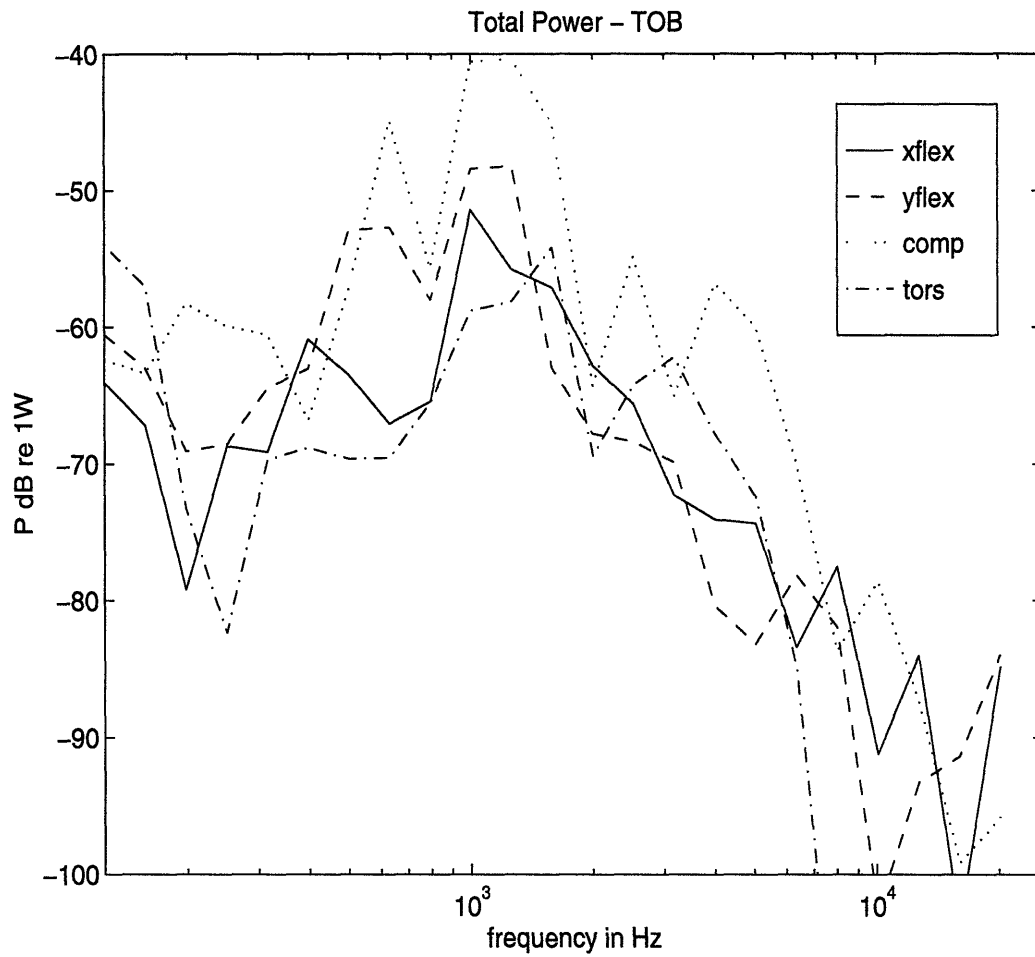


Figure 2-18: Third octave band average of measured power of elastic waves for the strut *a6e6* (*Z* excitation) with  $\Delta f = 8\text{Hz}$  (Ref[20]).

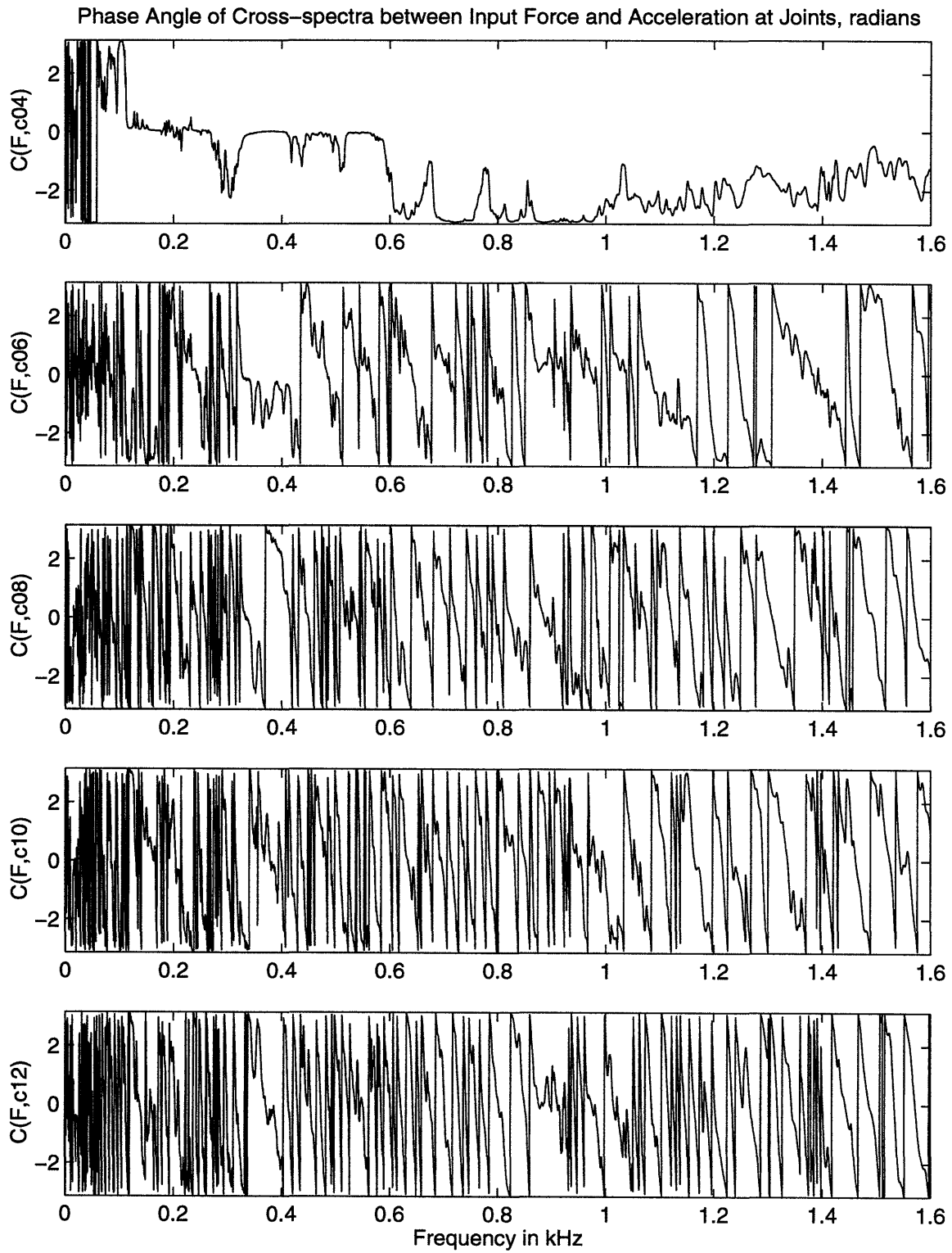


Figure 2-19: Phase angle of cross-spectra of total elastic wave field between the input and the acceleration at the joints of the truss with  $\Delta f = 0.5Hz$ .

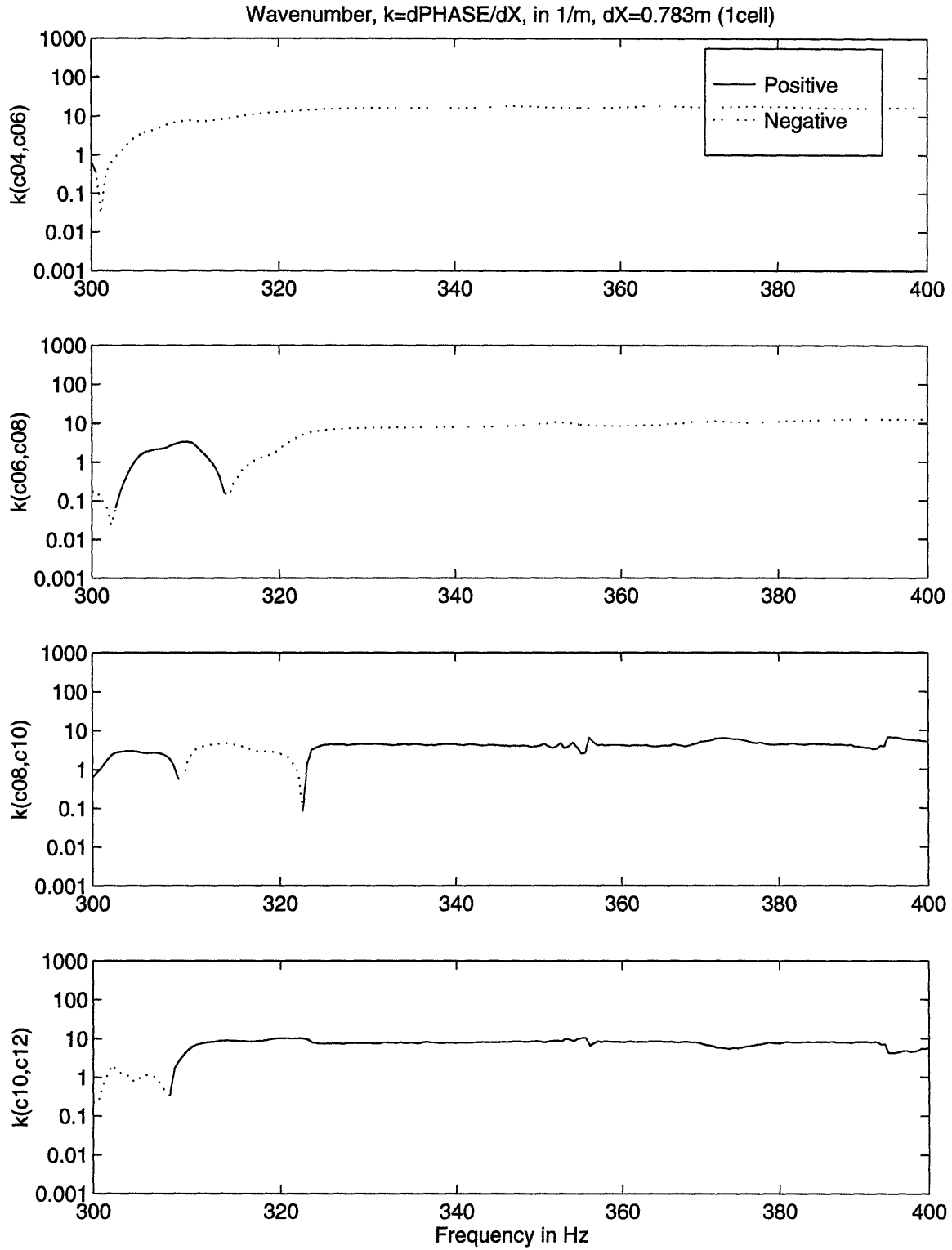


Figure 2-20: Extracted wavenumber between two adjacent joints as a function of frequency with  $\Delta f = 0.5\text{Hz}$ .

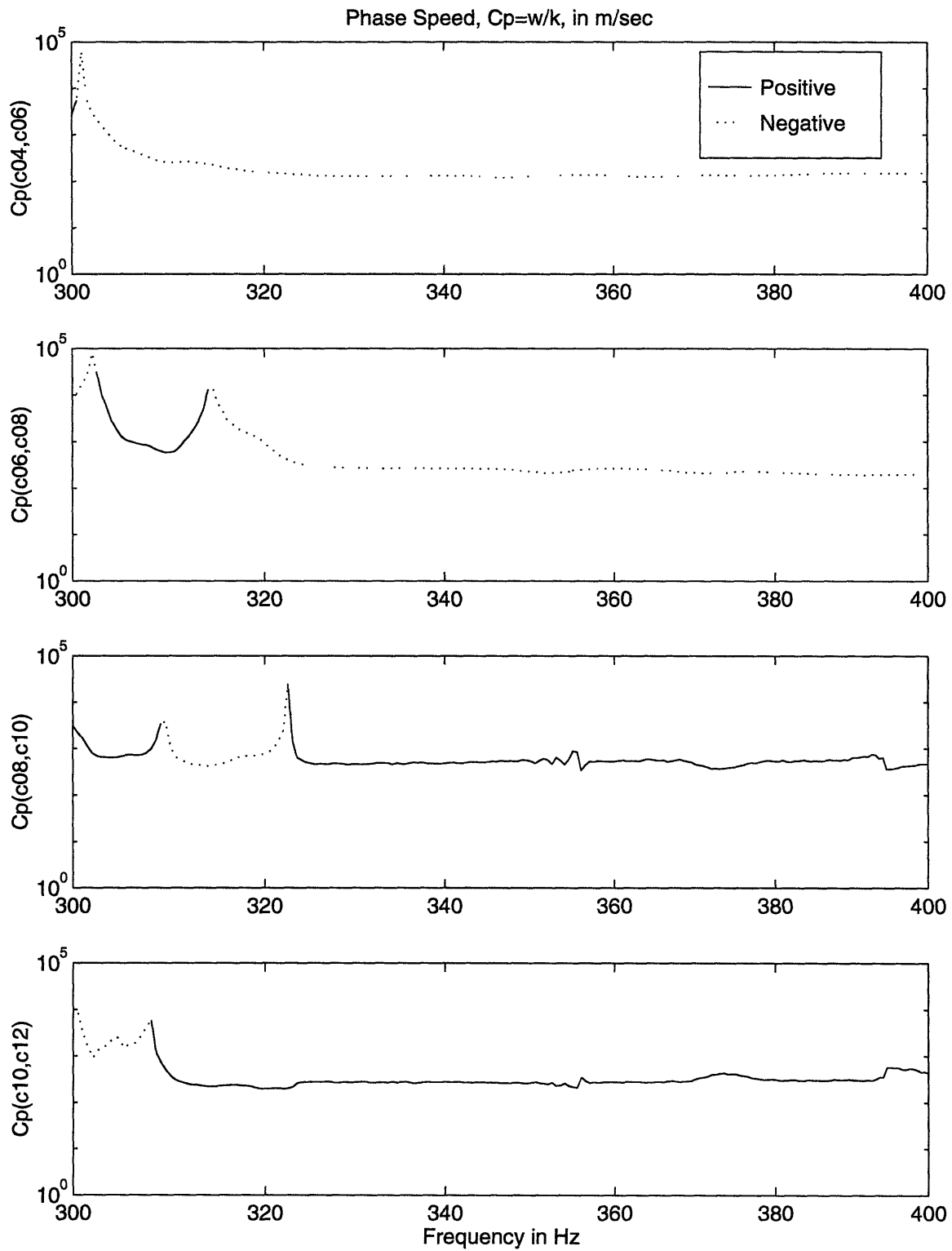


Figure 2-21: Extracted phase speed between two adjacent joints as a function of frequency with  $\Delta f = 0.5 Hz$ .

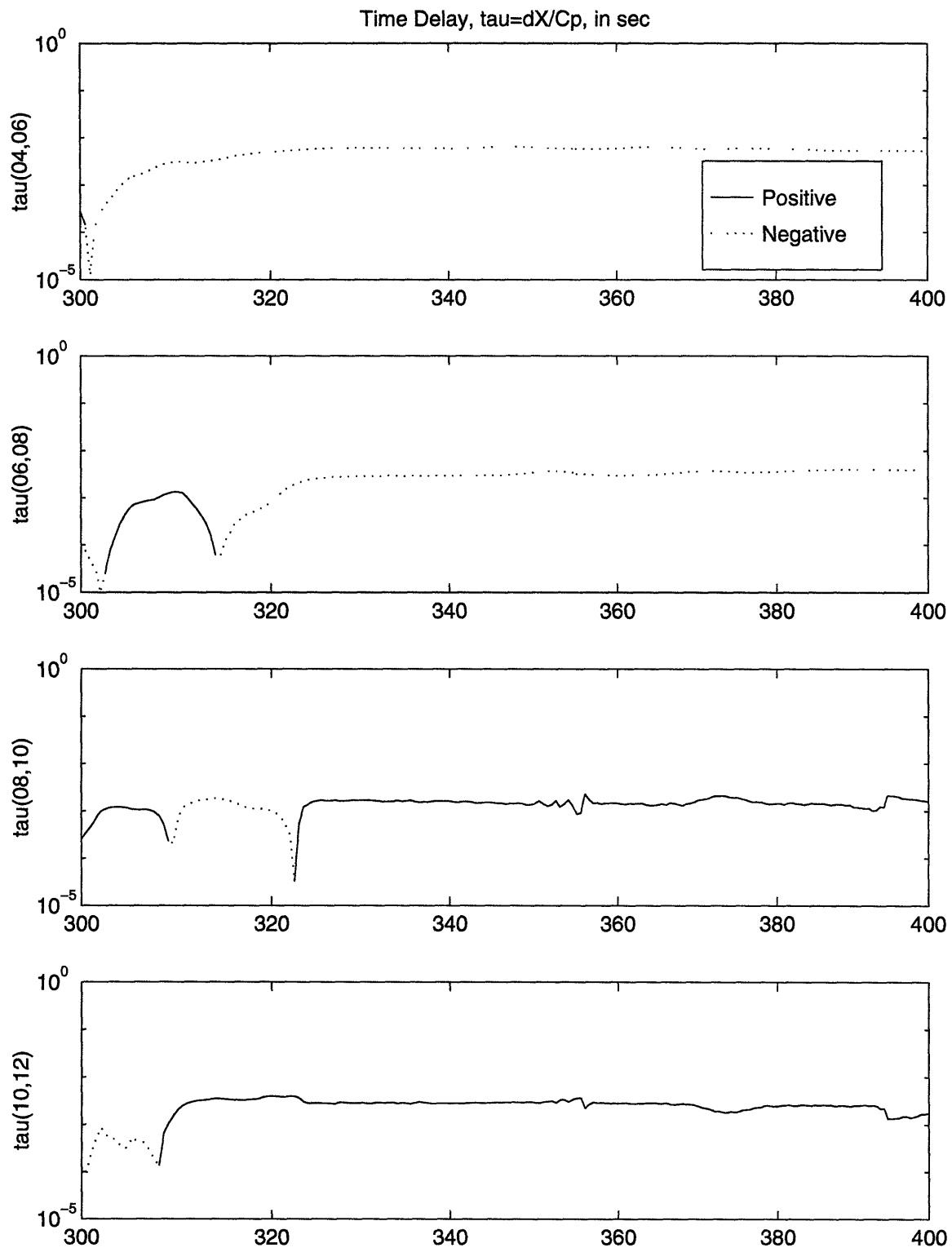


Figure 2-22: Extracted time delay between two adjacent joints as a function of frequency with  $\Delta f = 0.5 Hz$ .

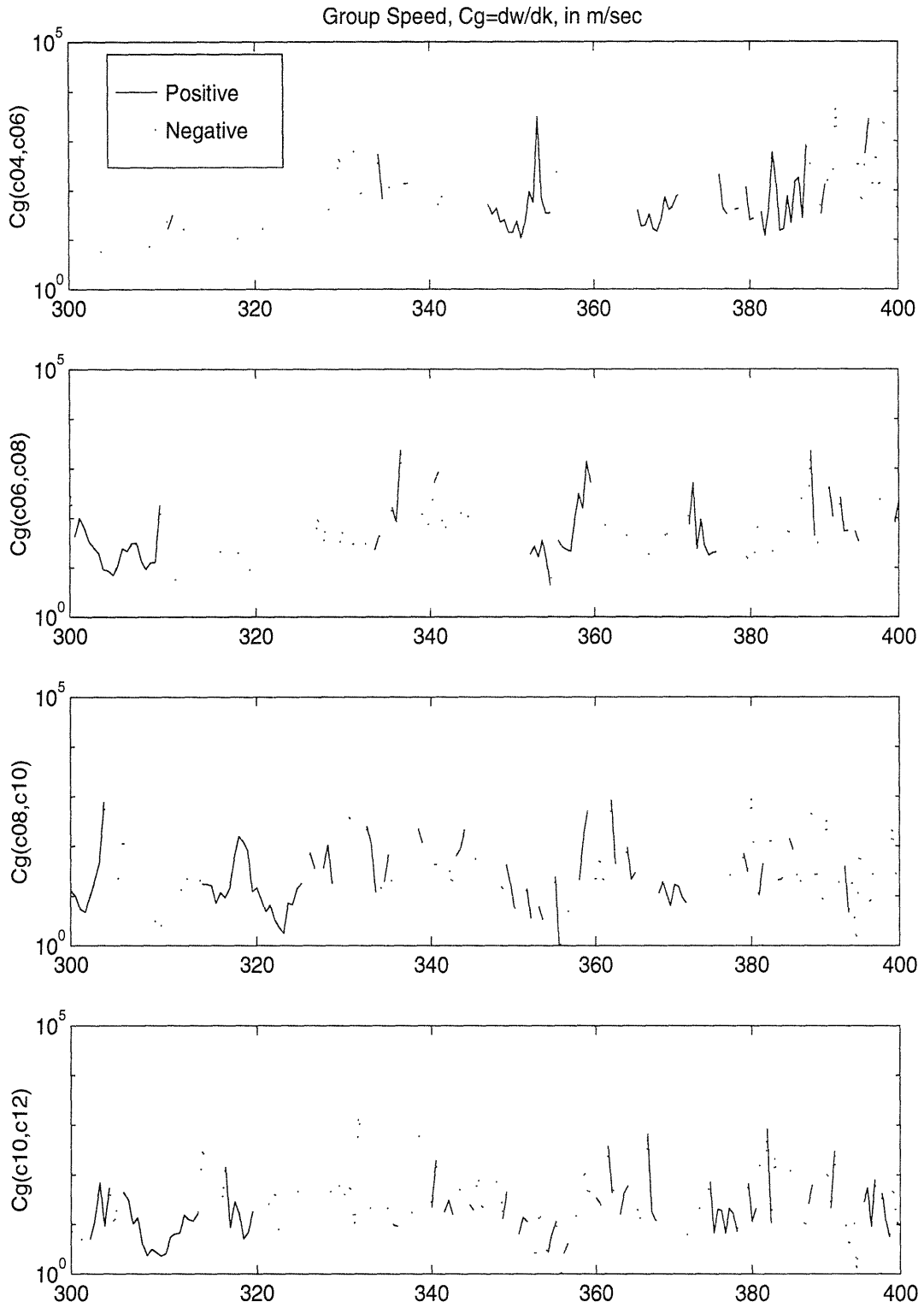


Figure 2-23: Extracted group speed between two adjacent joints as a function of frequency with  $\Delta f = 0.5 Hz$ .

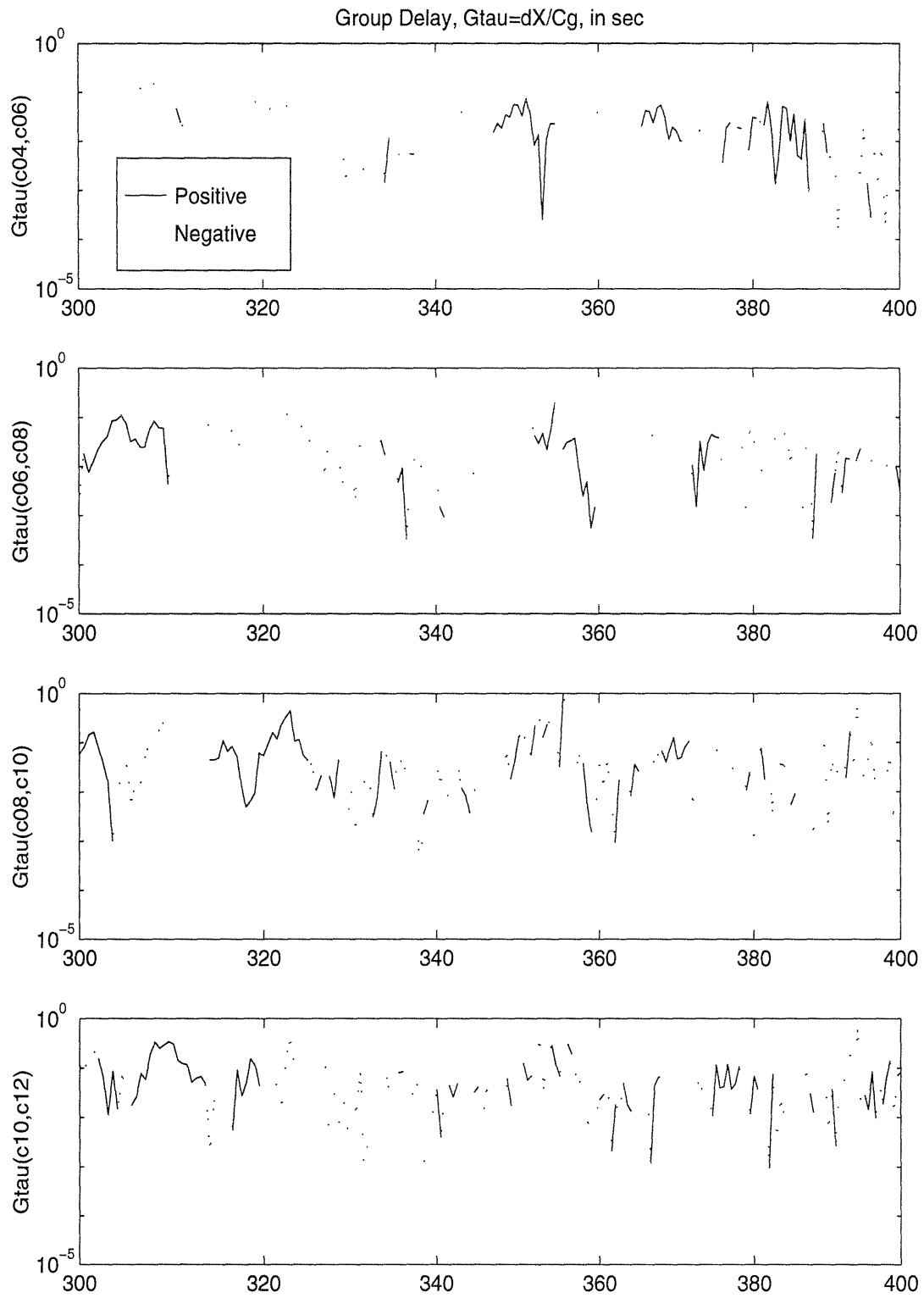


Figure 2-24: Extracted group delay between two adjacent joints as a function of frequency with  $\Delta f = 0.5 Hz$ .

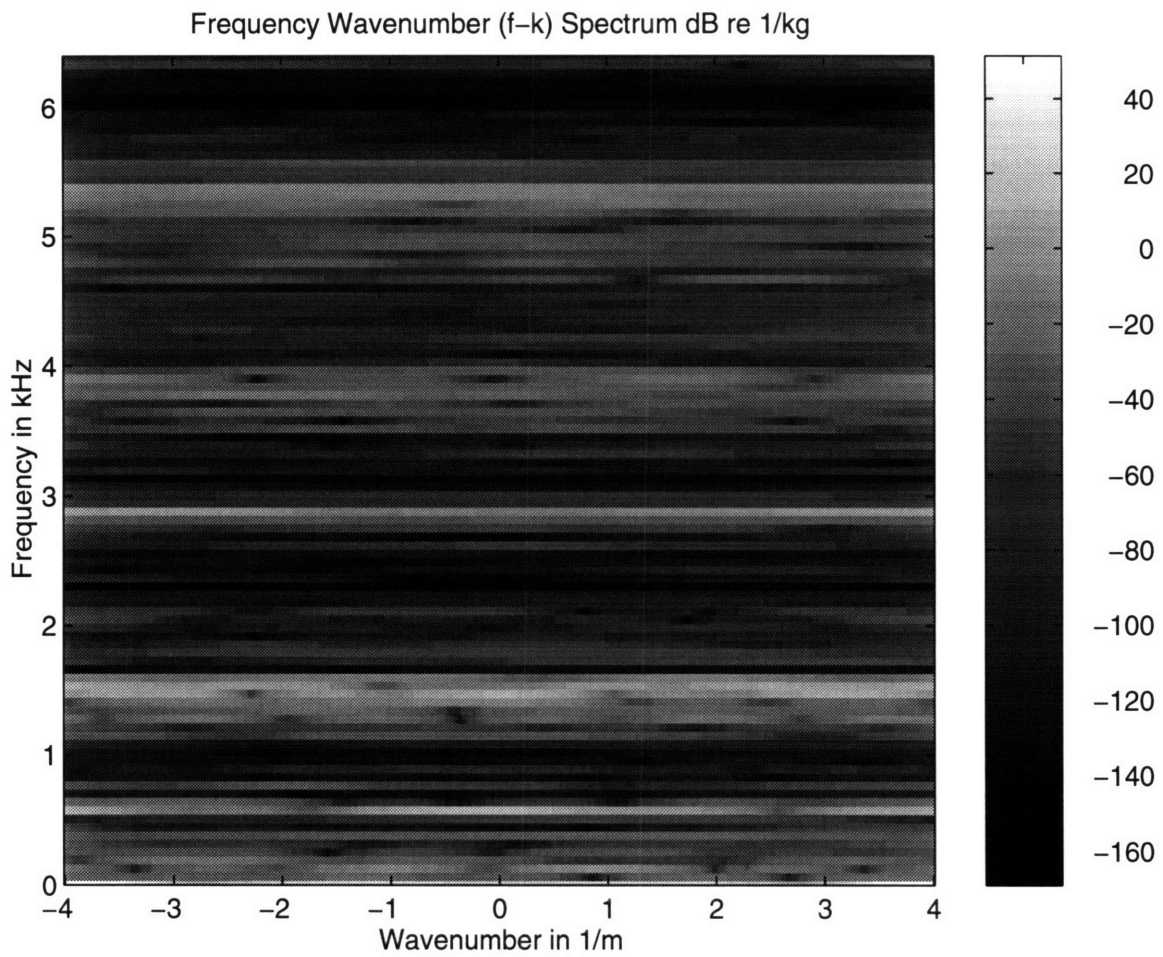


Figure 2-25: Frequency-wavenumber (f-k) spectrum of inertance ( $Z$  excitation) at the  $c$  joints with  $\Delta f = 2Hz$ .



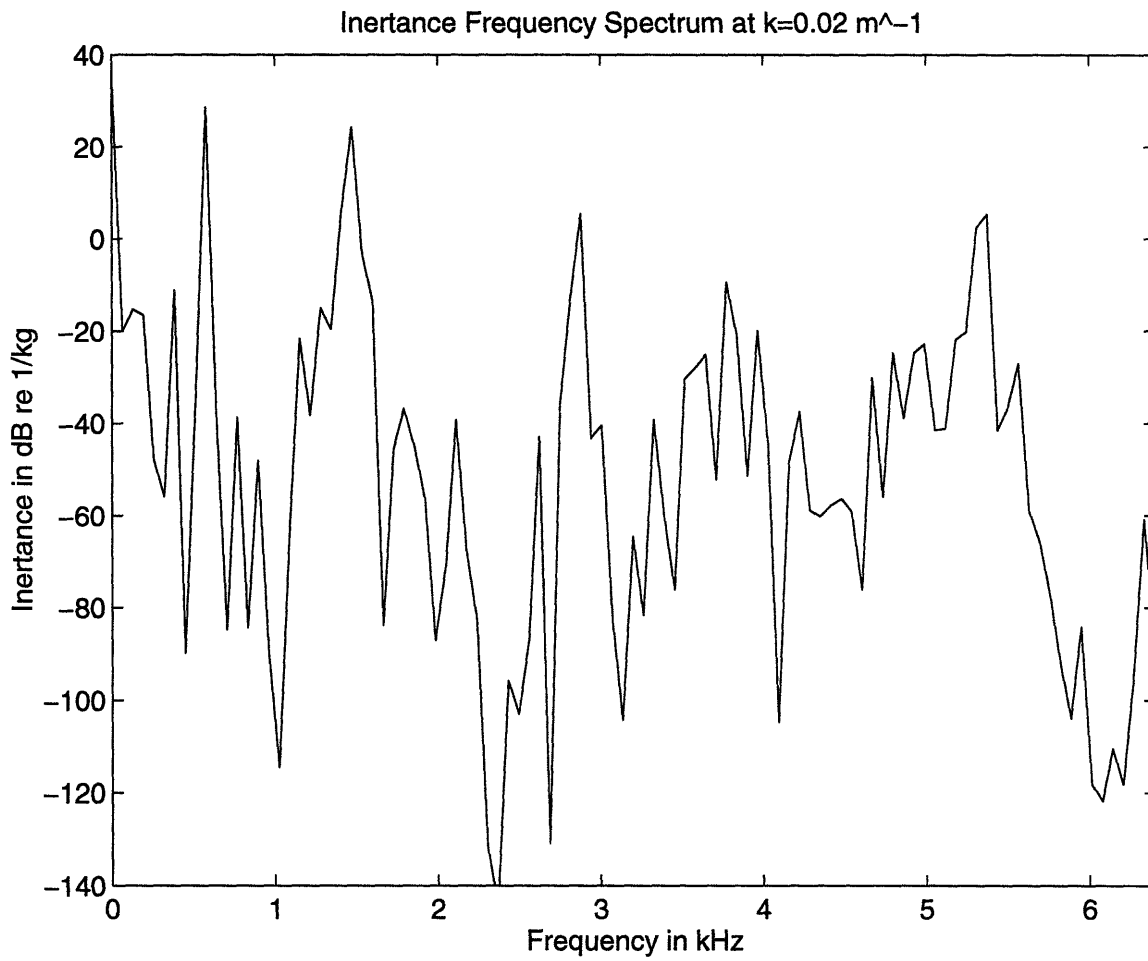


Figure 2-26: Cross section of inertance frequency-wavenumber spectrum at  $k = 0.02 \text{ m}^{-1}$ .

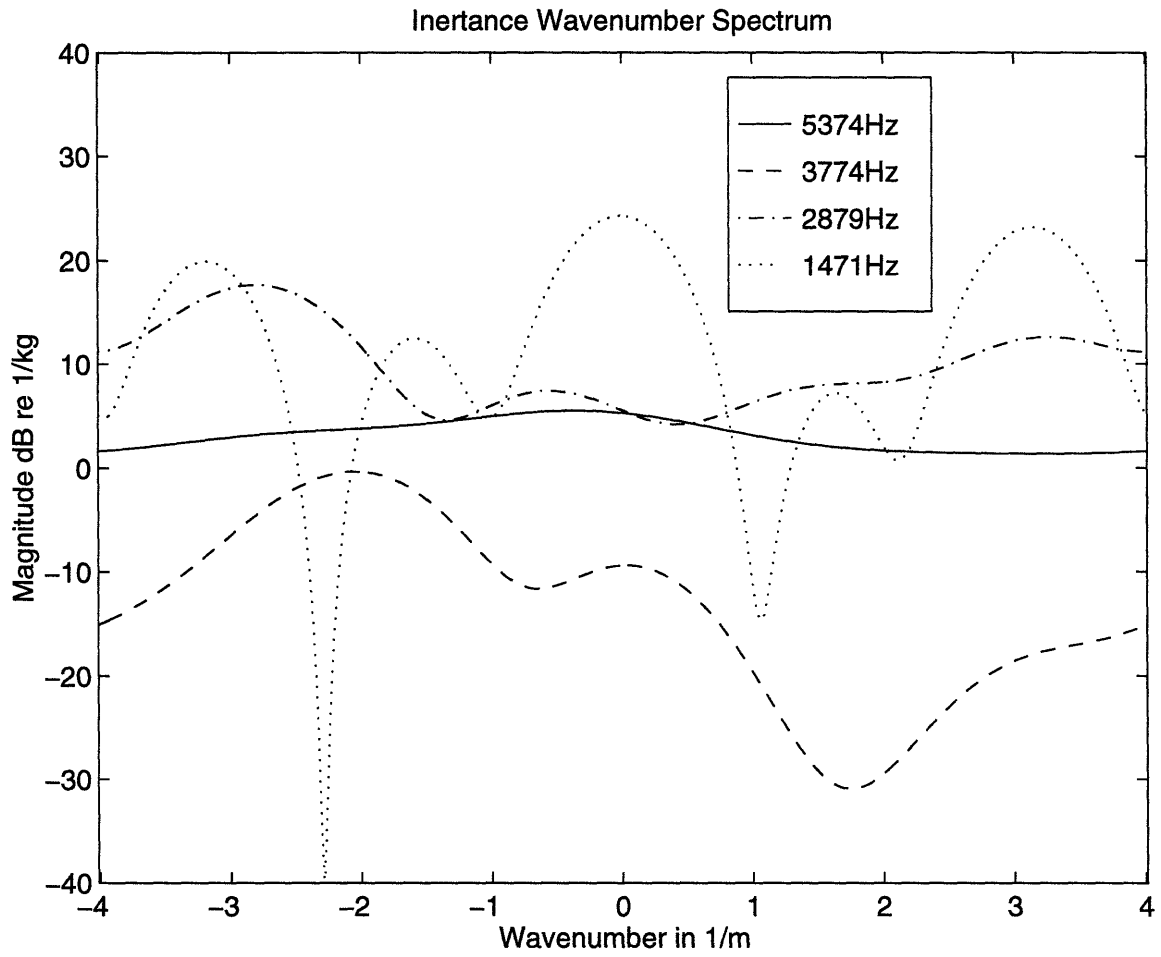


Figure 2-27: Inertance wavenumber spectrum of high inertance bands.

# Chapter 3

## Early Arrival Times of Elastic Waves

### 3.1 Bandpass Filtering

An early attempt to measure the arrival time was conducted by Heath[1] by using flexural wave speeds from the Euler-Bernoulli beam theory. However, the truss follows the Timoshenko beam theory with increasing frequency in flexural wave propagation, as shown by Machens and Dyer[3].

I measured the major early arrival times of elastic waves and compared with the calculated arrival time using the Timoshenko beam theory for the flexural wave. The application of the Timoshenko beam theory to the MIT truss case is discussed in Appendix A. A transient input signal is used instead of the stationary random signal to suppress unfavorable measurement of noise. I used impulse response functions rather than correlation to detect wave arrival since, in a multi-path problem, the resolution of the former is better than that of the latter. I deconvolved the source signal from the output signals to find the impulse response functions. Since the dispersive flexural wave propagation is included, a band-limited analysis is required.

However, two conflicts arise[16]:

- the need for a narrow-bandwidth analysis to confine dispersion within useful bounds.
- the need for a wide-bandwidth analysis to suppress overlapping of adjacent correlation peaks.

I used a Gaussian octave bandpass filter to reconcile these conflicts. A Gaussian bandpass filter in the signal amplitude can be expressed as

$$G(f) = \exp\left(-\frac{(f_o - |f|)^2}{2\sigma_f^2}\right) \quad (3.1)$$

where  $f_o$  is the center frequency at which  $G(f) = 1$ , and  $\sigma_f$  is a bandwidth parameter to make the magnitude of filter  $6dB$  down at the band edges[21]. The advantage of a Gaussian bandpass filter over a usual finite impulse response bandpass filter is the Gaussian filter's effective side lobe suppression due to the smallest possible duration-bandwidth product of a Gaussian pulse[22]. A Gaussian bandpass filter with the center frequency at  $16kHz$  and its impulse response are shown in Fig. 3-1.

I calculate the complex envelope of the impulse response function, since this is very convenient for looking at the arrival of energy at joints compared to a simple impulse response function[21].

## 3.2 Early Arrival Times

The calculated first arrival times with an assumption of no change of wave type are shown in Table 3.1. The group speed of the flexural wave of the Timoshenko beam theory is used since it is faster than the phase speed and the elastic wave field propagates with this group speed. At the *c04* joint, there are three possible paths from the source (*SRC*):  $SRC \rightarrow c04$ ,  $SRC \rightarrow a04 \rightarrow c04$ , and  $SRC \rightarrow c04 \rightarrow a04 \rightarrow c04$ . However, in reality the measured arrival time is longer than these calculated values

since the joints act as wave transformers, scattering from one strut to others, and from one wave type to the other two.

Table 3.1: The first arrival time of elastic waves with single wave type propagation.

Joint	Distance ( $m$ )	Arrival time ( $msec$ )				
		$T_{comp}$	$T_{tors}$	$T_{f16kHz}$	$T_{f8kHz}$	$T_{f4kHz}$
c04	0.545	0.11	0.18	0.26	0.32	0.42
c06	1.125	0.22	0.36	0.53	0.66	0.86
c08	2.090	0.41	0.67	0.99	1.22	1.60
c10	3.061	0.60	0.99	1.45	1.79	2.34
c12	4.031	0.79	1.30	1.90	2.35	3.08

The input signal used in the experiment is not an ideal impulse but generated from two signal generators. Thus its behavior has some disadvantages for direct application of conventional finite impulse response (FIR) filters. Fig. 3-2 shows the characteristics of the input signal and it clearly shows limits of realization of an ideal impulse in my experiment. Its disadvantages are difficulties in matched filter calculations due to the long tail of the input signal, and wide side-lobes in the frequency domain.

I lowpass filtered the impulse response functions with a cut-off frequency of  $f_c = 25.6kHz$  to avoid aliasing, since the sampling frequency of the data acquisition system is  $65,536Hz$ . A FIR filter is applied due to phase distortion concerns. The frequency response function of this FIR filter is shown in Fig. 3-3, and the lowpass filtered impulse response functions with full time length, and up to  $5msec$ , are shown in Fig. 3-4 and Fig. 3-5 respectively. These two figures show the time delay of the energy arrival at each joint.

Fig. 3-5 clearly shows the long tail of the input signal (at *SRC*), and this is due to the anomaly of the applied input compared to an ideal impulse. Thus it is difficult to get bandpass filtered impulse response functions with low side lobes by using FIR bandpass filters. The lowpass filtered impulse response functions at the joints are difficult to interpret since all dispersive waves with different group speeds are mixed in these plots.

To mitigate the foregoing difficulties, Gaussian octave bandpass filtered impulse response functions with complex envelop representation are used to plot the impulse response functions. A Gaussian octave bandpass filter has advantages such as low side-lobe levels, and a complex envelope representation makes easy observation of the arrival trend, since there is no oscillating temporal pattern.

Gaussian octave bandpass filtered impulse response functions with the center frequency of  $16kHz$ ,  $8kHz$ ,  $4kHz$ ,  $2kHz$ ,  $1kHz$ ,  $0.5kHz$ ,  $0.25kHz$ , and  $0.125kHz$  are shown in Fig. 3-6, Fig. 3-7, Fig. 3-8, Fig. 3-9, Fig. 3-10, Fig. 3-11, Fig. 3-12, and Fig. 3-13 respectively. For the  $16kHz$  octave band impulse response function, it is easy to look at the energy arrival and decay at each joint, compared to the lowpass filtered impulse response functions. One sees an initial rise of the energy, a peak reached later in time with increasing distance of the joint from the source, and finally a slow or gradual decay. This pattern is observed from the  $16kHz$  to the  $2kHz$  octave band. However, below the  $2kHz$  octave band it is hard to find these trends, and this is due to the bandwidth conflict of the dispersive flexural wave propagation and the global behavior of the truss in the low frequency region.

The Gaussian octave bandpass filtered impulse response functions with center frequency of  $16kHz$ ,  $8kHz$ , and  $4kHz$  are shown as a function of time, up to  $5msec$ , in Fig.3-14, Fig.3-15, and Fig.3-16 respectively. The  $16kHz$  and  $8kHz$  octave band impulse response functions show the major early arrivals of each wave packet more clearly compared to that of the  $4kHz$  octave band impulse response function. It is harder to find the wave packet arrivals in the latter because the Gaussian resolution, as seen at the source, is too wide to resolve individual paths.

Table 3.2, Table 3.3, and Table 3.4 summarize all possible candidates of the major early arrival times calculated for the shortest path, including all combinations of the possible elastic waves based on Fig.3-14, Fig.3-15, and Fig.3-16, and they are plotted in these figures with 'o' symbols. The  $16kHz$  and  $8kHz$  octave band impulse response functions show good agreement with the predicted values. See, for example, the second arrival at joint c04 in the  $8kHz$  Gaussian octave band (Fig.3-15), and

the predicted value in Table 3.3 for the same joint. This agreement comes from the assumption of a combination of the torsional and the flexural wave. But, it is hard to find agreements in the  $4kHz$  octave band impulse response except for the first arrival at each joint. It seems that the compressional waves are dominant first arrivals, and the flexural waves are dominant at the later arrivals. However, there is no specific preference in elastic wave type distribution during the early arrival times except for the above properties.

The major early arrival times for the three highest octave bands are shown in Fig. 3-17 with the shortest path as the  $X$  axis. The dotted lines are linear regressions of the first arrival time at each joint. It shows that there is a linear relationship of the early arrival times with increasing octave band. At the  $16kHz$  octave band the arrival times at each joint have approximately constant group delay. This means the dispersive flexural wave is not the dominant first arrival of energy. However, this trend disappears with decreasing frequency and at the  $4kHz$  octave band the arrival trend does not have constant group delay. From these plots the group speeds of the first arrivals are approximately  $3450m/sec$ ,  $3140m/sec$ , and  $2980m/sec$  for the  $16kHz$ ,  $8kHz$ , and  $4kHz$  Gaussian octave band respectively. Apparently these speeds are slower than the compressional wave speed in the aluminum struts ( $5092m/sec$ ) and this is because a pure compressional wave cannot be propagated from the source to the observation point (see Table 3.2).

This figure is re-plotted with the axial distance as the  $X$  axis in Fig. 3-18. Again the dotted lines are linear regressions of the first arrival times. The offsets at the distance of zero are due to the time delays of energy arrival from the source location since the first joint has the same axial location as the source. The wave speeds of the first arrivals in this plot are  $3120m/sec$ ,  $2950m/sec$ , and  $2830m/sec$  for the  $16kHz$ ,  $8kHz$ , and  $4kHz$  Gaussian octave band respectively.

Theoretically, if pure compressional wave propagation exists through the shortest path, the observed axial wave speed via these joints becomes  $C_{comp}/\sqrt{2} = 3600m/sec$ , since the bottom of each cell of the truss is a square and the length between the two

adjacent joints is  $\sqrt{2}$  times longer than a side of the bottom square. However, the extracted wave speeds of the first arrivals are slower than this wave speed through the virtual beam. This is due to the wave bearing characteristics of the truss.

The group delay in Fig. 3-18 does not agree with that in Fig. 2-17 and Fig. 2-24. This can be easily shown by comparing the arrival times at the farthest joint in Fig. 3-18. All of them are less than  $3msec$ , which are less than the results in Chapter 2. This is so because a time frame length of  $0.125sec$  was used in time domain experiment to mitigate noise, overlap, and reverberation.

The decay rates of the elastic waves in Fig. 3-6, Fig. 3-7, and Fig. 3-8 look constant and invariant with position. From these figures it is clear that the decay is not single, but double: one with large decay rate and the other with small decay rate. To investigate this, the decay rate of the total elastic wave field is extracted from the Gaussian bandpass filtered impulse response functions, assuming exponential decay of the energy,  $E(t)$ ,

$$E(t) = E_0 e^{-\eta_0(\omega)t} + E_1 e^{-\eta_1(\omega)t}, \quad (3.2)$$

where  $\omega$  is angular frequency and  $\eta_0(\omega)$  and  $\eta_1(\omega)$  are the two temporal decay rates, which are functions of frequency. I define  $\eta_0$  as the steeper temporal decay rate and  $\eta_1$  as the smaller temporal decay rate. Since the energy in the truss is coupled, it is natural that the number of decay rates can be more than one.

Fig. 3-19, Fig. 3-20, and Fig. 3-21 show Gaussian bandpass filtered impulse response functions and their least square fitted curves, following equation Eq. (3.2), at each joint of the truss with the center frequency at  $16kHz$ ,  $8kHz$  and  $4kHz$  respectively. Fig. 3-22 shows two decay rates as a function of the shortest path with three Gaussian octave bands. These figures show that the steeper decay rate,  $\eta_0$ , increases with increasing frequency and becomes flatter with decreasing frequency. The second decay rate,  $\eta_1$ , is smaller than the major decay rate, and decreases with increasing frequency. This decay rate,  $\eta_1$ , is, with a few exceptions, approximately invariant with position. The two decay rates in different octave bands at the joints are shown in Table 3.5. From this table it is clear that there is no constant exponential energy



decay rate of the truss for the transient case.

The temporal patterns of Fig. 3-19 to Fig. 3-22 have many significant properties. First, it takes time for the truss to reach its early multipath build up, from 0 to about  $10msec$ , roughly linear with increasing axial distance of the measurement from the location of the source. This is so for each of the 16, 8,  $4kHz$  Gaussian octave bands. (The build up delay is not in the model of Eq. (3.2).) Note that this delay corresponds to some sort of average speed of about  $400m/sec$  for the shortest paths in the truss. The average arrival time at joint  $c12$  with all the possible early arrivals is calculated from Table 3.2, Table 3.3, and Table 3.4 and it is about  $1.6msec$ . This may be interpreted such that the maximum energy build up is reached after the waves reverberate about 6 times the total shortest path length in the truss; thus the mean-free-path of energy build up in the truss is 6 times the total shortest path length in the truss[19].

Second, the transition in Eq. (3.2) from the  $\eta_0$  to the  $\eta_1$  decay rate is at about  $45\sim 50msec$  in the  $16kHz$  band,  $60\sim 70msec$  in the  $8kHz$  band, and  $60\sim 85msec$  in the  $4kHz$  band. The mean time to transition in all bands, and for measurements at all joint locations, is about  $60msec$ . This may be interpreted such that the mean-free-path of energy decay is also about 6 times the total shortest path length in the truss; that is, the waves reverberate 6 times the truss length to reach equilibrium with the absorption processes in the truss, before reaching the final state of the slow decay rate  $\eta_1$ . However, this is not as robust as the first result, since decay rates depend on frequency. The energy build up and decay processes in the truss are schematically shown Fig. 3-23. Energy build up is an elastic process, whereas energy decay is a loss process which depends on frequency.

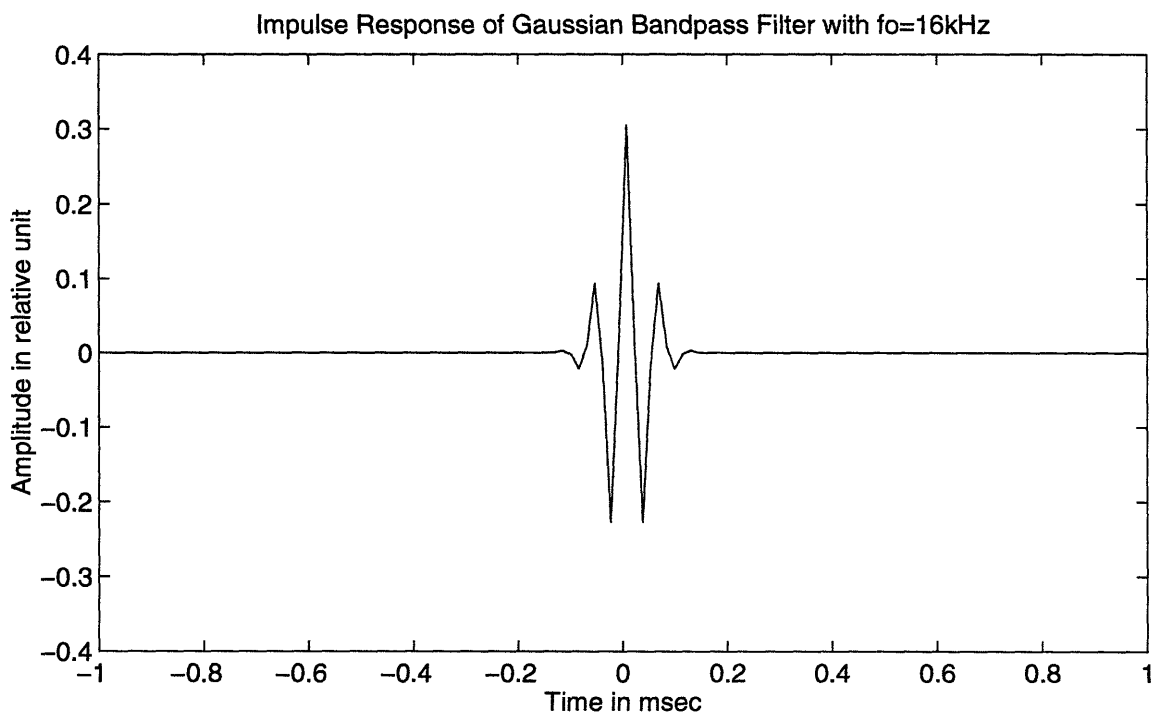
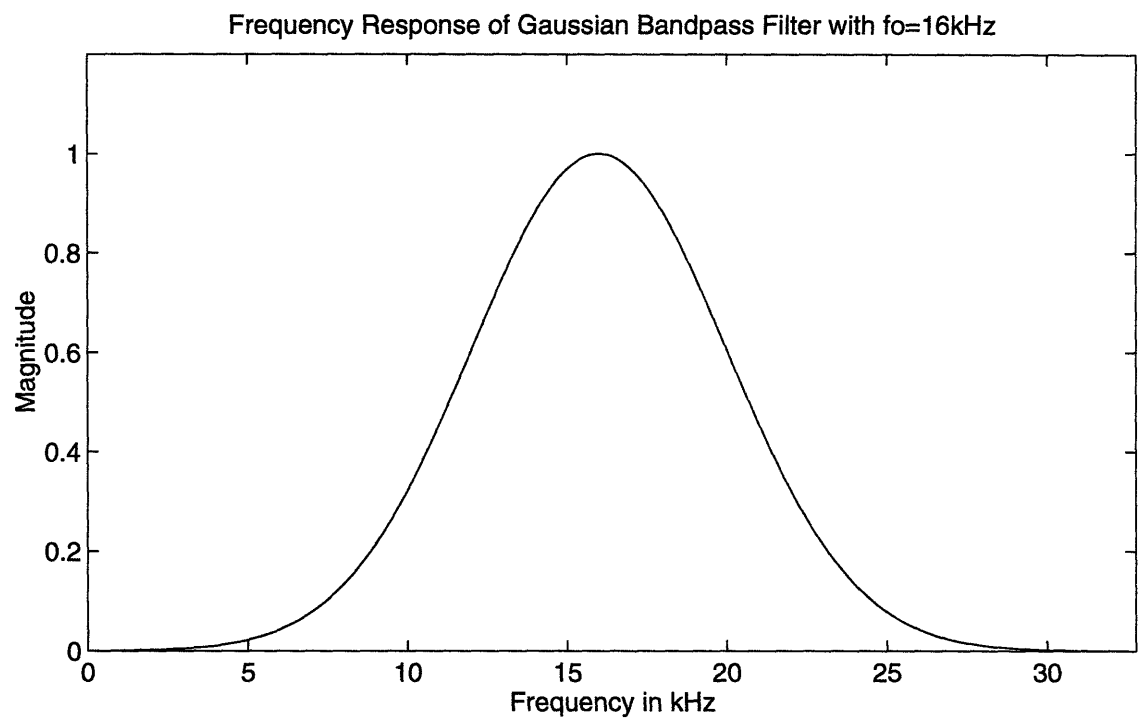


Figure 3-1: Frequency response (top) and impulse response (bottom) of Gaussian bandpass filter.

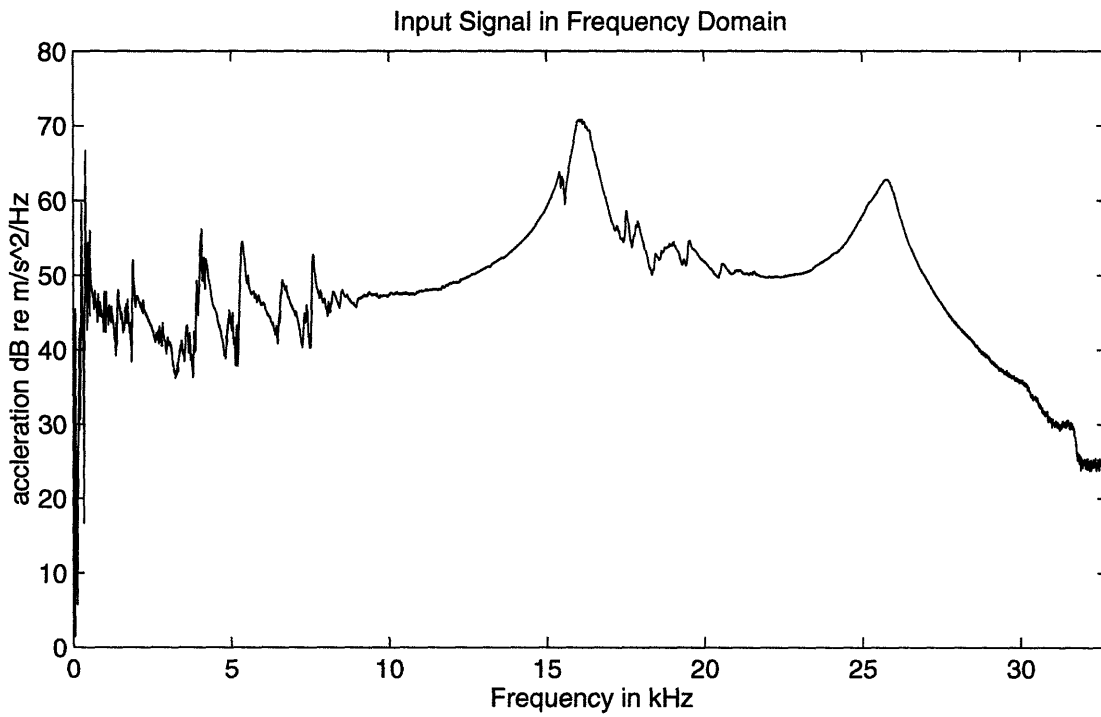
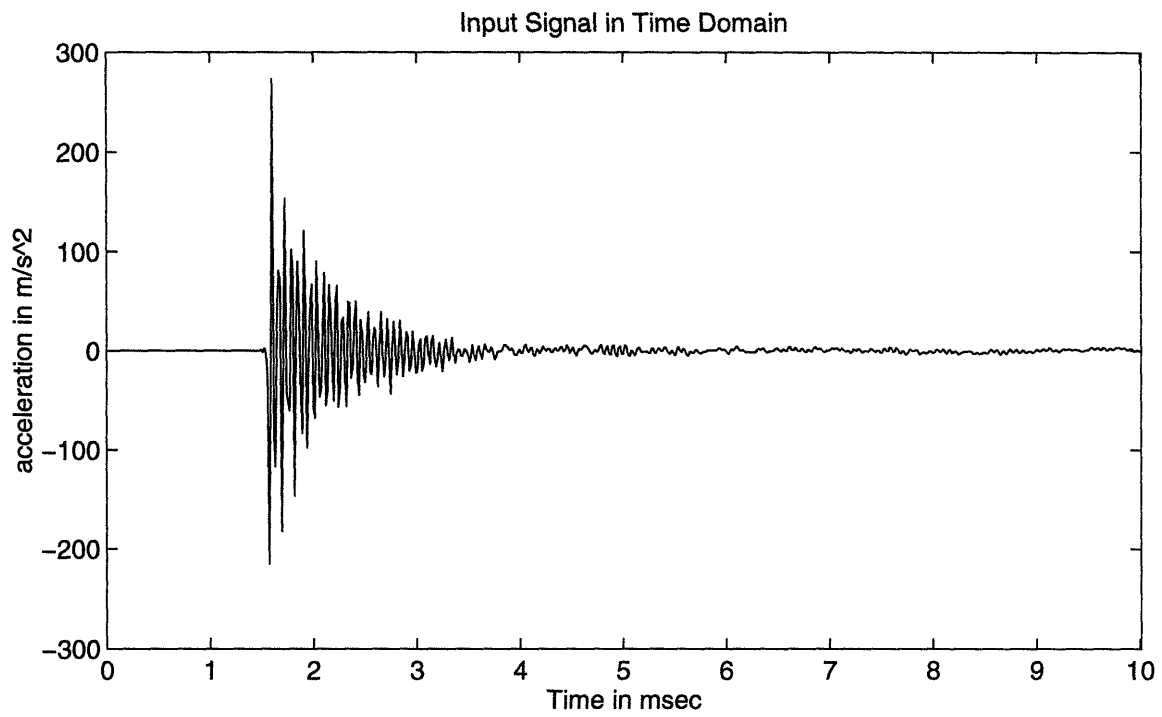


Figure 3-2: Characteristics of the input signal.

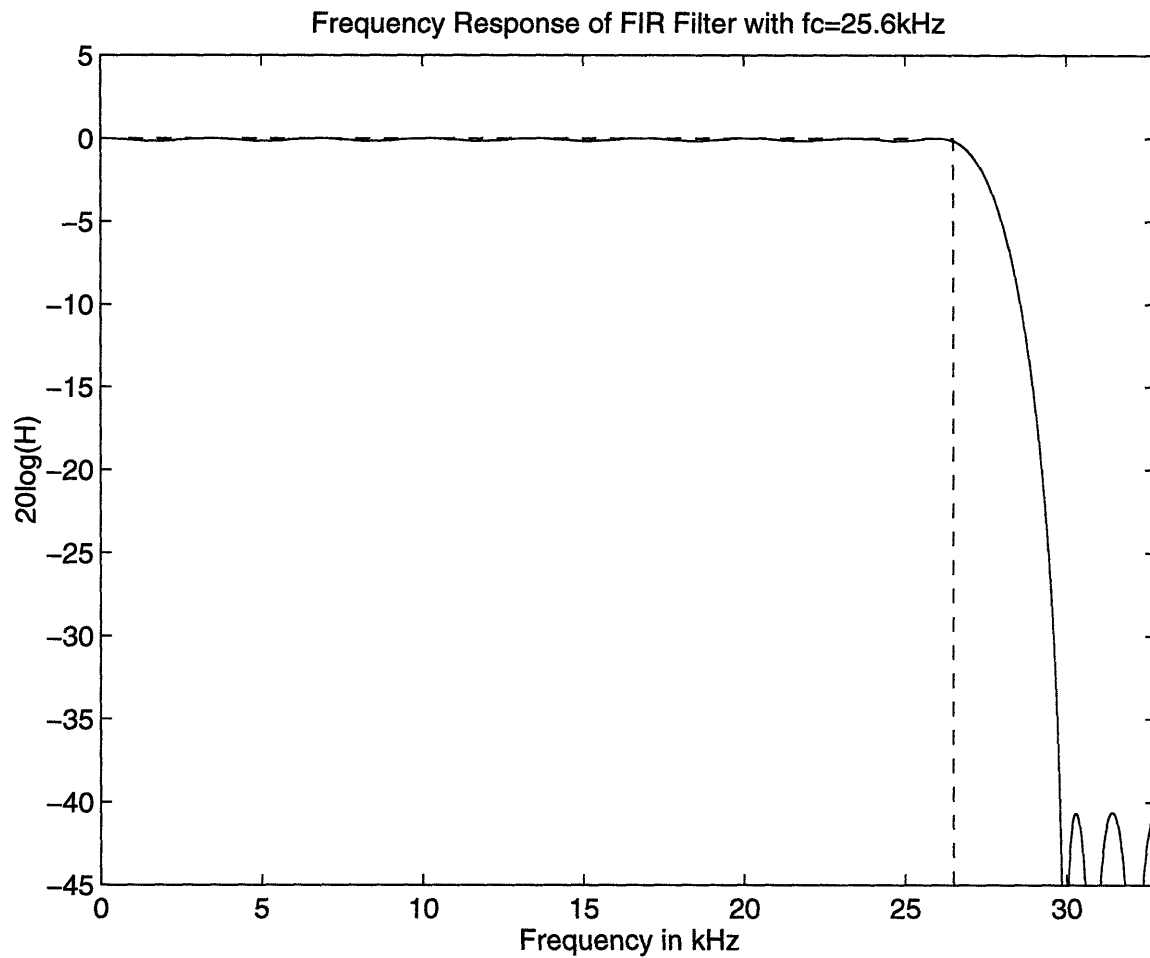


Figure 3-3: Frequency response of FIR lowpass filter with cut-off frequency  $f_c = 25.6\text{kHz}$  (solid) and rectangular lowpass filter (dashed).

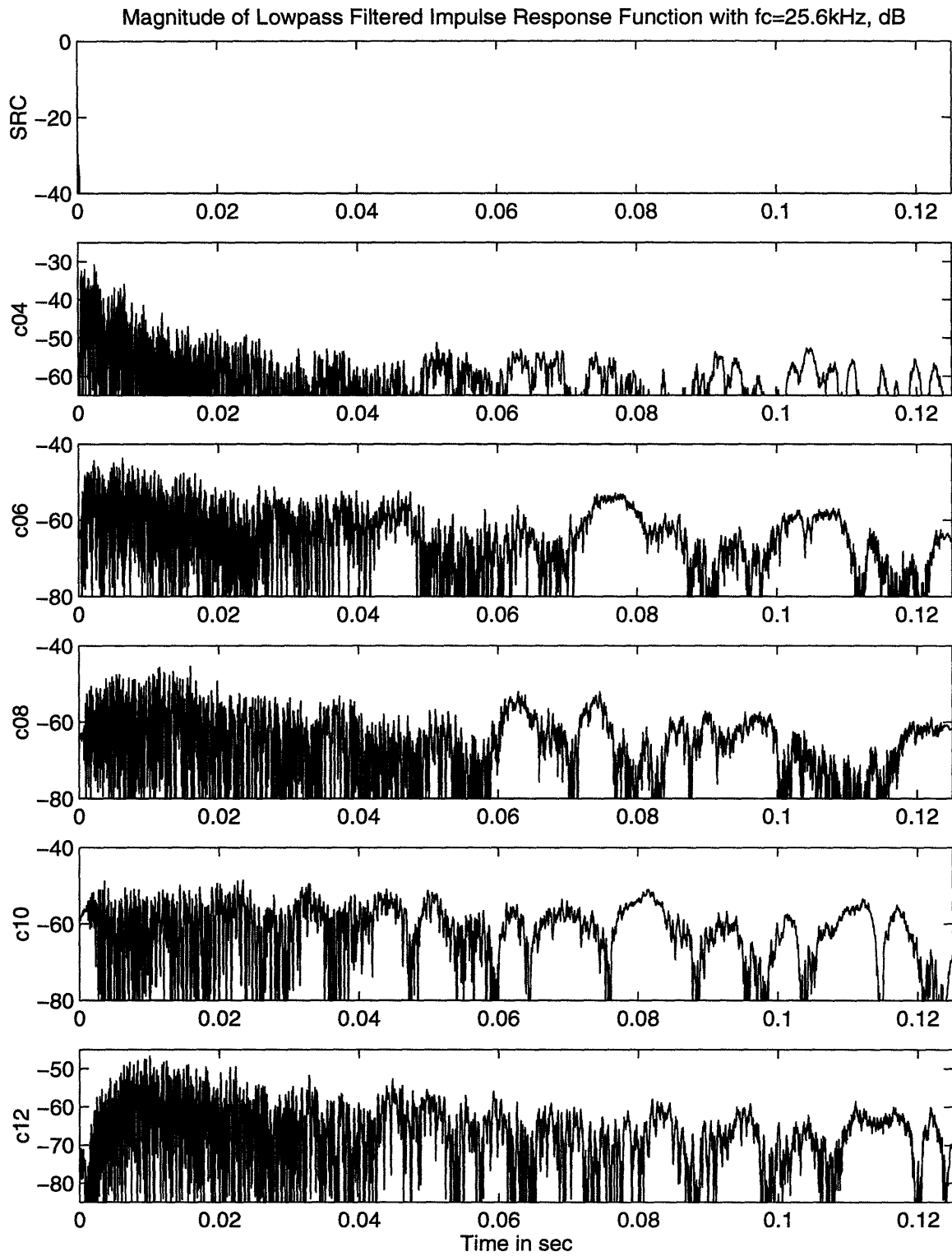


Figure 3-4: Magnitude of lowpass filtered impulse response function from 0 to 0.125sec with  $f_c = 25.6\text{kHz}$ .

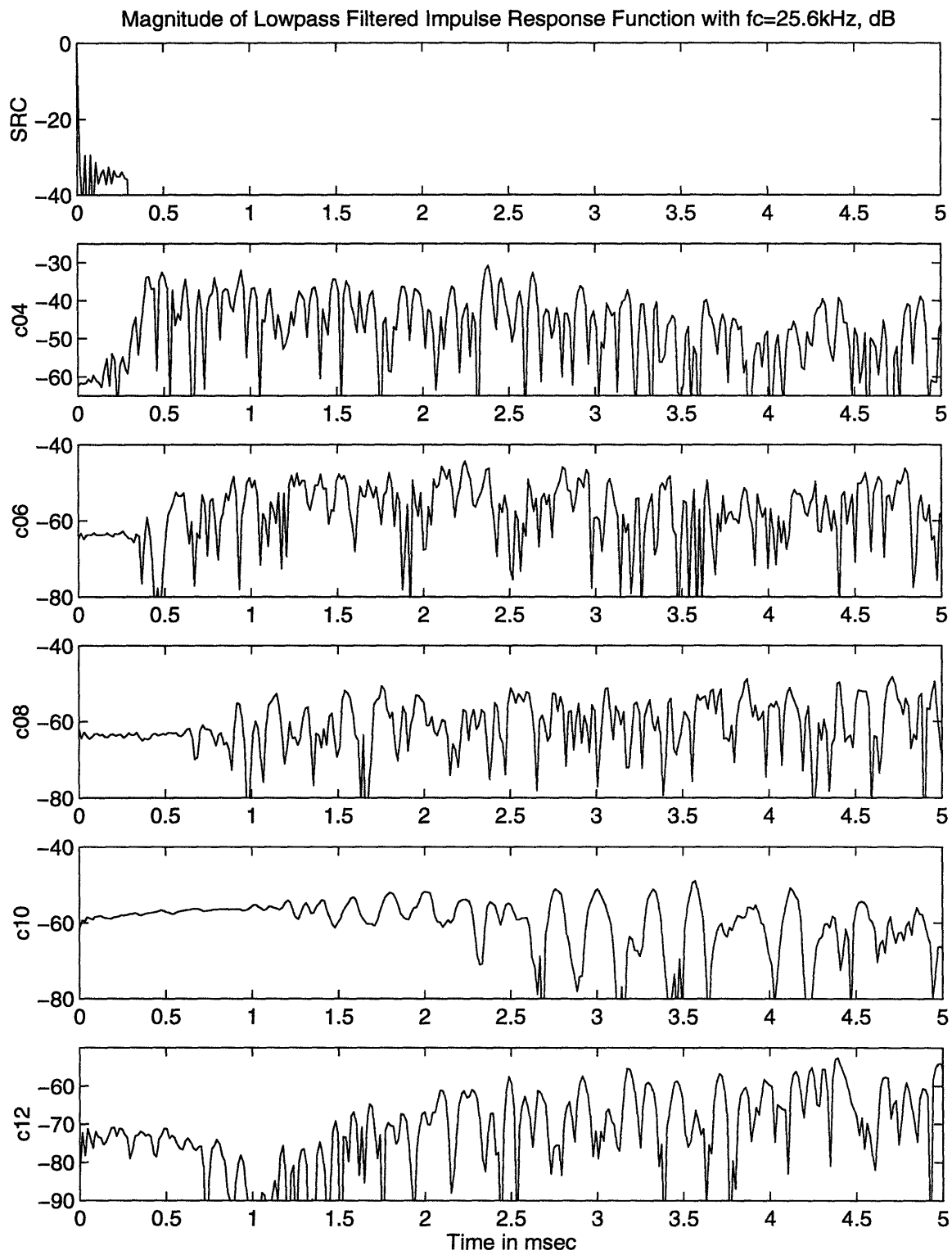


Figure 3-5: Magnitude of lowpass filtered impulse response function from 0 to 5msec with  $f_c = 25.6kHz$ .

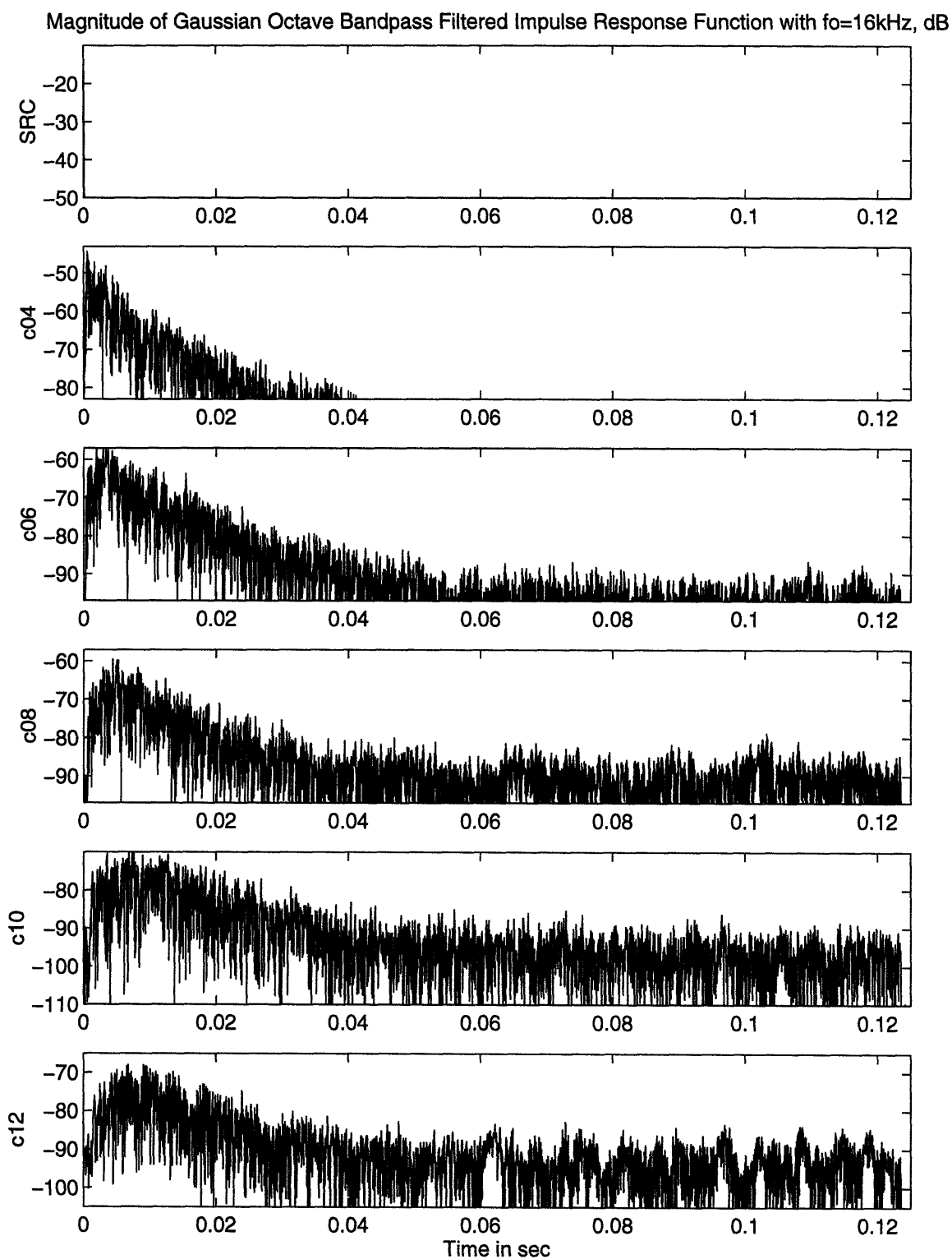


Figure 3-6: Magnitude of Gaussian octave bandpass filtered impulse response function from 0 to 0.125sec with center frequency of  $f_o = 16\text{kHz}$ .

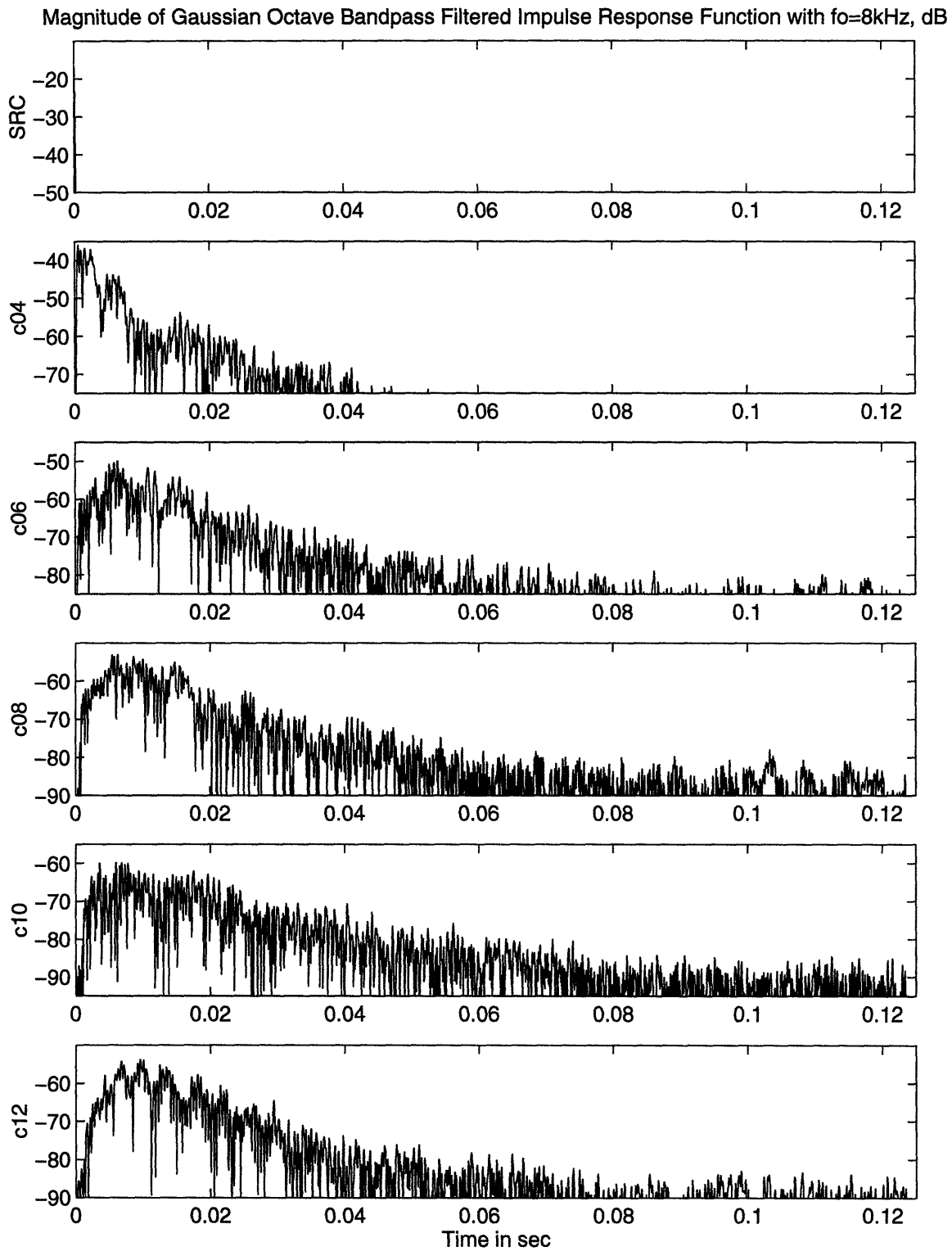


Figure 3-7: Magnitude of Gaussian octave bandpass filtered impulse response function from 0 to 0.125sec with  $f_o = 8\text{kHz}$ .



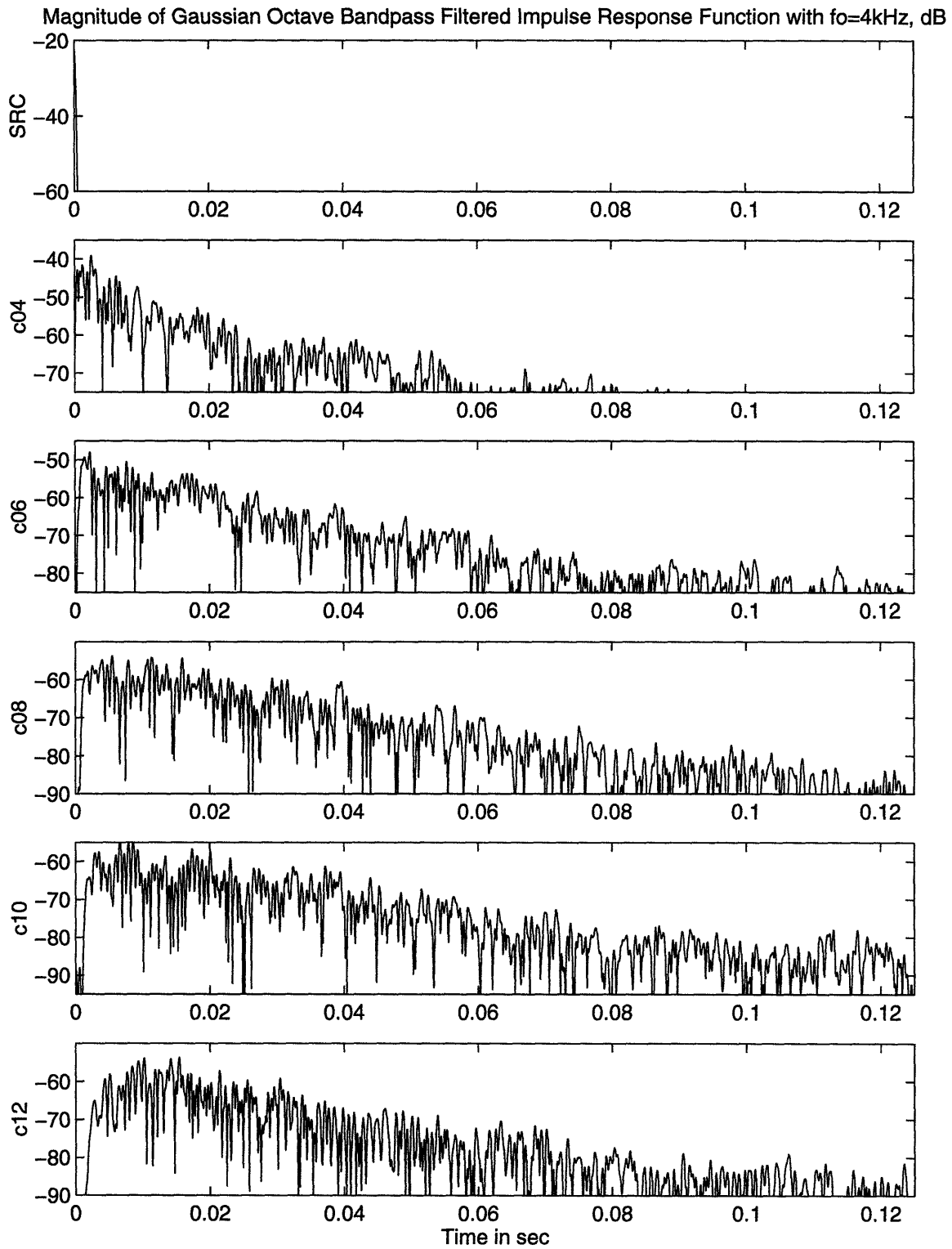


Figure 3-8: Magnitude of Gaussian octave bandpass filtered impulse response function from 0 to 0.125sec with  $f_o = 4\text{kHz}$ .

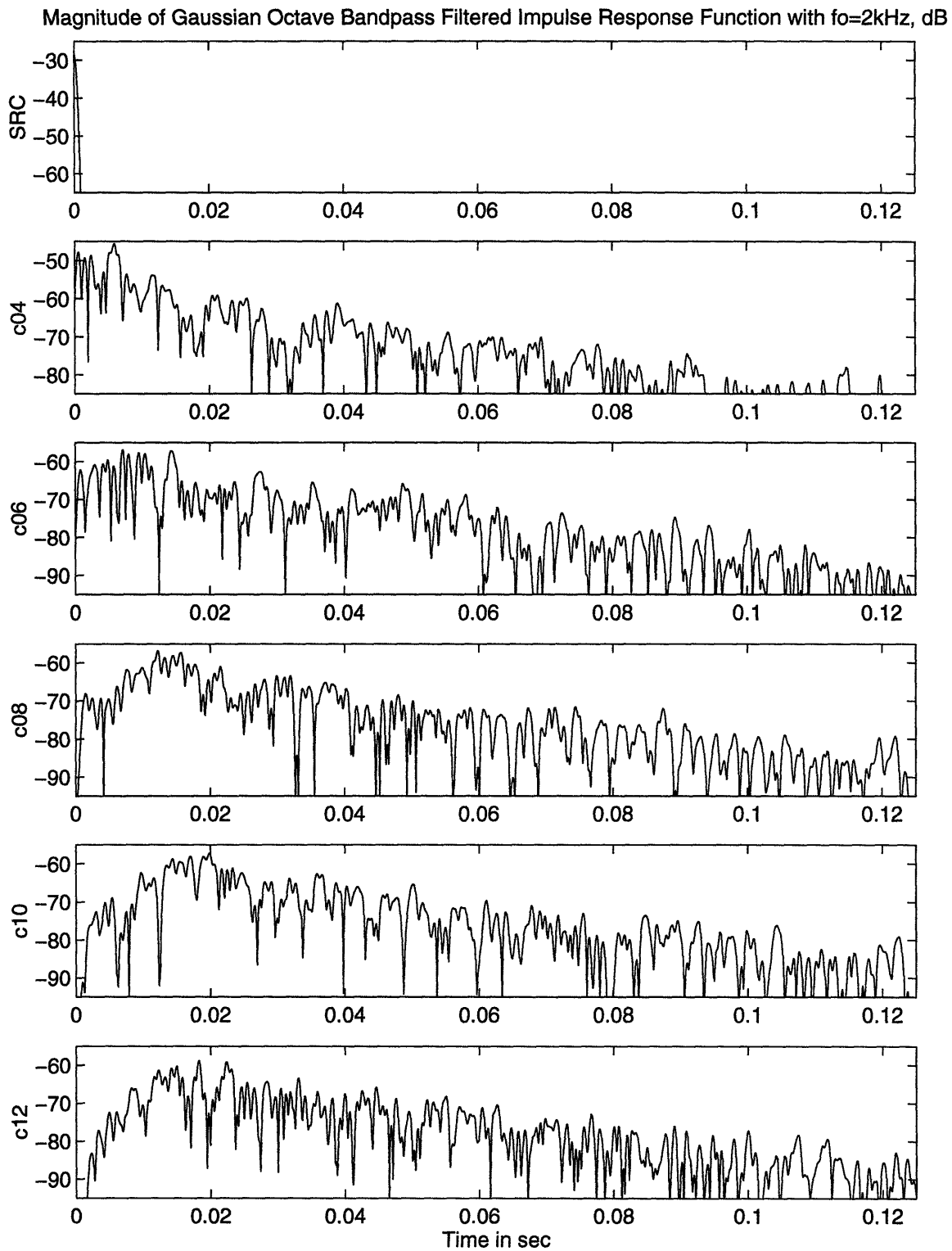


Figure 3-9: Magnitude of Gaussian octave bandpass filtered impulse response function from 0 to 0.125sec with  $f_o = 2\text{kHz}$ .

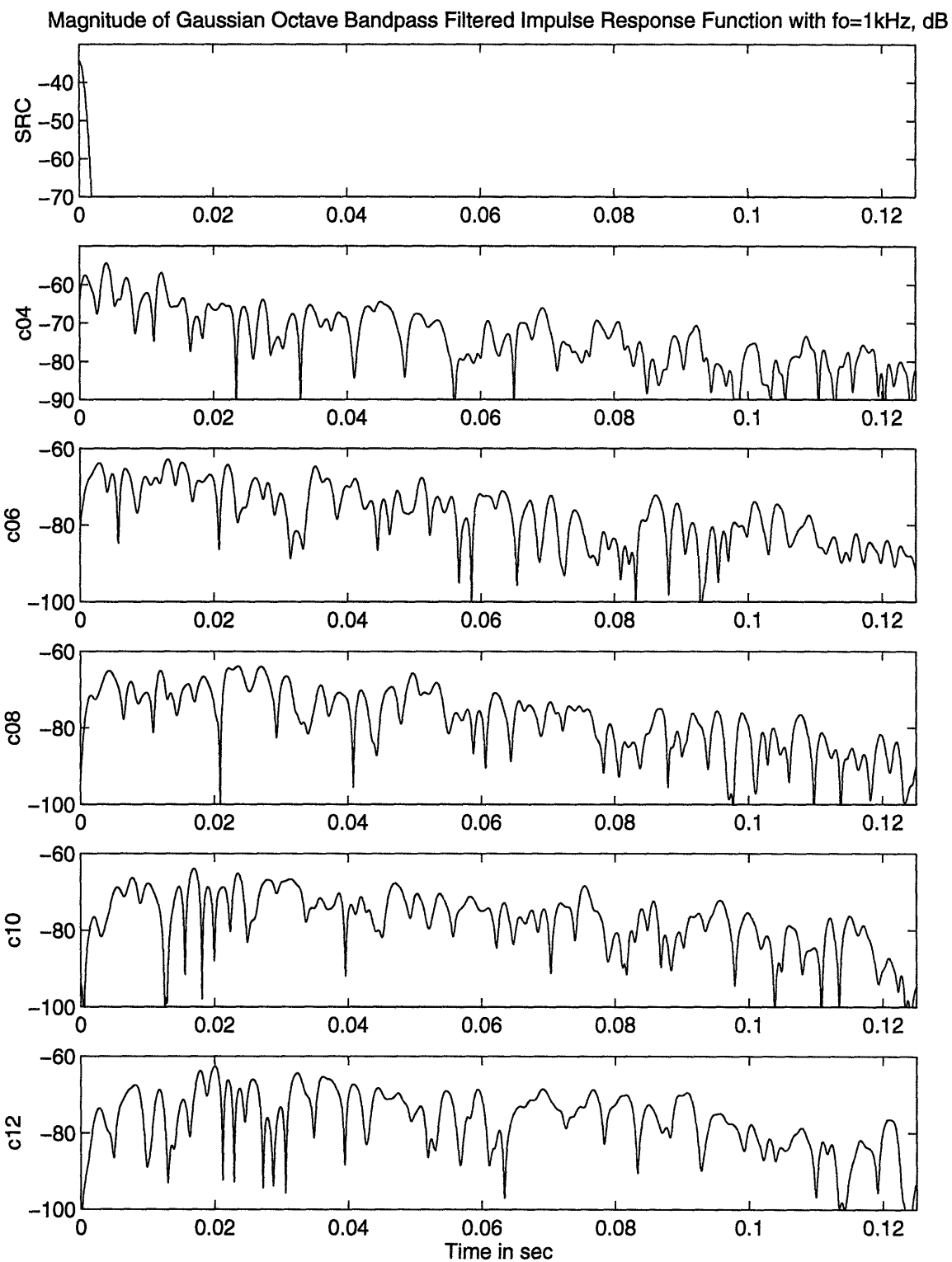


Figure 3-10: Magnitude of Gaussian octave bandpass filtered impulse response function from 0 to 0.125sec with  $f_o = 1\text{kHz}$ .

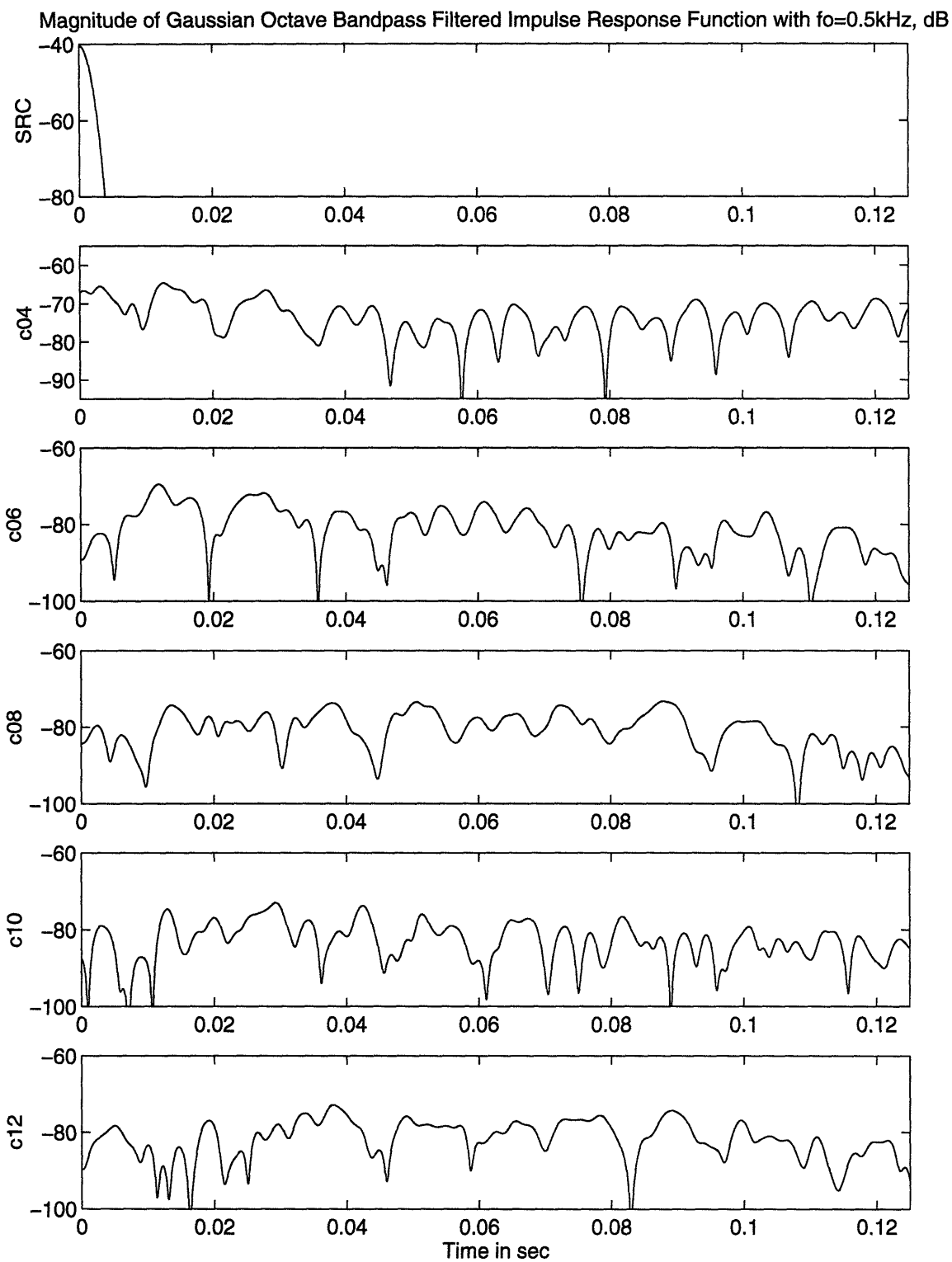


Figure 3-11: Magnitude of Gaussian octave bandpass filtered impulse response function from 0 to 0.125sec with  $f_o = 0.5\text{kHz}$ .

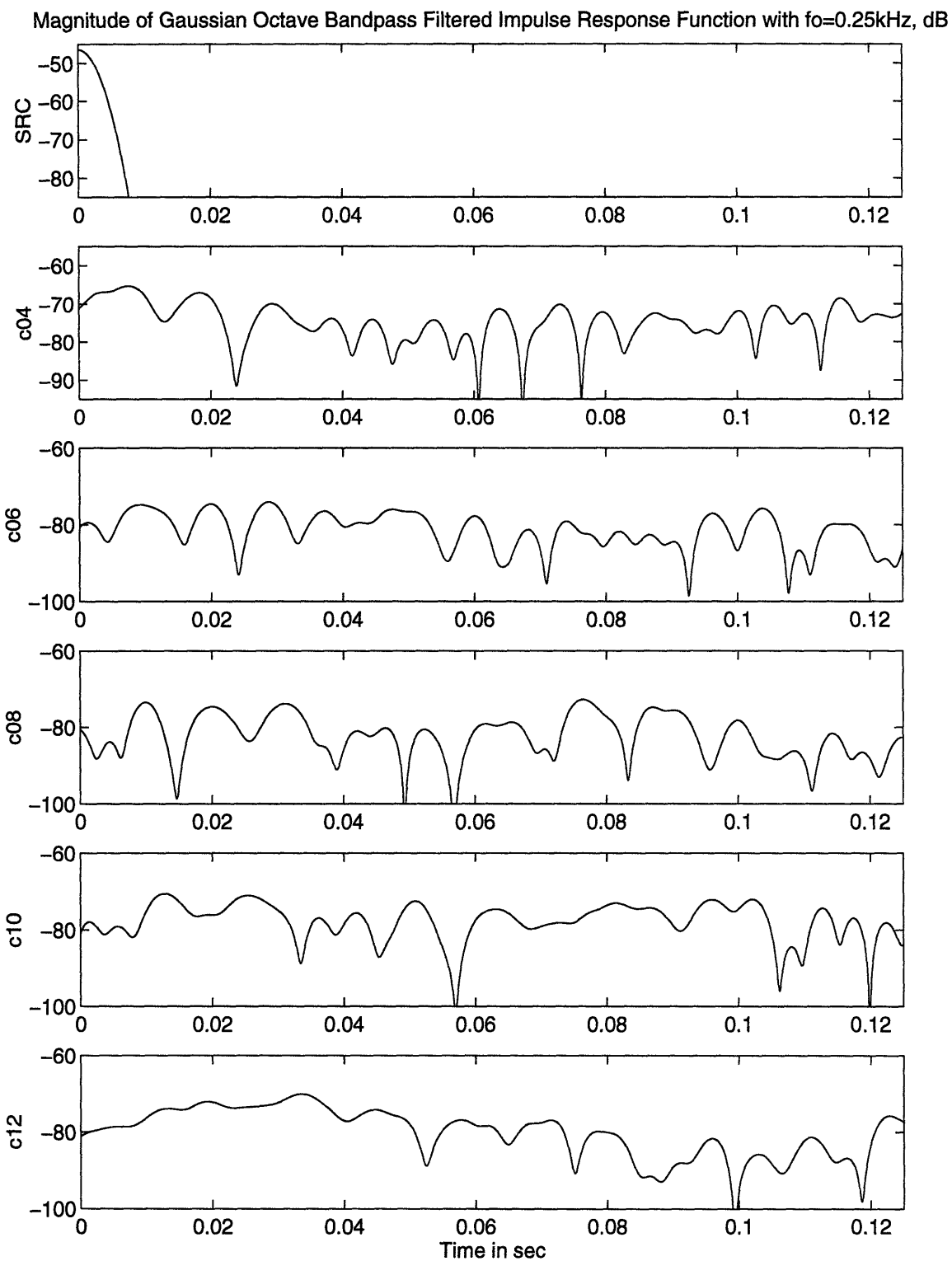


Figure 3-12: Magnitude of Gaussian octave bandpass filtered impulse response function from 0 to 0.125sec with  $f_o = 0.25\text{kHz}$ .

Magnitude of Gaussian Octave Bandpass Filtered Impulse Response Function with  $f_o=0.125kHz$ , dB

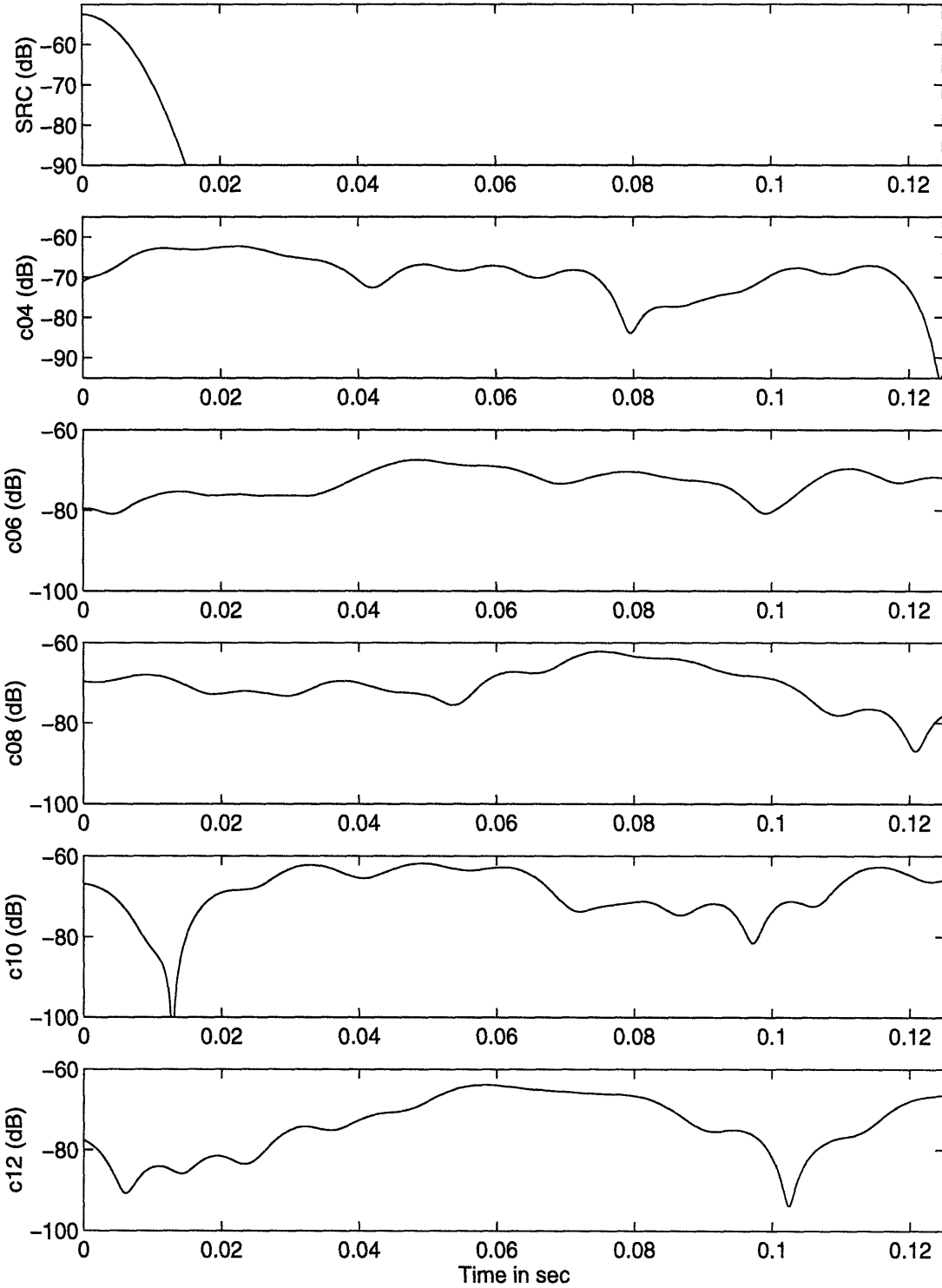


Figure 3-13: Magnitude of Gaussian octave bandpass filtered impulse response function from 0 to 0.125sec with  $f_o = 0.125kHz$ .

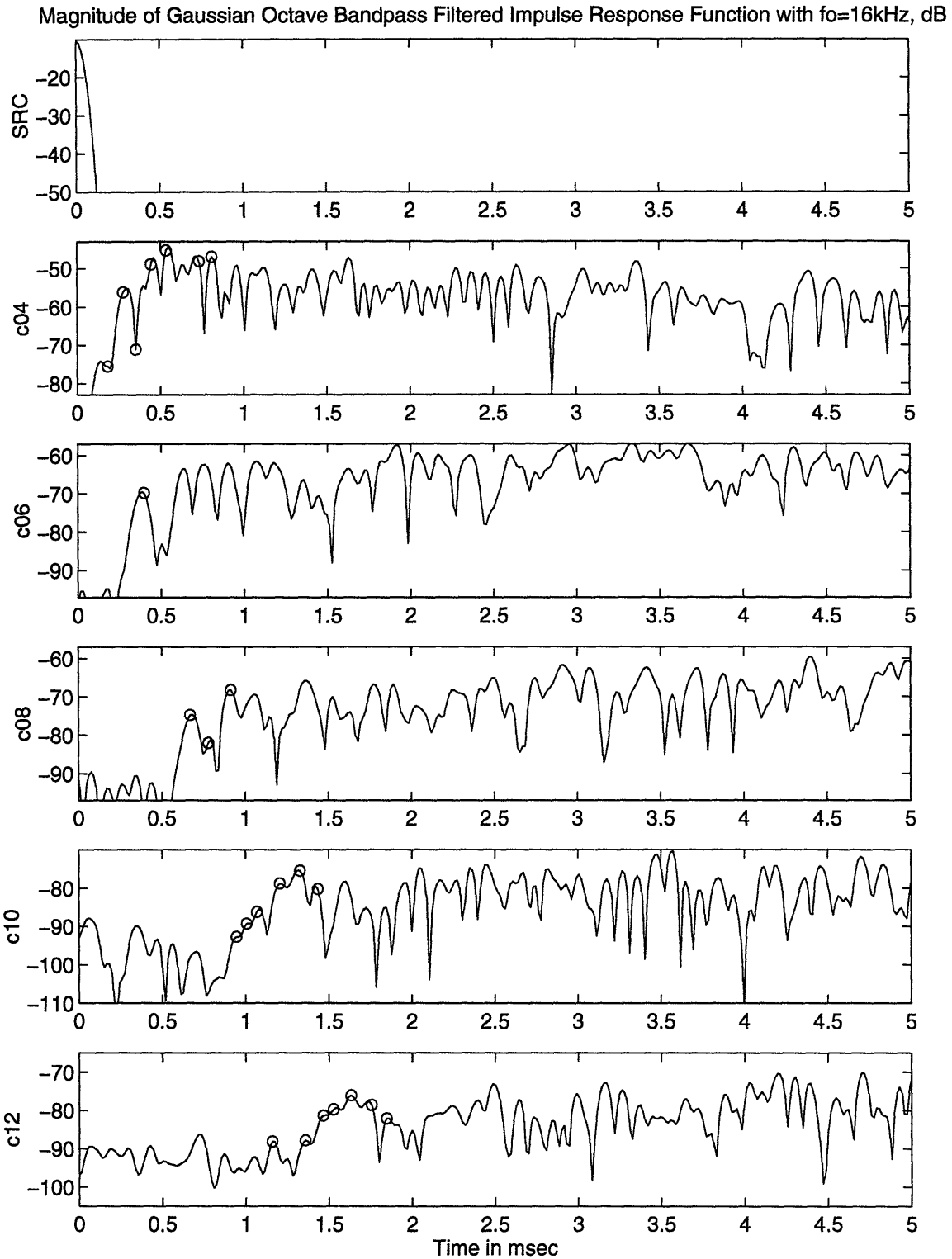


Figure 3-14: Magnitude of Gaussian octave bandpass filtered impulse response function from 0 to 5msec with  $f_o = 16kHz$  and predicted major early arrival times (o).

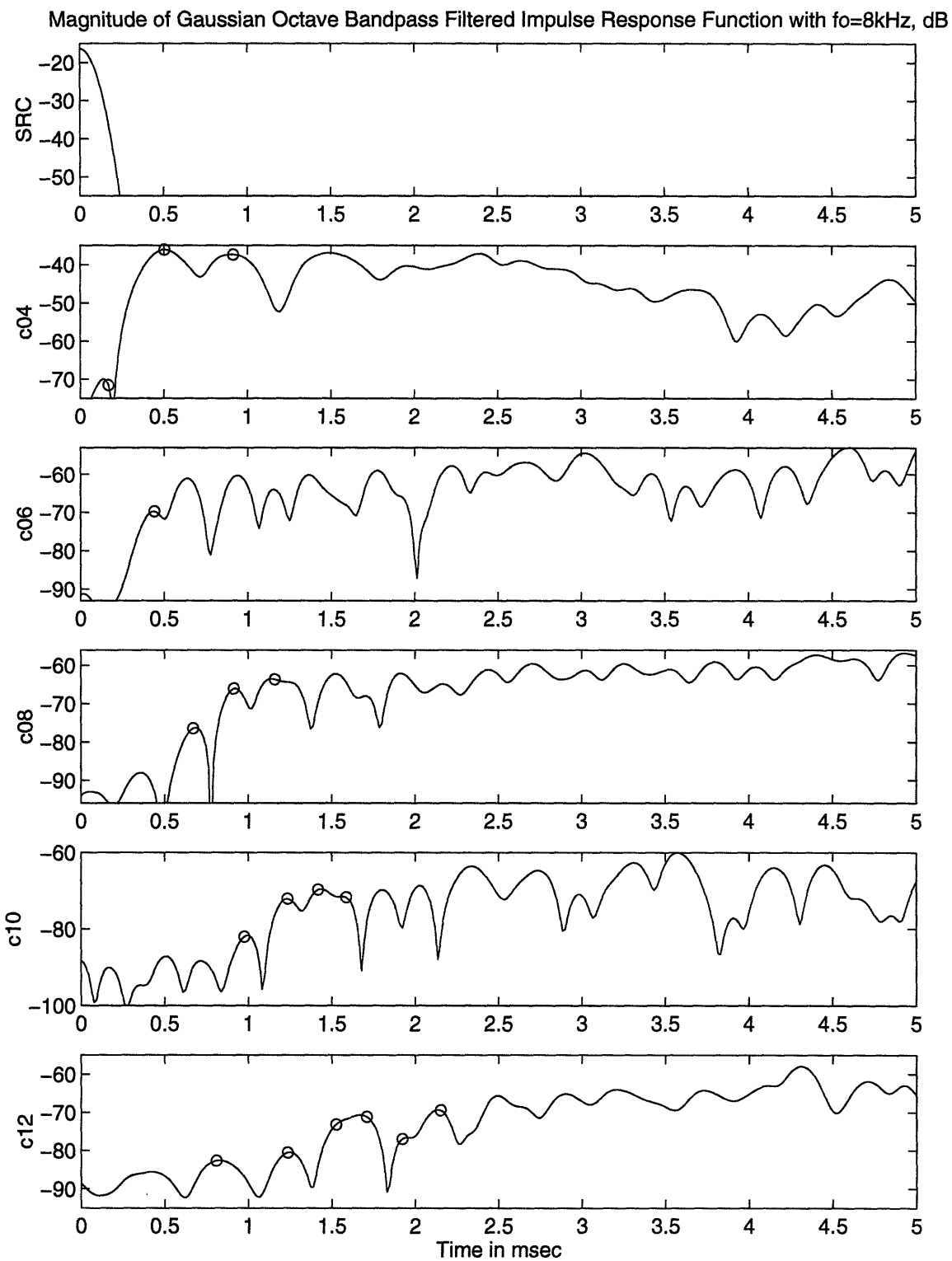


Figure 3-15: Magnitude of Gaussian octave bandpass filtered impulse response function from 0 to 5 msec with  $f_o = 8\text{kHz}$  and predicted major early arrival times ( $\circ$ ).



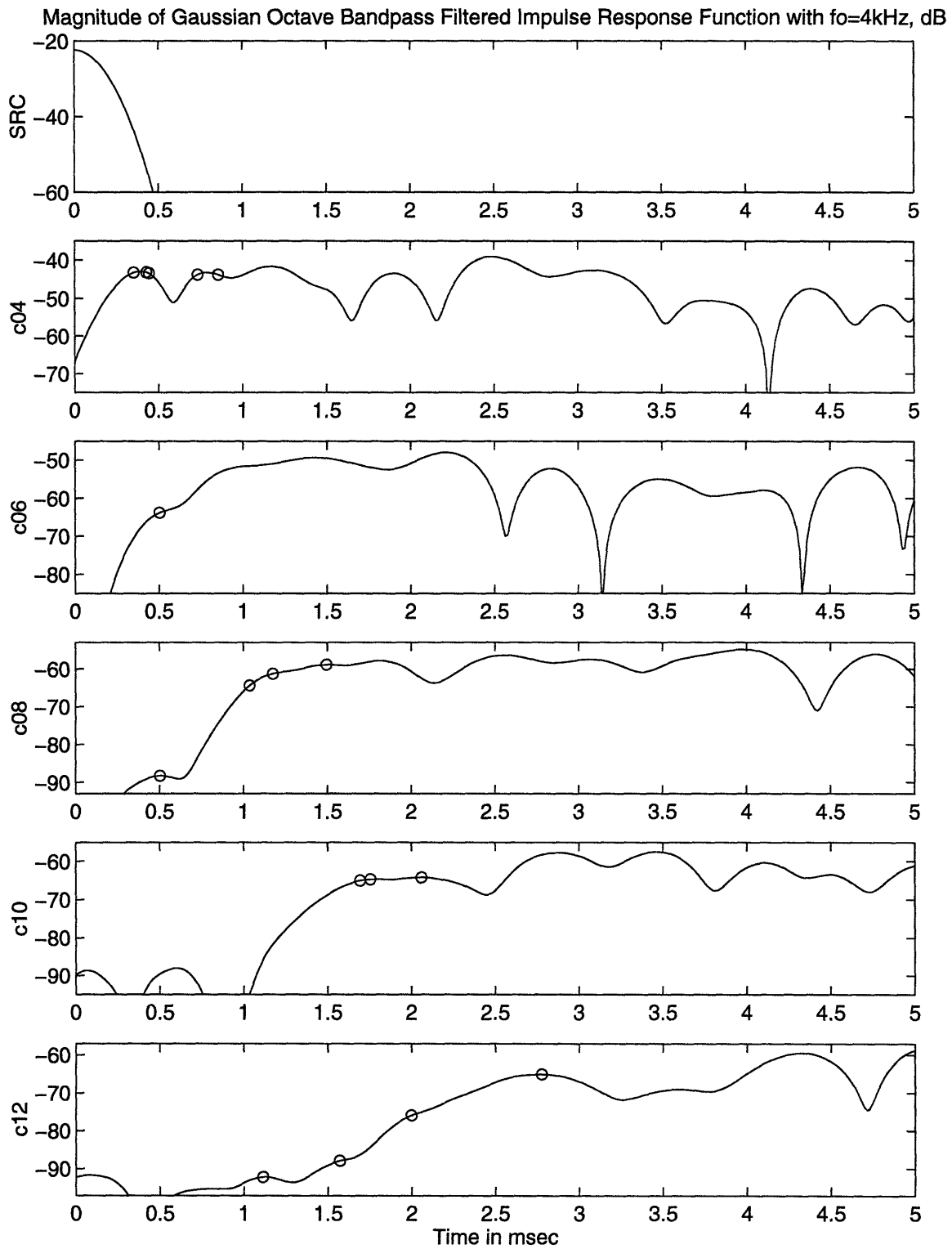


Figure 3-16: Magnitude of Gaussian octave bandpass filtered impulse response function from 0 to 5 msec with  $f_o = 4kHz$  and predicted major early arrival times (o).

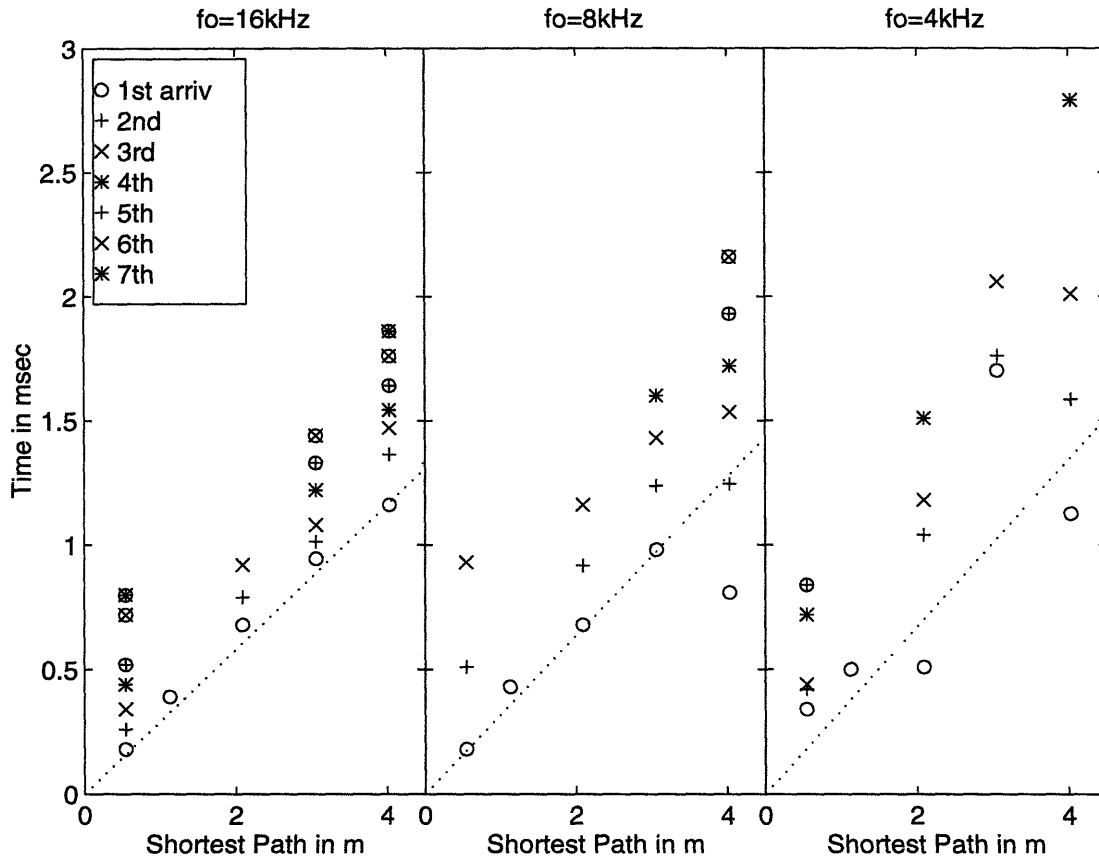


Figure 3-17: Major early arrival times of octave bandpass filtered impulse response function with the shortest path as the X axis. Dotted lines are linear regressions of the first arrival times.

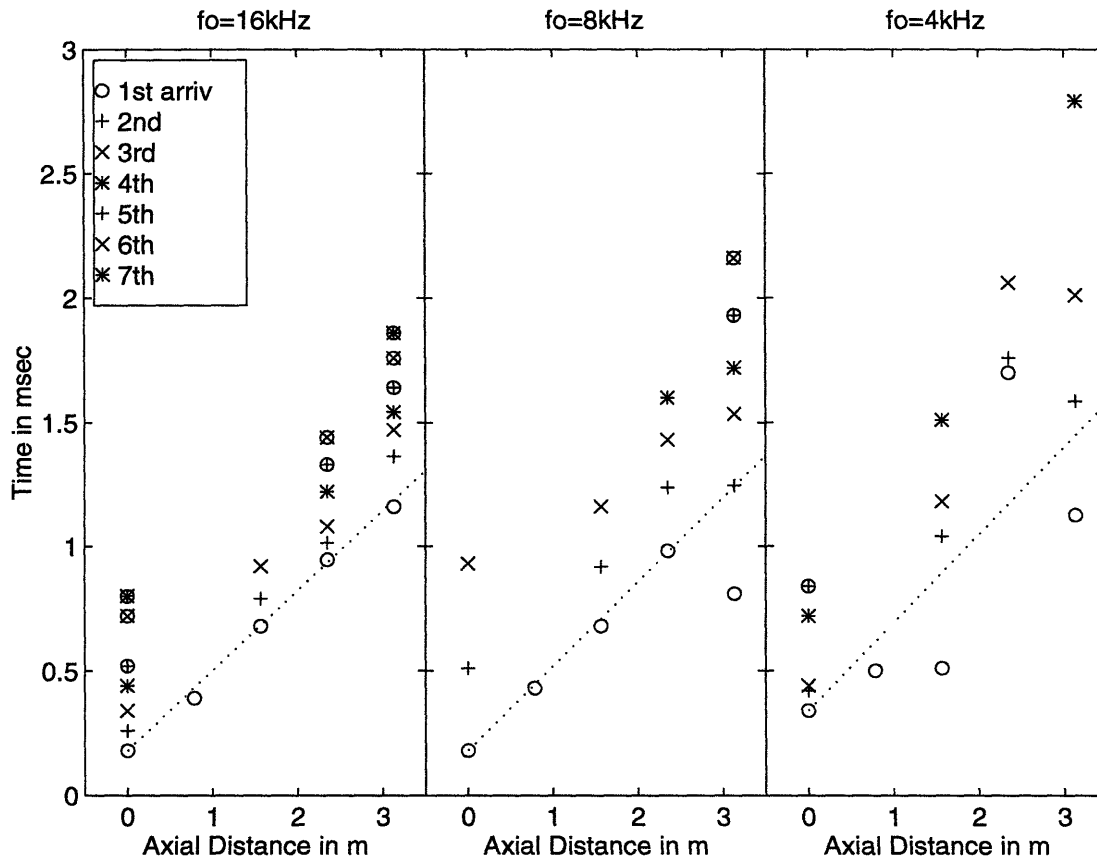


Figure 3-18: Major early arrival times of octave bandpass filtered impulse response function with the axial distance as the  $X$  axis. Dotted lines are linear regressions of the first arrival times.

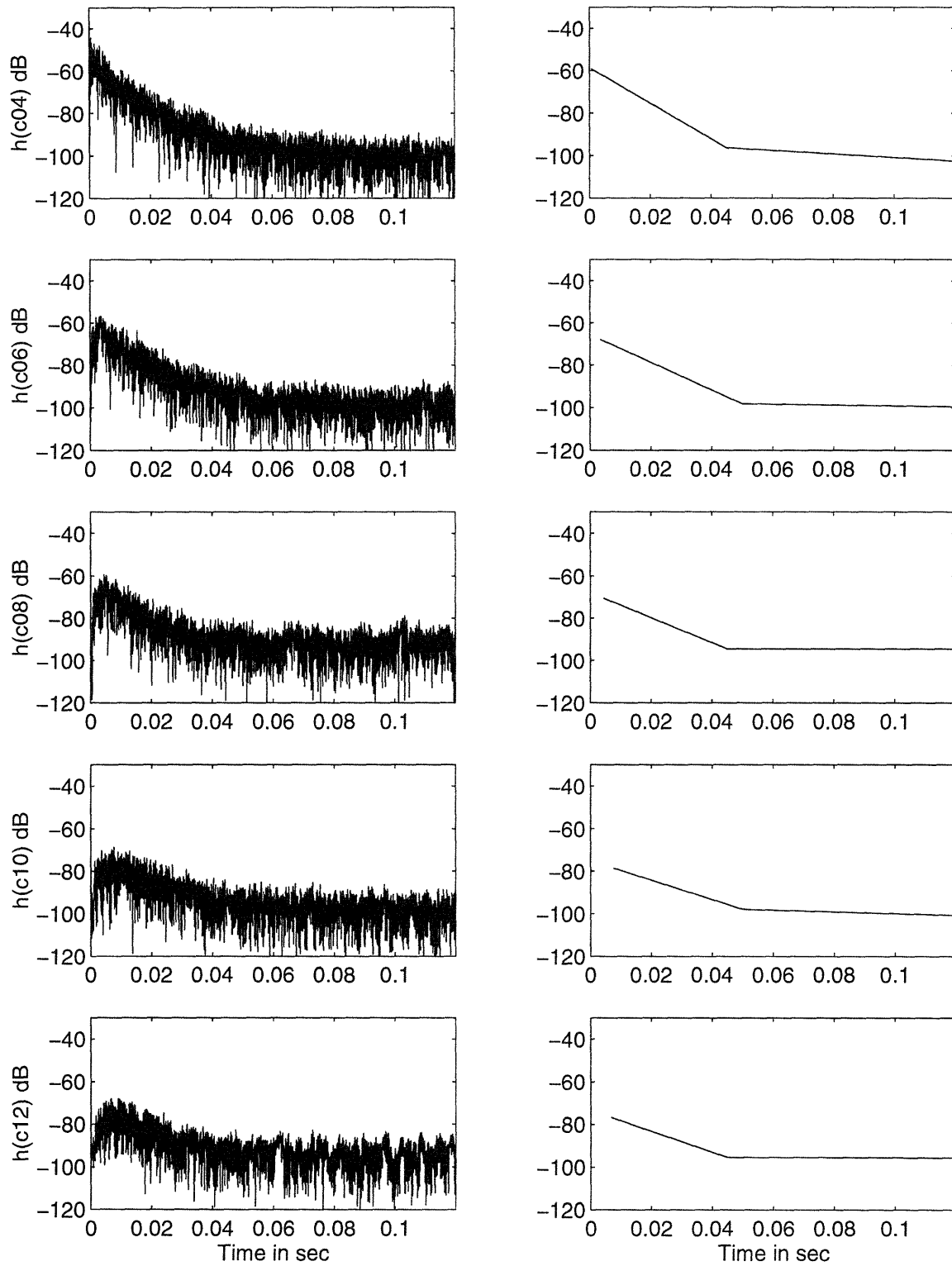


Figure 3-19: Least square fitted curves of Gaussian octave bandpass filtered impulse response function with  $f_o = 16kHz$ .

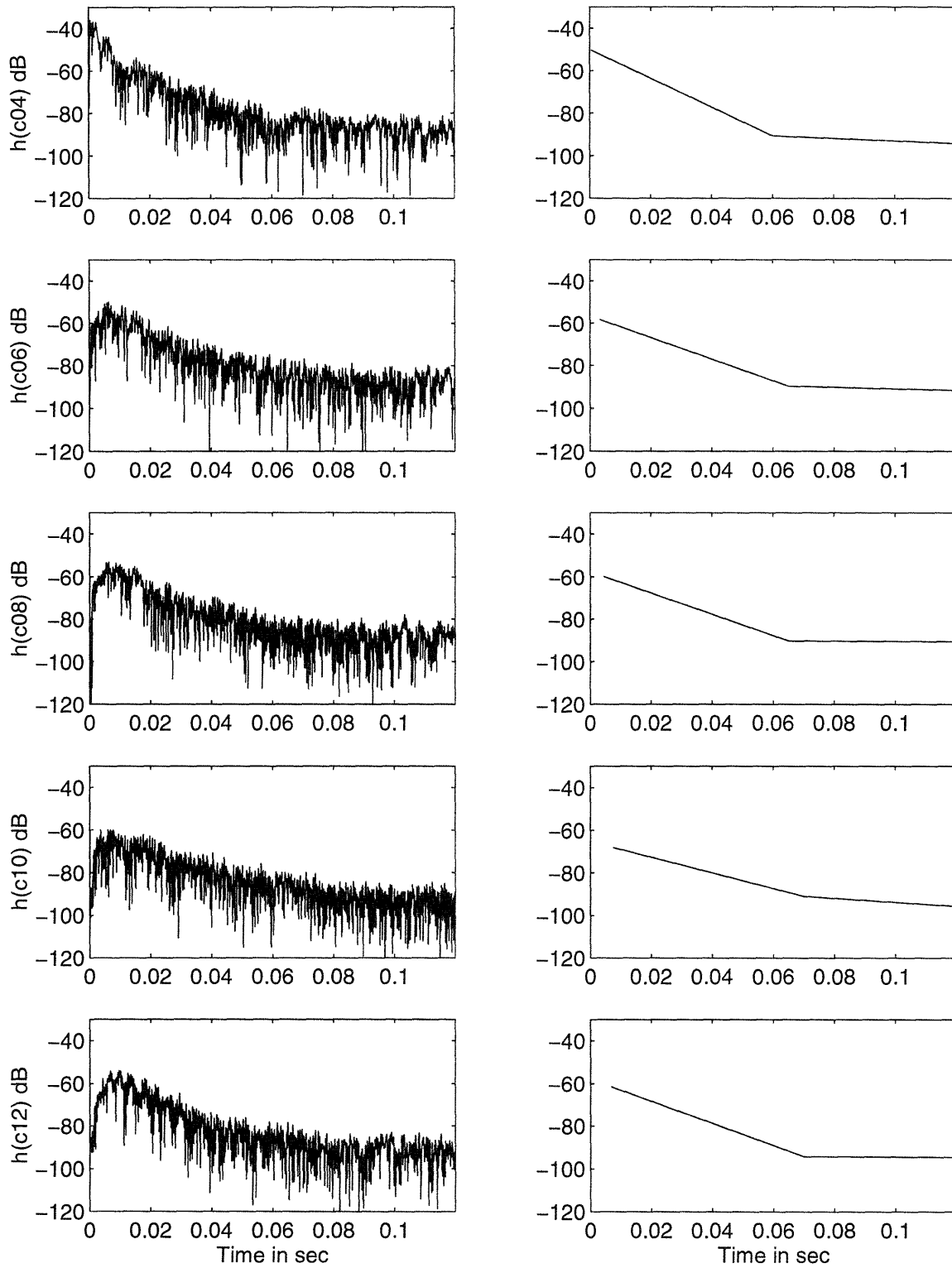


Figure 3-20: Least square fitted curves of Gaussian octave bandpass filtered impulse response function with  $f_o = 8kHz$ .

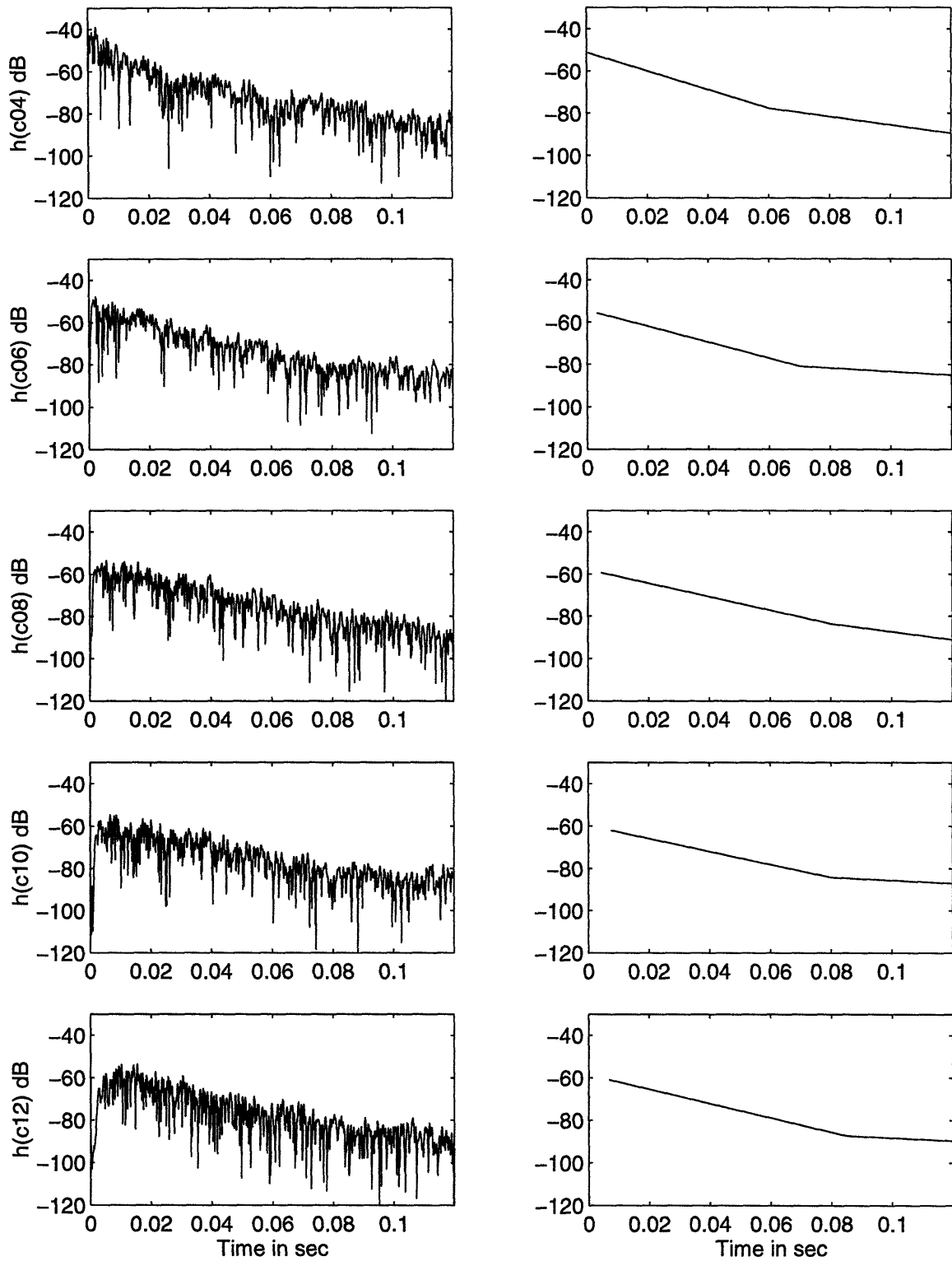


Figure 3-21: Least square fitted curves of Gaussian octave bandpass filtered impulse response function with  $f_o = 4kHz$ .

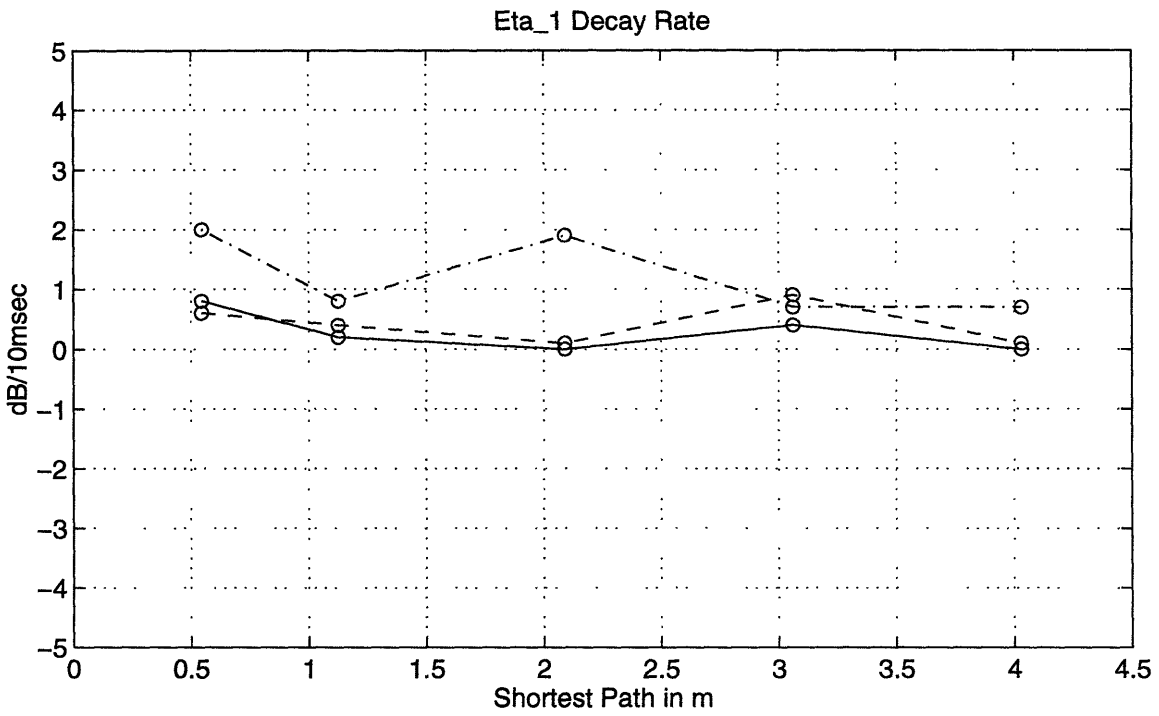
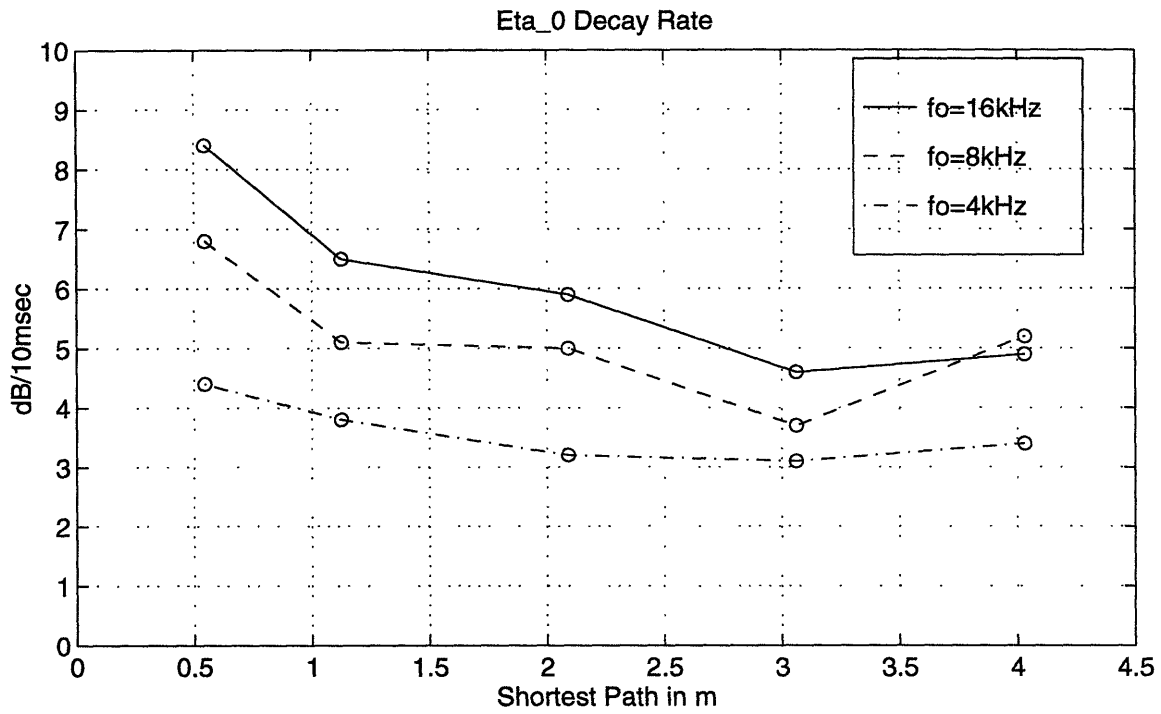


Figure 3-22: Decay rates of Gaussian octave bandpass filtered impulse response function.

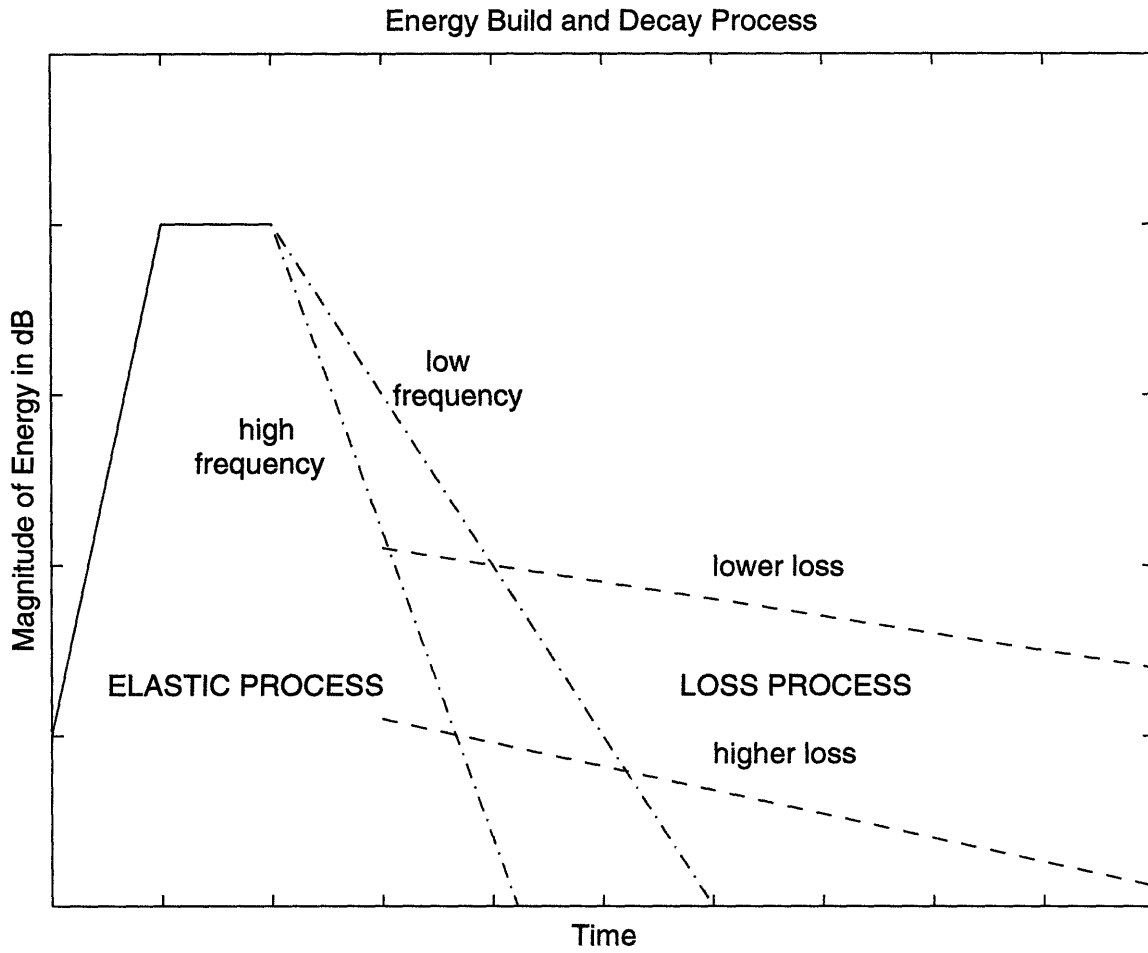


Figure 3-23: Schematic of energy build up and decay processes in the truss



Table 3.2: Early arrival times of Gaussian bandpass filtered elastic waves with  $f_o = 16kHz$ .

Joint	Number	$T_{arrv}$ (msec)	# of Comp.	# of Tors.	# of Flex.
c04	1	0.18	0	1	0
	2	0.26	0	0	1
	3	0.34	2	0	0
	4	0.44	1	1	0
	5	0.52	1	0	1
	6	0.72	0	3	0
	7	0.80	0	2	1
c06	1	0.39	0	2	1
c08	1	0.68	3	0	2
	2	0.79	1	1	3
	3	0.92	0	1	4
c10	1	0.94	2	4	1
		0.95	3	2	2
	2	1.00	1	5	1
		1.02	3	1	3
		1.02	1	4	2
	3	1.08	2	2	3
	4	1.22	1	3	3
	5	1.33	1	1	5
	6	1.44	0	1	6
	c12	1	1.16	6	1
1.16			3	6	0
2		1.36	2	5	2
		1.36	3	2	4
		1.37	4	0	5
		1.37	4	0	5
3		1.46	4	0	5
		1.46	1	5	3
		1.47	2	3	4
		1.47	0	6	3
		1.48	3	1	5
		1.48	1	4	4
		1.48	1	4	4
4		1.54	2	2	5
		1.54	0	5	4
		1.55	1	3	5
5		1.64	2	0	7
		1.64	1	3	5
6		1.76	0	2	7
7		1.86	1	0	8

Table 3.3: Early arrival times of Gaussian bandpass filtered elastic waves with  $f_o = 8kHz$ .

Joint	Number	$T_{arrv}$ (msec)	# of Comp.	# of Tors.	# of Flex.	
c04	1	0.18	0	1	0	
	2	0.51	0	2	0	
	3	0.93	0	2	1	
c06	1	0.43	1	1	1	
c08	1	0.68	2	2	1	
		0.68	0	5	0	
	2	0.91	1	1	3	
		0.91	1	2	2	
		0.93	0	3	2	
3	1.16	1	0	4		
c10	1	0.97	4	1	2	
		0.97	1	4	2	
		0.97	1	6	0	
		0.98	5	0	2	
		0.99	2	3	2	
		0.99	0	6	1	
		1.00	3	3	1	
	2	1.23	2	4	1	
		1.24	2	0	5	
		1.24	0	5	2	
	3	1.43	1	1	5	
	4	1.60	0	6	1	
	c12	1	0.81	8	1	0
		2	1.24	3	5	1
1.25			5	2	2	
3		1.53	3	3	3	
		1.53	1	6	2	
		1.54	5	0	4	
		1.54	3	2	4	
4		1.72	2	2	5	
		1.72	2	3	4	
5		1.93	2	1	6	
		1.93	0	4	5	
6		2.16	1	0	8	
		2.16	1	1	7	

Table 3.4: Early arrival times of Gaussian bandpass filtered elastic waves with  $f_o = 4kHz$ .

Joint	Number	$T_{arrv}$ (msec)	# of Comp.	# of Tors.	# of Flex.
c04	1	0.34	2	0	0
	2	0.42	0	0	1
	3	0.44	1	1	0
	4	0.72	0	3	0
	5	0.84	1	0	1
c06	1	0.50	2	0	1
c08	1	0.51	4	0	1
	2	1.04	1	2	2
	3	1.18	0	2	3
	4	1.51	1	0	4
c10	1	1.70	3	0	4
		1.70	0	3	4
	2	1.76	2	1	4
	3	2.06	0	2	5
c12	1	1.12	3	6	0
		1.13	7	1	1
	2	1.58	3	4	2
		1.59	0	7	2
	3	2.01	3	2	4
		2.01	0	5	4
	4	2.79	0	2	7

Table 3.5: Decay rates of Gaussian octave bandpass filtered elastic waves.

Decay Rate ( $dB/10msec$ )		
Gaussian octave band $f_o = 16kHz$		
Joint	$\eta_0$	$\eta_1$
c04	8.4	0.8
c06	6.5	0.2
c08	5.9	0.0
c10	4.6	0.4
c12	4.9	0.0
Gaussian octave band $f_o = 8kHz$		
Joint	$\eta_0$	$\eta_1$
c04	6.8	0.6
c06	5.1	0.4
c08	5.0	0.1
c10	3.7	0.9
c12	5.2	0.1
Gaussian octave band $f_o = 4kHz$		
Joint	$\eta_0$	$\eta_1$
c04	4.4	2.0
c06	3.8	0.8
c08	3.2	1.9
c10	3.1	0.7
c12	3.4	0.7

# Chapter 4

## Conclusions

### 4.1 Summary and Conclusions

A study of elastic waves in a three-dimensional truss with use of spatial spectral analysis and temporal impulse analysis, was conducted within a single-input/multiple-output context. The frequency and time domain experiments were performed to investigate both the magnitude and phase of the transfer function at the joints of the truss.

The results of the *frequency domain* study can be summarized:

- Spatial coherence of the total elastic wave field is high throughout the truss except at stopbands caused by the periodicity of the truss and in bands at which the strut lengths equal the integral multiples of half the elastic wavelengths. The strongest stopbands are  $3kHz$ ,  $5kHz$ ,  $10kHz$ ,  $14kHz$ , etc.
- The extracted wavenumber, phase speed, time delay, group speed and group delay from the phase of the cross-spectra show that the elastic waves propagate both in positive and negative axial directions through the joints of the truss due to reverberation and scattering.

- The frequency-wavenumber spectrum shows that high inertance spectrum bands lie between approximately  $-10dB$  and  $10dB$  re  $1/kg$  and the wavenumber spectrum in these bands becomes flatter with increasing frequency. The wave propagates through the joints both in positive and negative axial direction and this is caused by phase randomness.

The results of the *time domain* study can be summarized:

- The transient elastic wave energy travels with approximately constant group delay in the high frequency bands, and the measured arrival times agree with the predicted times in the two highest octave bands.
- Decay rates of the elastic wave field are not constant, but functions of frequency and location; The major decay rate increases with increasing frequency up to  $8.4dB/10msec$  in the  $16kHz$  octave band, and decreases with increasing distance down to near  $3.0dB/10msec$  in the  $4kHz$  octave band. The minor decay rate is approximately invariant with position and decreases with increasing frequency from  $2.0$  to  $0.0dB/10msec$ .
- The mean-free-paths of energy build up and energy decay are about 6 times the total axial length of the truss; that is, the waves reverberate 6 times the truss length to reach the maximum energy build up, and also the equilibrium with the absorption processes in the truss. However, the latter is not as robust as the former since decay rates depend on frequency.

From the above results, I conclude that a broad wavenumber distribution at the joints of the truss is developed over all frequency bands. Thus the wave propagates in both positive and negative axial directions and this is due to the multi-paths of the truss structure. The multiple paths cause phase randomness even though the phase of the cross-spectra at the joints shows an approximately linear relationship. The results of time domain experiment shows roughly constant group delay of wave propagation with a transient input source. However, this tendency will disappear after the truss becomes fully energized and the phase at the joints becomes random.

## 4.2 Future Work

I investigated the spatial spectra of the MIT truss to understand the response at the joints with a simple single-input/multiple-output system.

However, in a real application the truss will carry many equipments which may or may not be correlated with each other. Thus it would be desirable to study the truss as a multiple-input/multiple-output system with correlated and uncorrelated sources.

If the sources are completely uncorrelated, superposition of single-input/multiple-output systems can characterize this multiple-input/multiple-output system. For the partially correlated source case, problems in designing reasonable sources should be overcome to investigate a multiple-input/multiple-output system.

I used as input only forcing at a base strut. However, to fully understand the spatial spectra of truss structures, experiments with different input locations, such as on plates and joints as well as with different truss configurations, are also desirable.

# Appendix A

## Timoshenko Beam Theory

The Timoshenko beam theory includes effects of rotary inertia and shear deformation which are neglected in the Euler-Bernoulli beam theory[23]. With a free vibration, the Timoshenko beam equation can be expressed as

$$\frac{EI}{\rho A} \frac{\partial^4 z}{\partial x^4} + \frac{\partial^2 z}{\partial t^2} - \frac{I}{A} \left(1 + \frac{E}{KG}\right) \frac{\partial^4 z}{\partial x^2 \partial t^2} + \frac{\rho I}{KGA} \frac{\partial^4 z}{\partial t^4} = 0 \quad (\text{A.1})$$

where

- $E$  = Young's modulus,
- $G$  = shear modulus,
- $I$  = area moment of inertia,
- $A$  = area of beam,
- $\rho$  = density of beam,
- $K$  = Timoshenko's shear coefficient, and
- $z$  = transverse displacement of beam.

The dispersion relation of the Timoshenko beam equation Eq. (A.1) becomes

$$k = \frac{1}{2} \sqrt{2\mathbf{A}\omega^2 + 2\sqrt{(\mathbf{A}^2 - 4\mathbf{C})\omega^4 + 4\mathbf{B}\omega^2}} \quad (\text{A.2})$$

where

$$\mathbf{A} = \frac{\rho}{E} + \rho KG, \quad \mathbf{B} = \frac{\rho A}{EI}, \quad \text{and} \quad \mathbf{C} = \frac{\rho^2}{EKG}.$$



Eq. (A.2) is different from the dispersion relation of an Euler-Bernoulli beam which is

$$k = \sqrt[4]{\frac{\rho A}{EI}} \sqrt{\omega}. \quad (\text{A.3})$$

The phase speed and group speed of waves on a Euler-Bernoulli beam are

$$\begin{aligned} C_{phase} &= \frac{\omega}{k} \\ &= \sqrt{\omega \sqrt{\frac{EI}{\rho A}}} \\ &= \sqrt{\omega \kappa \sqrt{\frac{E}{\rho}}}, \end{aligned} \quad (\text{A.4})$$

$$\begin{aligned} C_{group} &= \frac{\partial \omega}{\partial k} \\ &= 2 \sqrt{\omega \kappa \sqrt{\frac{E}{\rho}}} \end{aligned} \quad (\text{A.5})$$

where  $\kappa$  is a radius of gyration. For the MIT truss the radius of gyration becomes

$$\kappa = \frac{1}{2} \sqrt{r_{outer}^2 + r_{inner}^2} \quad (\text{A.6})$$

thus  $\kappa = 0.0039m$ .

The phase speed and group speed of flexural wave on a Timoshenko beam are

$$\begin{aligned} C_{phase} &= \frac{\omega}{k} \\ &= \frac{\omega}{\frac{1}{2} \sqrt{2\mathbf{A}\omega^2 + 2\sqrt{(\mathbf{A}^2 - 4\mathbf{C})\omega^4 + 4\mathbf{B}\omega^2}}}, \end{aligned} \quad (\text{A.7})$$

$$\begin{aligned} C_{group} &= \frac{\partial \omega}{\partial k} \\ &= 4 \frac{\sqrt{2\mathbf{A}\omega^2 + 2\sqrt{(\mathbf{A}^2 - 4\mathbf{C})\omega^4 + 4\mathbf{B}\omega^2}}}{4\mathbf{A}\omega + \frac{(4\mathbf{A}^2 - 16\mathbf{C})\omega^3 + 8\mathbf{B}\omega}{\sqrt{(\mathbf{A}^2 - 4\mathbf{C})\omega^4 + \mathbf{B}\omega^2}}} \end{aligned} \quad (\text{A.8})$$

For more accurate calculation I choose the Timoshenko's shear coefficient of a thin-walled round tube as

$$K = \frac{2(1 + \nu)}{4 + 3\nu}, \quad (\text{A.9})$$

and set  $\nu$  be 1/2 to satisfy the Timoshenko beam equation in the limit of zero wavelength in the waves on high frequency region; thus,  $K$  becomes 0.545 instead of 0.5[24][25]. The dispersion relation and flexural wave speed of the MIT truss with the Timoshenko and Euler-Bernoulli beam theory are shown in Fig. A-1 and Fig. A-2 respectively. The wave speeds of the truss are shown in Table A.1.

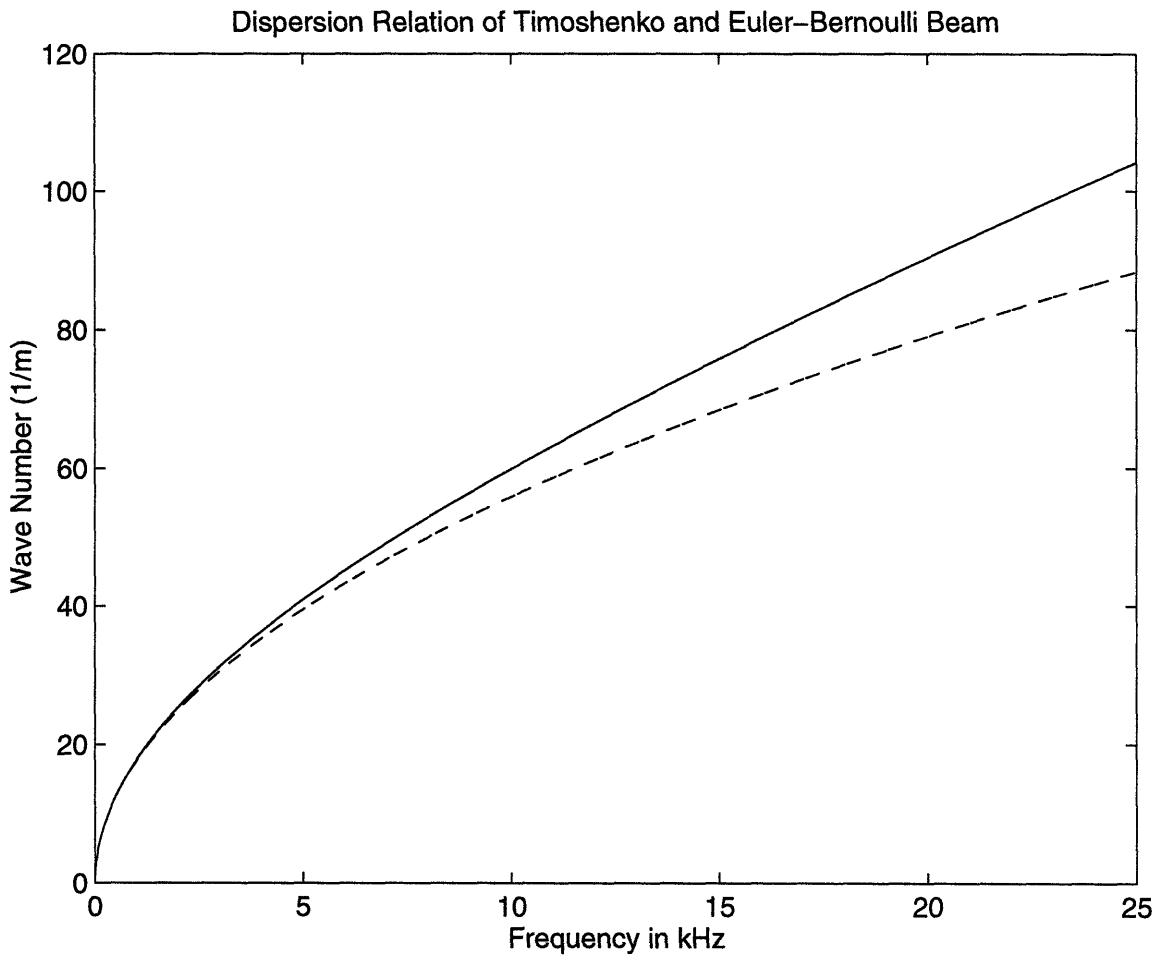


Figure A-1: Dispersion relation of Timoshenko beam (solid) and Euler-Bernoulli beam (dashed).

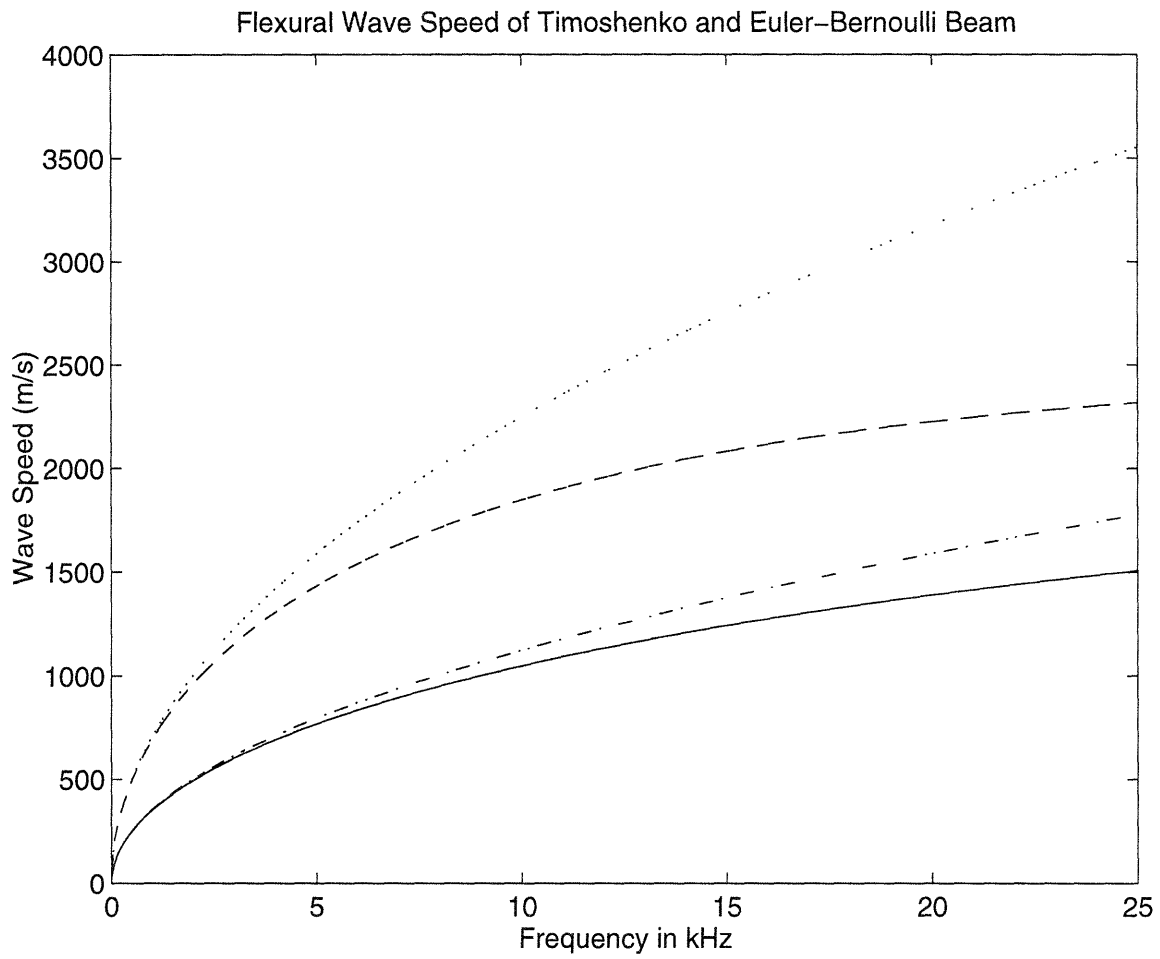


Figure A-2: Flexural wave speed of Timoshenko and Euler-Bernoulli beams. Solid and dashed lines are phase speed of Timoshenko and Euler-Bernoulli beam respectively, and dash-dot and dotted lines are group speed of Timoshenko and Euler-Bernoulli beam respectively.

Table A.1: Elastic wave speeds in the MIT truss.

Young's Modulus of Aluminum ( <i>GPa</i> )				
70				
Shear Modulus of Aluminum ( <i>GPa</i> )				
26				
Density of Aluminum ( <i>kg/m<sup>3</sup></i> )				
2700				
Compressional wave Speed ( <i>m/sec</i> )				
5092				
Torsional wave Speed ( <i>m/sec</i> )				
3103				
Flexural wave Speed ( <i>m/sec</i> )				
Octave Band	Euler-Bernoulli Beam		Timoshenko Beam	
$f_o$ ( <i>kHz</i> )	$C_{phase}$	$C_{group}$	$C_{phase}$	$C_{group}$
0.125	126	251	126	251
0.25	178	355	177	354
0.5	251	503	250	497
1	355	711	353	696
2	503	1005	496	964
4	711	1422	691	1309
8	1005	2011	951	1715
16	1422	2844	1275	2116

# Appendix B

## MATLAB Codes

### Chapter 2

```
%%%%%%%%%%%%%%%%%%%%%%%%%%%%%%%%%%%%%%%%%%%%%%%%%%%%%%%%%%%%%%%%%%%%%%%%%%%%%%
%%
%% Coherence of Elastic Waves at Joints of Truss
%%
%%%%%%%%%%%%%%%%%%%%%%%%%%%%%%%%%%%%%%%%%%%%%%%%%%%%%%%%%%%%%%%%%%%%%%%%%%%%%%
%% Force at B4 in Z-direction & REF at C04 acclerometer
clear;
%%%%%%%%%%%%%%%%%%%%%%%%%%%%%%%%%%%%%%%%%%%%%%%%%%%%%%%%%%%%%%%%%%%%%%%%%%%%%%
%[data,q1,q2,q3,q4,q5,q6,q7]=ReadUniversal('s5b4b4z_25K.unv');
%%%%%%%%%%%%%%%%%%%%%%%%%%%%%%%%%%%%%%%%%%%%%%%%%%%%%%%%%%%%%%%%%%%%%%%%%%%%%%
%% frequency band 25kHz
load /arctic1/jhpark/truss/Feb13/b4c4z_old
mf=25600
%%%%%%%%%%%%%%%%%%%%%%%%%%%%%%%%%%%%%%%%%%%%%%%%%%%%%%%%%%%%%%%%%%%%%%%%%%%%%%
%% frequency band 5kHz WhiteNoise 25kH
%load /arctic1/jhpark/truss/Feb13/b4b4zS5_25K
%mf= 6400
%%%%%%%%%%%%%%%%%%%%%%%%%%%%%%%%%%%%%%%%%%%%%%%%%%%%%%%%%%%%%%%%%%%%%%%%%%%%%%
%% frequency band 1kHz WhiteNoise 25kH
%load /arctic1/jhpark/truss/Feb13/b4b4zS1_25K
%mf= 1600
%% mf % maxmun frequency in Hz
nf=3200; % number of frequency data
f=[0:mf/nf:mf];
fk=f./1e3; % frequency in kHz
%% impedance head correction curve
x=[1000,2000,4000,10000,20000,30000];
y=[0,0,0,-.8,-5.5,-10];
yi=spline(x,y,f);
yi=(10.^(yi/10)).';
ff=real(data(:,1)); % force auto-spectrum
ff=ff./(yi.^2); % force correction
aa=real(data(:,24)); % accel auto-spectrum
%% This is C joint arrangement
c02=real(data(:,4)); %c02 4
c04=real(data(:,2)); %c04 2
c06=real(data(:,11)); %c06 11
c08=real(data(:,15)); %c08 15
c10=real(data(:,19)); %c10 19
c12=real(data(:,23)); %c12 23
%% cross-spectrum w.r.t. ref as force
cf02=data(:,27)./yi; %cf02 27
```

```

cf04=data(:,25)./yi; %cf04 25
cf06=data(:,34)./yi; %cf06 34
cf08=data(:,38)./yi; %cf08 38
cf10=data(:,42)./yi; %cf10 42
cf12=data(:,46)./yi; %cf12 46
%%%% cross-spectrum w.r.t. ref as acceleration at c04
ca02=data(:,48); %ca02
ca04=c04; %ca04
ca06=data(:,55); %ca06
ca08=data(:,59); %ca08
ca10=data(:,63); %ca10
ca12=data(:,67); %ca12
clear data q1 q2 q3 q4 q5 q6 q7
%%%%%%%%%%%%%%%%%%%%%%%%%%%%%%%%%%%%%%%%%%%%%%%%%%%%%%%%%%%%%%%%%%%%%%%%
%%%%
%%%%          Coherence Factor ref: Force at C04
%%%%
%%%%          |Saf|^2
%%%%          Kf = -----
%%%%          SaaSff
%%%%
%%%%%%%%%%%%%%%%%%%%%%%%%%%%%%%%%%%%%%%%%%%%%%%%%%%%%%%%%%%%%%%%%%%%%%%%
Kf0402 =(abs(cf02)).^2./(ff.*c02);
Kf0404 =(abs(cf04)).^2./(ff.*c04);
Kf0406 =(abs(cf06)).^2./(ff.*c06);
Kf0408 =(abs(cf08)).^2./(ff.*c08);
Kf0410 =(abs(cf10)).^2./(ff.*c10);
Kf0412 =(abs(cf12)).^2./(ff.*c12);
%%%%%%%%%%%%%%%%%%%%%%%%%%%%%%%%%%%%%%%%%%%%%%%%%%%%%%%%%%%%%%%%%%%%%%%%
%%%%
%%%%          Coherence Factor ref: Accel at B04
%%%%
%%%%          |a1a2*|^2
%%%%          Ka = ----- , |a1a2*|^2 = (abs(conj(a2a1*)))^2
%%%%          a1a1*a2a2*
%%%%
%%%%%%%%%%%%%%%%%%%%%%%%%%%%%%%%%%%%%%%%%%%%%%%%%%%%%%%%%%%%%%%%%%%%%%%%
Ka0402 =(abs(ca02)).^2/(c04.*c02);
Ka0404 =(abs(ca04)).^2/(c04.*c04);
Ka0406 =(abs(ca06)).^2/(c04.*c06);
Ka0408 =(abs(ca08)).^2/(c04.*c08);
Ka0410 =(abs(ca10)).^2/(c04.*c10);
Ka0412 =(abs(ca12)).^2/(c04.*c12);
%%%%% unwrap phase of cross-spectrum
phase1=unwrap(angle(cf04));
phase2=unwrap(angle(cf06));
phase3=unwrap(angle(cf08));
phase4=unwrap(angle(cf10));
phase5=unwrap(angle(cf12));
%%%%% dPHASE
del_phase1=phase2-phase1;
del_phase2=phase3-phase2;
del_phase3=phase4-phase3;
del_phase4=phase5-phase4;
%%%%% dPHASE/dX = k, dX=4.7/6=0.7833
k1=del_phase1./((4.7/6)*ones(size(phase1)));
k2=del_phase2./((4.7/6)*ones(size(phase1)));
k3=del_phase3./((4.7/6)*ones(size(phase1)));
k4=del_phase4./((4.7/6)*ones(size(phase1)));
%%%%% Cp=w/k, Phase Speed
c1=(f.*2*pi)./k1.';
c2=(f.*2*pi)./k2.';
c3=(f.*2*pi)./k3.';
c4=(f.*2*pi)./k4.';
%%%%% tau = dX/Cp, Time Delay
Tc1=(ones(size(c1)).*(4.7/6))./c1;
Tc2=(ones(size(c1)).*(4.7/6))./c2;
Tc3=(ones(size(c1)).*(4.7/6))./c3;

```

```

Tc4=(ones(size(c1)).*(4.7/6))./c4;
%%%% Cg=dw/dk, Group Speed
omega=f.*(2*pi);
dw=diff(omega);
dk1=diff(k1);
dk2=diff(k2);
dk3=diff(k3);
dk4=diff(k4);
Cg1=dw./dk1';
Cg2=dw./dk2';
Cg3=dw./dk3';
Cg4=dw./dk4';
%%%% Tg=dX/Cg, Group Delay
Tg1=(ones(size(Cg1)).*(4.7/6))./Cg1;
Tg2=(ones(size(Cg1)).*(4.7/6))./Cg2;
Tg3=(ones(size(Cg1)).*(4.7/6))./Cg3;
Tg4=(ones(size(Cg1)).*(4.7/6))./Cg4;
%%%% to find phase slope in degrees by finite difference
up1=diff((phase1.*(180/pi)).');
up2=diff((phase2.*(180/pi)).');
up3=diff((phase3.*(180/pi)).');
up4=diff((phase4.*(180/pi)).');
up5=diff((phase5.*(180/pi)).');
dfk=diff(fk);
%%%% slope
slp1=up1./dfk;
slp2=up2./dfk;
slp3=up3./dfk;
slp4=up4./dfk;
slp5=up5./dfk;
%%%% total slope
asl1=mean(slp1);
asl2=mean(slp2);
asl3=mean(slp3);
asl4=mean(slp4);
asl5=mean(slp5);
slopeTOT=[asl1 asl2 asl3 asl4 asl5];
%%%% f16 octave band slope
af16s11=mean(slp1(1416:2830));
af16s12=mean(slp2(1416:2830));
af16s13=mean(slp3(1416:2830));
af16s14=mean(slp4(1416:2830));
af16s15=mean(slp5(1416:2830));
slopef16=[af16s11 af16s12 af16s13 af16s14 af16s15];
%%%% f8
af8s11=mean(slp1(708:1416));
af8s12=mean(slp2(708:1416));
af8s13=mean(slp3(708:1416));
af8s14=mean(slp4(708:1416));
af8s15=mean(slp5(708:1416));
slopef8=[af8s11 af8s12 af8s13 af8s14 af8s15];
%%%% f4
af4s11=mean(slp1(355:708));
af4s12=mean(slp2(355:708));
af4s13=mean(slp3(355:708));
af4s14=mean(slp4(355:708));
af4s15=mean(slp5(355:708));
slopef4=[af4s11 af4s12 af4s13 af4s14 af4s15];
S='TOT f16 f8 f4'
SLOPE=[slopeTOT' slopef16' slopef8' slopef4'];
slope= ( round ( SLOPE.*100 ) ) ./100
%%%% change mf & mfk for plot axis
% delta f
df=mf/nf
mfk=floor(mf/1e3);
if mfk==1
    mfk=1.5;
end

```

```

%%%%% axis tailoring
mfk;
mf=mfk*1e3;
%%%%%%%%%%%%%%%%%%%%%%%%%%%%%%%%%%%%%%%%%%%%%%%%%%%%%%%%%%%%%%%%%%%%%%%%
figure(1)
orient tall
subplot(511)
plot(fk,Kf0404)
axis([0 mfk 0 1])
ylabel('Coh(F,c04)')
title('Coherence Function between Input Force and Acceleration at Joints')
subplot(512)
plot(fk,Kf0406)
axis([0 mfk 0 1])
ylabel('Coh(F,c06)')
subplot(513)
plot(fk,Kf0408)
axis([0 mfk 0 1])
ylabel('Coh(F,c08)')
subplot(514)
plot(fk,Kf0410)
axis([0 mfk 0 1])
ylabel('Coh(F,c10)')
subplot(515)
plot(fk,Kf0412)
axis([0 mfk 0 1])
ylabel('Coh(F,c12)')
xlabel('Frequency in kHz')
%%%%%%%%%%%%%%%%%%%%%%%%%%%%%%%%%%%%%%%%%%%%%%%%%%%%%%%%%%%%%%%%%%%%%%%%
figure(2)
orient tall
subplot(511)
semilogy(fk,(abs(cf04)))
axis([0 mfk 1e-5 1e0])
ylabel('C(F,c04)')
title('Magnitude of Cross-spectra between Input Force and Acceleration at Joints in Nm/s^2')
subplot(512)
semilogy(fk,(abs(cf06)))
axis([0 mfk 1e-6 1e-1])
ylabel('C(F,c06)')
subplot(513)
semilogy(fk,(abs(cf08)))
axis([0 mfk 1e-6 1e-1])
ylabel('C(F,c08)')
subplot(514)
semilogy(fk,(abs(cf10)))
axis([0 mfk 1e-7 1e-2])
ylabel('C(F,c10)')
subplot(515)
semilogy(fk,(abs(cf12)))
axis([0 mfk 1e-7 1e-2])
ylabel('C(F,c12)')
xlabel('Frequency in kHz')
%%%%%%%%%%%%%%%%%%%%%%%%%%%%%%%%%%%%%%%%%%%%%%%%%%%%%%%%%%%%%%%%%%%%%%%%
figure(3)
orient tall
subplot(511)
plot(fk,angle(cf04))
axis([0 mfk -pi pi])
ylabel('C(F,c04)')
title('Phase Angle of Cross-spectra between Input Force and Acceleration at Joints, radians')
subplot(512)
plot(fk,angle(cf06))
axis([0 mfk -pi pi])
ylabel('C(F,c06)')
subplot(513)
plot(fk,angle(cf08))
axis([0 mfk -pi pi])

```



```

ylabel('C(F,c08)')
subplot(514)
plot(fk,angle(cf10))
axis([0 mfk -pi pi])
ylabel('C(F,c10)')
subplot(515)
plot(fk,angle(cf12))
axis([0 mfk -pi pi])
ylabel('C(F,c12)')
xlabel('Frequency in kHz')
%%%%%%%%%%%%%%%%%%%%%%%%%%%%%%%%%%%%%%%%%%%%%%%%%%%%%%%%%%%%%%%%%%%%%%%%
figure(4)
orient tall
subplot(511)
plot(fk,phase1)
axis([0 mfk -1.5e3 1e2])
ylabel('C(F,c04)')
title('Phase Angle of Cross-spectra between Input Force and Acceleration at Joints, radians')
subplot(512)
plot(fk,phase2)
axis([0 mfk -1.5e3 1e2])
ylabel('C(F,c06)')
subplot(513)
plot(fk,phase3)
axis([0 mfk -1.5e3 1e2])
ylabel('C(F,c08)')
subplot(514)
plot(fk,phase4)
axis([0 mfk -1.5e3 1e2])
ylabel('C(F,c10)')
subplot(515)
plot(fk,phase5)
axis([0 mfk -1.5e3 1e2])
ylabel('C(F,c12)')
xlabel('Frequency in kHz')
%%%%%%%%%%%%%%%%%%%%%%%%%%%%%%%%%%%%%%%%%%%%%%%%%%%%%%%%%%%%%%%%%%%%%%%%
figure(5)
orient tall
subplot(411)
loglog(f,k1,'-',f,abs(k1),':')
axis([0 mf 1e-3 1e3])
set(gca,'YTick',[1e-3 1e-2 1e-1 1 1e1 1e2 1e3])
ylabel('k(c04,c06)')
title('Wavenumber,k = dPHASE/dX, in 1/m, dX=0.783m (1cell)')
legend('Positive','Negative')
subplot(412)
loglog(f,k2,'-',f,abs(k2),':')
axis([0 mf 1e-3 1e3])
set(gca,'YTick',[1e-3 1e-2 1e-1 1 1e1 1e2 1e3])
ylabel('k(c06,c08)')
subplot(413)
loglog(f,k3,'-',f,abs(k3),':')
axis([0 mf 1e-3 1e3])
set(gca,'YTick',[1e-3 1e-2 1e-1 1 1e1 1e2 1e3])
ylabel('k(c08,c10)')
subplot(414)
loglog(f,k4,'-',f,abs(k4),':')
axis([0 mf 1e-3 1e3])
set(gca,'YTick',[1e-3 1e-2 1e-1 1 1e1 1e2 1e3])
ylabel('k(c10,c12)')
xlabel('Frequency in Hz')
%%%%%%%%%%%%%%%%%%%%%%%%%%%%%%%%%%%%%%%%%%%%%%%%%%%%%%%%%%%%%%%%%%%%%%%%
figure(6)
orient tall
subplot(411)
loglog(f,c1,'-',f,abs(c1),':')
axis([0 mf 1e0 1e5])
ylabel('Cp(c04,c06)')

```

```

title('Phase Speed, Cp=w/k, in m/sec')
legend('Positive','Negative')
subplot(412)
loglog(f,c2,'-',f,abs(c2),':')
axis([0 mf 1e0 1e5])
ylabel('Cp(c06,c08)')
subplot(413)
loglog(f,c3,'-',f,abs(c3),':')
axis([0 mf 1e0 1e5])
%grid
ylabel('Cp(c08,c10)')
subplot(414)
loglog(f,c4,'-',f,abs(c4),':')
axis([0 mf 1e0 1e5])
ylabel('Cp(c10,c12)')
xlabel('Frequency in Hz')
%%%%%%%%%%%%%%%%%%%%%%%%%%%%%%%%%%%%%%%%%%%%%%%%%%%%%%%%%%%%%%%%%%%%%%%%
figure(7)
orient tall
subplot(411)
loglog(f,Tc1,'-',f,abs(Tc1),':')
ylabel('tau(04,06)')
axis([0 mf 1e-5 1e0])
legend('Positive','Negative')
title('Time Delay, tau=dX/Cp, in sec')
subplot(412)
loglog(f,Tc2,'-',f,abs(Tc2),':')
ylabel('tau(06,08)')
axis([0 mf 1e-5 1e0])
subplot(413)
loglog(f,Tc3,'-',f,abs(Tc3),':')
ylabel('tau(08,10)')
axis([0 mf 1e-5 1e0])
subplot(414)
loglog(f,Tc4,'-',f,abs(Tc4),':')
ylabel('tau(10,12)')
axis([0 mf 1e-5 1e0])
%%%%%%%%%%%%%%%%%%%%%%%%%%%%%%%%%%%%%%%%%%%%%%%%%%%%%%%%%%%%%%%%%%%%%%%%
figure(8)
orient tall
subplot(411)
loglog(f(1:length(f)-1),Cg1,'-',f(1:length(f)-1),abs(Cg1),':')
ylabel('Cg(c04,c06)')
axis([0 mf 1e0 1e5])
legend('Positive','Negative')
title('Group Speed, Cg=dw/dk, in m/sec')
subplot(412)
loglog(f(1:length(f)-1),Cg2,'-',f(1:length(f)-1),abs(Cg2),':')
ylabel('Cg(c06,c08)')
axis([0 mf 1e0 1e5])
subplot(413)
loglog(f(1:length(f)-1),Cg3,'-',f(1:length(f)-1),abs(Cg3),':')
ylabel('Cg(c08,c10)')
axis([0 mf 1e0 1e5])
subplot(414)
loglog(f(1:length(f)-1),Cg4,'-',f(1:length(f)-1),abs(Cg4),':')
ylabel('Cg(c10,c12)')
axis([0 mf 1e0 1e5])
%%%%%%%%%%%%%%%%%%%%%%%%%%%%%%%%%%%%%%%%%%%%%%%%%%%%%%%%%%%%%%%%%%%%%%%%
figure(9)
orient tall
subplot(411)
loglog(f(1:length(f)-1),Tg1,'-',f(1:length(f)-1),abs(Tg1),':')
ylabel('Gtau(c04,c06)')
axis([0 mf 1e-5 1e0])
legend('Positive','Negative')
title('Group Delay, Gtau=dX/Cg, in sec')
subplot(412)

```



```

ba10=data(:,63);
ba12=data(:,67);
clear data q1 q2 q3 q4 q5 q6 q7
%%%%%%%%%%%%%%%%%%%%%%%%%%%%%%%%%%%%%%%%%%%%%%%%%%%%%%%%%%%%%%%%%%%%%%%%
%%%%%
%%%%%          Coherence Factor ref: Force at B04
%%%%%
%%%%%          |Saf|^2
%%%%% Kf = -----
%%%%%          SaaSff
%%%%%
%%%%%%%%%%%%%%%%%%%%%%%%%%%%%%%%%%%%%%%%%%%%%%%%%%%%%%%%%%%%%%%%%%%%%%%%
Kf0402 =(abs(bf02)).^2/(ff.*b02);
Kf0404 =(abs(bf04)).^2/(ff.*b04);
Kf0406 =(abs(bf06)).^2/(ff.*b06);
Kf0408 =(abs(bf08)).^2/(ff.*b08);
Kf0410 =(abs(bf10)).^2/(ff.*b10);
Kf0412 =(abs(bf12)).^2/(ff.*b12);
%%%%%%%%%%%%%%%%%%%%%%%%%%%%%%%%%%%%%%%%%%%%%%%%%%%%%%%%%%%%%%%%%%%%%%%%
%%%%%
%%%%%          Coherence Factor ref: Accel at B04
%%%%%
%%%%%          |a1a2*|^2
%%%%% Ka = ----- , |a1a2*|^2 = (abs(conj(a2a1*)))^2
%%%%%          a1a1*a2a2*
%%%%%
%%%%%%%%%%%%%%%%%%%%%%%%%%%%%%%%%%%%%%%%%%%%%%%%%%%%%%%%%%%%%%%%%%%%%%%%
Ka0402 =(abs(ba02)).^2/(b04.*b02);
Ka0404 =(abs(ba04)).^2/(b04.*b04);
Ka0406 =(abs(ba06)).^2/(b04.*b06);
Ka0408 =(abs(ba08)).^2/(b04.*b08);
Ka0410 =(abs(ba10)).^2/(b04.*b10);
Ka0412 =(abs(ba12)).^2/(b04.*b12);
%%%%% change mf & mfk for plot axis
% delta f
df=mf/nf
mfk=floor(mf/1e3);
if mfk==1
    mfk=1.5;
end
%%%%% axis tailoring
mfk;
mf=mfk*1e3;
%%%%%%%%%%%%%%%%%%%%%%%%%%%%%%%%%%%%%%%%%%%%%%%%%%%%%%%%%%%%%%%%%%%%%%%%
figure(1)
orient tall
subplot(511)
plot(fk,Kf0404)
axis([0 mfk 0 1])
ylabel('Coh(F,b04)')
title('Coherence Function between Input Force and Acceleration at Base Struts')
subplot(512)
plot(fk,Kf0406)
axis([0 mfk 0 1])
ylabel('Coh(F,b06)')
subplot(513)
plot(fk,Kf0408)
axis([0 mfk 0 1])
ylabel('Coh(F,b08)')
subplot(514)
plot(fk,Kf0410)
axis([0 mfk 0 1])
ylabel('Coh(F,b10)')
subplot(515)
plot(fk,Kf0412)
axis([0 mfk 0 1])
ylabel('Coh(F,b12)')
xlabel('Frequency in kHz')

```

```

%%%%%%%%%%%%%%%%%%%%%%%%%%%%%%%%%%%%%%%%%%%%%%%%%%%%%%%%%%%%%%%%%%%%%%%%
return
%%%%%%%%%%%%%%%%%%%%%%%%%%%%%%%%%%%%%%%%%%%%%%%%%%%%%%%%%%%%%%%%%%%%%%%%

```

```

%%%%%%%%%%%%%%%%%%%%%%%%%%%%%%%%%%%%%%%%%%%%%%%%%%%%%%%%%%%%%%%%%%%%%%%%
%%%%%
%%%%% Natural Frequencies of Truss Struts
%%%%%
%%%%%%%%%%%%%%%%%%%%%%%%%%%%%%%%%%%%%%%%%%%%%%%%%%%%%%%%%%%%%%%%%%%%%%%%
E=70e9;
G=26e9;
rho=2700;
kappa=3.9e-3;
Cl=sqrt(E/rho);
Ct=sqrt(G/rho);
%%%%% lengths of struts
L1=0.484;
L2=0.700;
L3=0.810;
%%%%%%%%%%%%%%%%%%%%%%%%%%%%%%%%%%%%%%%%%%%%%%%%%%%%%%%%%%%%%%%%%%%%%%%%
%%%%% for L=0.484
%%%%%%%%%%%%%%%%%%%%%%%%%%%%%%%%%%%%%%%%%%%%%%%%%%%%%%%%%%%%%%%%%%%%%%%%
flong=0;
ftors=0;
i=1; %dummy control var
while flong < 25e3,
flong=i*Cl*L1;
flongL1(i)=flong;
i=i+1;
end
i=1; %dummy control var
while ftors < 25e3,
ftors=i*Ct*L1;
ftorsL1(i)=ftors;
i=i+1;
end
%%%%% fn for bending wave of an E-B beam
%%%%% fn=(b_nL)^2*Cl*kappa/(2*pi*L^2)
bL=[4.730041 7.853205 10.995608 14.137165];
fflexL1 = bL.^2.*Cl*kappa/(2*pi*L1^2);
i=4; %dummy control var
while fflexL1(i) < 25e3,
bL(i+1)=bL(i)+pi;
fflexL1(i+1)=bL(i+1)^2*Cl*kappa/(2*pi*L1^2);
i=i+1;
end
SignlongL1=ones(1,length(flongL1));
SigntorsL1=ones(1,length(ftorsL1));
SignflexL1=ones(1,length(fflexL1));
%%%%%%%%%%%%%%%%%%%%%%%%%%%%%%%%%%%%%%%%%%%%%%%%%%%%%%%%%%%%%%%%%%%%%%%%
%%%%% for L=0.700
%%%%%%%%%%%%%%%%%%%%%%%%%%%%%%%%%%%%%%%%%%%%%%%%%%%%%%%%%%%%%%%%%%%%%%%%
flong=0;
ftors=0;
i=1; %dummy control var
while flong < 25e3,
flong=i*Cl*L2;
flongL2(i)=flong;
i=i+1;
end
i=1; %dummy control var
while ftors < 25e3,
ftors=i*Ct*L2;
ftorsL2(i)=ftors;
i=i+1;
end
%%%%% fn for bending wave of an E-B beam

```

```

%%%%% fn=(b_nL)^2*C1*kappa/(2*pi*L^2)
bL=[4.730041 7.853205 10.995608 14.137165];
fflexL2 = bL.^2.*C1*kappa/(2*pi*L2^2);
i=4; %dummy control var
while fflexL2(i) < 25e3,
bL(i+1)=bL(i)+pi;
fflexL2(i+1)=bL(i+1)^2*C1*kappa/(2*pi*L2^2);
i=i+1;
end
SignlongL2=ones(1,length(flongL2));
SigntorsL2=ones(1,length(ftorsL2));
SignflexL2=ones(1,length(fflexL2));
%%%%%%%%%%%%%%%%%%%%%%%%%%%%%%%%%%%%%%%%%%%%%%%%%%%%%%%%%%%%%%%%%%%%%%%%
%%%%% for L=0.810
%%%%%%%%%%%%%%%%%%%%%%%%%%%%%%%%%%%%%%%%%%%%%%%%%%%%%%%%%%%%%%%%%%%%%%%%
flong=0;
ftors=0;
i=1; %dummy control var
while flong < 25e3,
flong=i*C1*L3;
flongL3(i)=flong;
i=i+1;
end
i=1; %dummy control var
while ftors < 25e3,
ftors=i*Ct*L3;
ftorsL3(i)=ftors;
i=i+1;
end
%%%%% fn for bending wave of an E-B beam
%%%%% fn=(b_nL)^2*C1*kappa/(2*pi*L^2)
bL=[4.730041 7.853205 10.995608 14.137165];
fflexL3 = bL.^2.*C1*kappa/(2*pi*L3^2);
i=4; %dummy control var
while fflexL3(i) < 25e3,
bL(i+1)=bL(i)+pi;
fflexL3(i+1)=bL(i+1)^2*C1*kappa/(2*pi*L3^2);
i=i+1;
end
SignlongL3=ones(1,length(flongL3));
SigntorsL3=ones(1,length(ftorsL3));
SignflexL3=ones(1,length(fflexL3));
%%%%%%%%%%%%%%%%%%%%%%%%%%%%%%%%%%%%%%%%%%%%%%%%%%%%%%%%%%%%%%%%%%%%%%%%
figure(1)
orient tall
subplot(311)
plot(flongL1/1e3,SignlongL1.*.6,'x',flongL2/1e3,SignlongL2.*.8,'o',...
flongL3/1e3,SignlongL3,'+',flongL1/1e3,SignlongL1.*.4,'.',...
flongL2/1e3,SignlongL2.*.4,'.',flongL3/1e3,SignlongL3.*.4,'.')
title('Resonance Frequency of Compressional Wave')
set(gca,'YTickLabels','')
ylabel('')
axis([0 25 0 1.2])
subplot(312)
plot(ftorsL1/1e3,SigntorsL1.*.6,'x',ftorsL2/1e3,SigntorsL2.*.8,'o',...
ftorsL3/1e3,SigntorsL3,'+',ftorsL1/1e3,SigntorsL1.*.4,'.',...
ftorsL2/1e3,SigntorsL2.*.4,'.',ftorsL3/1e3,SigntorsL3.*.4,'.')
title('Torsional Wave')
set(gca,'YTickLabels','')
ylabel('')
axis([0 25 0 1.2])
subplot(313)
plot(fflexL1/1e3,SignflexL1.*.6,'x',fflexL2/1e3,SignflexL2.*.8,'o',...
fflexL3/1e3,SignflexL3,'+',fflexL1/1e3,SignflexL1.*.4,'.',...
fflexL2/1e3,SignflexL2.*.4,'.',fflexL3/1e3,SignflexL3.*.4,'.')
title('Flexural Wave (Euler-Bernoulli Beam)')
set(gca,'YTickLabels','')
xlabel('Frequency in kHz')

```

```

ylabel('')
axis([0 25 0 1.2])
%%%%%%%%%%%%%%%%%%%%%%%%%%%%%%%%%%%%%%%%%%%%%%%%%%%%%%%%%%%%%%%%%%%%%%%%
figure(2)
orient tall
subplot(311)
plot(flongL3/1e3,SignlongL3*.6,'x',ftorsL3/1e3,SigntorsL3*.8,'o',...
fflexL3/1e3,SignflexL3,'+',flongL3/1e3,SignlongL3*.4,'.',...
ftorsL3/1e3,SigntorsL3*.4,'.',fflexL3/1e3,SignflexL3*.4,'.')
title('Resonance Frequency of Strut of l=810')
set(gca,'YTickLabels','')
ylabel('')
axis([0 25 0 1.2])
subplot(312)
plot(flongL2/1e3,SignlongL2*.6,'x',ftorsL2/1e3,SigntorsL2*.8,'o',...
fflexL2/1e3,SignflexL2,'+',flongL2/1e3,SignlongL2*.4,'.',...
ftorsL2/1e3,SigntorsL2*.4,'.',fflexL2/1e3,SignflexL2*.4,'.')
title('Strut of l=700')
set(gca,'YTickLabels','')
ylabel('')
axis([0 25 0 1.2])
subplot(313)
plot(flongL1/1e3,SignlongL1*.6,'x',ftorsL1/1e3,SigntorsL1*.8,'o',...
fflexL1/1e3,SignflexL1,'+',flongL1/1e3,SignlongL1*.4,'.',...
ftorsL1/1e3,SigntorsL1*.4,'.',fflexL1/1e3,SignflexL1*.4,'.')
title('Strut of l=484')
set(gca,'YTickLabels','')
xlabel('Frequency in kHz')
ylabel('')
axis([0 25 0 1.2])
%%%%%%%%%%%%%%%%%%%%%%%%%%%%%%%%%%%%%%%%%%%%%%%%%%%%%%%%%%%%%%%%%%%%%%%%
figure(3)
plot(flongL3/1e3,SignlongL3*.6,'x',ftorsL3/1e3,SigntorsL3*.8,'o',...
fflexL3/1e3,SignflexL3,'+',flongL3/1e3,SignlongL3*.4,'.',...
ftorsL3/1e3,SigntorsL3*.4,'.',fflexL3/1e3,SignflexL3*.4,'.')
hold
plot(flongL2/1e3,SignlongL2*.6,'x',ftorsL2/1e3,SigntorsL2*.8,'o',...
fflexL2/1e3,SignflexL2,'+',flongL2/1e3,SignlongL2*.4,'.',...
ftorsL2/1e3,SigntorsL2*.4,'.',fflexL2/1e3,SignflexL2*.4,'.')
plot(flongL1/1e3,SignlongL1*.6,'x',ftorsL1/1e3,SigntorsL1*.8,'o',...
fflexL1/1e3,SignflexL1,'+',flongL1/1e3,SignlongL1*.4,'.',...
ftorsL1/1e3,SigntorsL1*.4,'.',fflexL1/1e3,SignflexL1*.4,'.')
title('Resonance Frequency of Truss')
xlabel('Frequency in kHz')
ylabel('')
set(gca,'YTickLabels','')
axis([0 25 0 1.2])
hold
%%%%%%%%%%%%%%%%%%%%%%%%%%%%%%%%%%%%%%%%%%%%%%%%%%%%%%%%%%%%%%%%%%%%%%%%
return
%%%%%%%%%%%%%%%%%%%%%%%%%%%%%%%%%%%%%%%%%%%%%%%%%%%%%%%%%%%%%%%%%%%%%%%%

```

```

%%%%%%%%%%%%%%%%%%%%%%%%%%%%%%%%%%%%%%%%%%%%%%%%%%%%%%%%%%%%%%%%%%%%%%%%
%%%%%
%%%%% Global to Local transition of truss dynamics
%%%%%
%%%%%%%%%%%%%%%%%%%%%%%%%%%%%%%%%%%%%%%%%%%%%%%%%%%%%%%%%%%%%%%%%%%%%%%%
rho=2700; % density of Al6061
E=70e9; % Young's modulus
G=26e9; % Shear modulus
K=3.950e-3; % radius of gyration
f=[0:10:25e3];
w=f.*(2*pi);
Cl=sqrt(E/rho); % longitudinal wave speed
Ct=sqrt(G/rho); % torsional wave speed
%%%%% Timoshenko Beam
tc=0.545; % Timoshenko shear coeff. for thin-walled pipe 0.5^0.545

```

```

A=(rho/E+rho/(tc*G));
B=(rho/E/K^2);
C=(rho^2/(E*tc*G));
kT= sqrt(w.^2*2*A + sqrt(w.^4*(A^2-4*C)+w.^2*B*4).*2).*0.5;
CTp=w./kT;
CTg= ((sqrt(w.^2*A*2 + sqrt(w.^4*(A^2-4*C)+w.^2*B*4).*2)) ./ ...
      (w.*A^4+(w.^3*(A^2*4-16*C)+w.*B*8)./sqrt(w.^4*(A^2-4*C)+w.^2*B*4))).*4;
%%%% Euler Beam
kB=sqrt(w).*(rho/E/K^2)^(1/4);
CBp=sqrt(w).*(E*K^2/rho)^(1/4);
CBg=sqrt(w).*2.*(E*K^2/rho)^(1/4);
%%%%%%%%%%%%%%%%%%%%%%%%%%%%%%%%%%%%%%%%%%%%%%%%%%%%%%%%%%%%%%%%%%%%%%%%
% wave length
f=1e3,2*pi*ones(size(kB))./kB,...
%%%%%%%%%%%%%%%%%%%%%%%%%%%%%%%%%%%%%%%%%%%%%%%%%%%%%%%%%%%%%%%%%%%%%%%%
figure(1)
orient tall
subplot(211)
plot(f/1e3,(2*pi)./kT./2,'-',...
      f/1e3,Ct./f./2,'--',...
      f/1e3,C1./f./2,'-.',...
      f(1:1600)/1e3,ones(1,1600).*0.70,'-',...
      f(1:1600)/1e3,ones(1,1600).*0.81,'-',...
      f(1:1600)/1e3,ones(1,1600).*0.484,'-')
title('Half Wave Length vs. Frequency')
legend('flex','tors','comp')
text(13,.84,'Diagonal Strut')
text(13,.73,'Horizontal Strut')
text(13,.514,'Base Strut')
ylabel('Half Wave Length in meter')
xlabel('Frequency in kHz')
axis([0 25 0 1])
grid
subplot(212)
plot(f/1e3,(2*pi)./kT,'-',...
      f/1e3,Ct./f,'--',...
      f/1e3,C1./f,'-.',...
      f(1:1600)/1e3,ones(1,1600).*0.70,'-',...
      f(1:1600)/1e3,ones(1,1600).*0.81,'-',...
      f(1:1600)/1e3,ones(1,1600).*0.484,'-')
title('Wave Length vs. Frequency')
%legend('flex','tors','comp')
text(13,.84,'Diagonal Strut')
text(13,.73,'Horizontal Strut')
text(13,.514,'Base Strut')
ylabel('Wave Length in meter')
xlabel('Frequency in kHz')
axis([0 25 0 1])
grid
%%%%%%%%%%%%%%%%%%%%%%%%%%%%%%%%%%%%%%%%%%%%%%%%%%%%%%%%%%%%%%%%%%%%%%%%
return
%%%%%%%%%%%%%%%%%%%%%%%%%%%%%%%%%%%%%%%%%%%%%%%%%%%%%%%%%%%%%%%%%%%%%%%%

%%%%%%%%%%%%%%%%%%%%%%%%%%%%%%%%%%%%%%%%%%%%%%%%%%%%%%%%%%%%%%%%%%%%%%%%
%%%%%%
%%%%%% Array Processing with Cross-Spectra at Joints
%%%%%%%%%%%%%%%%%%%%%%%%%%%%%%%%%%%%%%%%%%%%%%%%%%%%%%%%%%%%%%%%%%%%%%%%
%load /arctic1/jhpark/truss/Feb13/b4b4zS25
%mf=25600
load /arctic1/jhpark/truss/Feb13/b4b4zS5_25K
mf=6400
%load /arctic1/jhpark/truss/Feb13/b4b4zS1_25K
%mf=1600
%
% put proper stuff in A
A(1,:)=(data(:,27)./data(:,1)).';

```



```

A(2,:)=(data(:,30)./data(:,1)).';
A(3,:)=(data(:,34)./data(:,1)).';
A(4,:)=(data(:,38)./data(:,1)).';
A(5,:)=(data(:,42)./data(:,1)).';
A(6,:)=(data(:,46)./data(:,1)).';
%Frequency wavenumber spectrum
i = sqrt(-1);
N=6
nf=3201
df=32
dx=0.783
nk=400
mk=pi/(dx)
dk=2*mk/nk
a=1
j = [0:N-1];
z([1:N],1) = (j*dx)';
z([1:N],2) = (0*j)';
for f=0:df:nf,
    f*mf/(1000*nf)
    fi=f/df+1;
    %calculate sx
    sx = zeros(N,N);
    for n=1:N,
        xa(n) = A(n,f+1);
    end
    sxa = xa.' * conj(xa);
    %calculate p(w,k)
    for k = -mk:dk:mk
        c = 1+ (k+mk)/dk;
        kt = [k;0];
        et = exp(-i*z*kt);
%     etn = et.*hamming(N);
%     norm = sum(hamming(N));
        pa(fi,c) = (et'*sxa*et)/(N*N);
%     pa(fi,c) = (etn'*sxa*etn)/(norm*norm);
    end
end
pa = 20*log10(abs(pa));
f=[0:nf/df]*mf/((nf/df)*1000);
k=a*[-mk:dk:mk];
%%%%%%%%%%%%%%%%%%%%%%%%%%%%%%%%%%%%%%%%%%%%%%%%%%%%%%%%%%%%%%%%%%%%%%%%
figure(1)
imagesc(k,f,pa)
axis('xy')
colormap(gray),colorbar
shading('flat')
xlabel('Wavenumber in 1/m');
ylabel('Frequency in kHz')
title('Frequency Wavenumber (f-k) Spectrum dB re 1/kg')
axis([-mk*a,mk*a,0,mf/1e3])
%%%%%%%%%%%%%%%%%%%%%%%%%%%%%%%%%%%%%%%%%%%%%%%%%%%%%%%%%%%%%%%%%%%%%%%%
figure(2)
plot(f,pa(:,202))
axis([0 mf/1e3 -140 40])
title('Inertance Frequency Spectrum at k=0.02 m^-1')
xlabel('Frequency in kHz')
ylabel('Inertance in dB re 1/kg')
%%%%%%%%%%%%%%%%%%%%%%%%%%%%%%%%%%%%%%%%%%%%%%%%%%%%%%%%%%%%%%%%%%%%%%%%
figure(3)
plot(k,pa(85,:),'-',k,pa(60,:),'-',k,pa(46,:),'-',k,pa(24,:),':')
l1=sprintf('%4.0fHz',floor(f(85).*1e3));
l2=sprintf('%4.0fHz',floor(f(60).*1e3));
l3=sprintf('%4.0fHz',floor(f(46).*1e3));
l4=sprintf('%4.0fHz',floor(f(24).*1e3));
legend(l1,l2,l3,l4)
axis([-mk*a mk*a -40 40])
title('Inertance Wavenumber Spectrum')

```

```

xlabel('Wavenumber in 1/m')
ylabel('Magnitude dB re 1/kg')
%%%%%%%%%%%%%%%%%%%%%%%%%%%%%%%%%%%%%%%%%%%%%%%%%%%%%%%%%%%%%%%%%%%%%%%%
%%%% find aliasing occurring frequency
%%%% with an assumption of the same elastic wave propagation
%%%% of aluminum struts
%%%%%%%%%%%%%%%%%%%%%%%%%%%%%%%%%%%%%%%%%%%%%%%%%%%%%%%%%%%%%%%%%%%%%%%%
clear
rho=2700; % density of Al6061
E=70e9; % Young's modulus
G=26e9; % Shear modulus
K=3.950e-3; % radius of gyration
f=linspace(0,4e3,2000);
w=f.*(2*pi);
Cl=sqrt(E/rho); % longitudinal wave speed
Ct=sqrt(G/rho); % torsional wave speed
Kl=(f./Cl).*2*pi; % longitudinal wavenumber
Kt=(f./Ct).*2*pi; % torsional wavenumber
%%%%%%%%%%%%%%%%%%%%%%%%%%%%%%%%%%%%%%%%%%%%%%%%%%%%%%%%%%%%%%%%%%%%%%%%
%%%% Timoshenko Beam
tc=0.545; % Timoshenko shear coeff. for thin-walled pipe 0.5~0.545
A=(rho/E+rho/(tc*G));
B=(rho/E/K^2);
C=(rho^2/(E*tc*G));
kT= sqrt(w.^2*A + sqrt(w.^4*(A^2-4*C)+w.^2*B*4).*2).*0.5;
CTp=w./kT;
CTg= ((sqrt(w.^2*A + sqrt(w.^4*(A^2-4*C)+w.^2*B*4).*2)) ./ ...
      (w.*A*4+(w.^3*(A^2*4-16*C)+w.*B*8)./sqrt(w.^4*(A^2-4*C)+w.^2*B*4))).*4;
%%%%%%%%%%%%%%%%%%%%%%%%%%%%%%%%%%%%%%%%%%%%%%%%%%%%%%%%%%%%%%%%%%%%%%%%
% wave length
% f/1e3,2*pi*ones(size(kB))./kB,...
% wavenumber
% k=2pi/wavelength, 2pi*freq/c
% Nyquist pi/dz
%%%%%%%%%%%%%%%%%%%%%%%%%%%%%%%%%%%%%%%%%%%%%%%%%%%%%%%%%%%%%%%%%%%%%%%%
figure(4)
plot(f/1e3,kT,'-',...
      f/1e3,Kt,'--',...
      f/1e3,Kl,'-.')
title('Wavenumber vs. Frequency')
legend('flex','tors','comp')
xlabel('Frequency in kHz')
ylabel('Wavenumber')
axis([0 4 0 pi/0.783])
%%%%%%%%%%%%%%%%%%%%%%%%%%%%%%%%%%%%%%%%%%%%%%%%%%%%%%%%%%%%%%%%%%%%%%%%
return
%%%%%%%%%%%%%%%%%%%%%%%%%%%%%%%%%%%%%%%%%%%%%%%%%%%%%%%%%%%%%%%%%%%%%%%%

```

### Chapter 3

```

%%%%%%%%%%%%%%%%%%%%%%%%%%%%%%%%%%%%%%%%%%%%%%%%%%%%%%%%%%%%%%%%%%%%%%%%
%%%%%
%%%%% Wave speed matrix to calculate arrival time
%%%%%
%%%%%%%%%%%%%%%%%%%%%%%%%%%%%%%%%%%%%%%%%%%%%%%%%%%%%%%%%%%%%%%%%%%%%%%%
clear
rho=2700; % density of Al6061
E=70e9; % Young's modulus
G=26e9; % Shear modulus
K=3.950e-3; % radius of gyration
f=[16e3 8e3 4e3 2e3 1e3 .5e3 .25e3 .125e3];
w=f.*2*pi;
%%%%% Timoshenko Beam
tc=0.545; % Timoshenko shear coeff. for thin-walled pipe 0.5^0.545
A=(rho/E+rho/(tc*G));
B=(rho/E/K^2);
C=(rho^2/(E*tc*G));
% Timoshenko
kT= sqrt(w.^2*A + sqrt(w.^4*(A^2-4*C)+w.^2*B*4).*2).*0.5;
CTp=w./kT;
CTg= ((sqrt(w.^2*A*2 + sqrt(w.^4*(A^2-4*C)+w.^2*B*4).*2)) ./ ...
(w.*A^4+(w.^3*(A^2-16*C)+w.*B*8)./sqrt(w.^4*(A^2-4*C)+w.^2*B*4))).*4;
kTa= sqrt(w.^2*A + sqrt(w.^4*A^2+w.^2*B*4).*2).*0.5;
CTpa=w./kTa;
CTga= ((sqrt(w.^2*A*2 + sqrt(w.^4*A^2+w.^2*B*4).*2)) ./ ...
(w.*A^4+(w.^3*A^2*4+w.*B*8)./sqrt(w.^4.*A^2+w.^2*B*4))).*4;
% Euler
CBp=sqrt(w.*(E*K^2/rho)^(1/4));
CBg=2*CBp;
Cl=sqrt(E/rho);
Ct=sqrt(G/rho);
Clt=[Cl Ct]';
Cg=[f' CTg' CTga' CBg'];
Cp=[f' CTp' CTpa' CBp'];
%%%%%%%%%%%%%%%%%%%%%%%%%%%%%%%%%%%%%%%%%%%%%%%%%%%%%%%%%%%%%%%%%%%%%%%%
%%%%% Timoshenko
% SRC at a4c4
% tmp(1,:) : distance between joints
%          C04 a04 b05 C06 b07 C08 b09 C10 b11 C12
Ttmp(1,1:10) = [.545 .165 .480 .480 .483 .482 .484 .487 .480 .490];
% tmp(2:11,:) : travel time in 'msec'
Ttmp(2,:)=Ttmp(1,:)/Cl*1e3;
Ttmp(3,:)=Ttmp(1,:)/Ct*1e3;
for i=1:8,
Ttmp(i+3,:)=Ttmp(1,:)/CTg(i)*1e3;
end
Ttmp;
%%%%% Travel time matrix W/O WAVE-FORM CHANGE AFTER JOINTS
%   dtime(1,1:5) : C04 C06 C08 C10 C12
%   dtime(1:11,1) : Dist Tc Tt Tf16 8 4 2 1 0.5 0.25 0.125
%%%%% C04
Ttime(:,1) = Ttmp(:,1);
%%%%% C06
Ttime(:,2) = Ttmp(:,2) + Ttmp(:,3) + Ttmp(:,4);
%%%%% C08
Ttime(:,3) = Ttime(:,2) + Ttmp(:,5) + Ttmp(:,6);
%%%%% C10
Ttime(:,4) = Ttime(:,3) + Ttmp(:,7) + Ttmp(:,8);
%%%%% C12
Ttime(:,5) = Ttime(:,4) + Ttmp(:,9) + Ttmp(:,10);
round(Ttime.*100)/100;
%%%%%%%%%%%%%%%%%%%%%%%%%%%%%%%%%%%%%%%%%%%%%%%%%%%%%%%%%%%%%%%%%%%%%%%%
%%%%% Euler-Bernoulli
% SRC at a4c4
% tmp(1,:) : distance between joints
%          C04 a04 b05 C06 b07 C08 b09 C10 b11 C12

```

```

% tmp(2:11,:) : travel time in 'msec'
Btmp(1:3,1:10) = Ttmp(1:3,1:10);
for i=1:8,
Btmp(i+3,:)=Btmp(1,:)/CBg(i)*1e3;
end
Btmp;
%%%%% Travel time matrix W/O WAVE-FORM CHANGE AFTER JOINTS
%  dtime(1,1:5) : C04 C06 C08 C10 C12
%  dtime(1:11,1) : Dist Tc Tt Tf16 8 4 2 1 0.5 0.25 0.125
%%%%% C04
Btime(:,1) = Btmp(:,1);
%%%%% C06
Btime(:,2) = Btmp(:,2) + Btmp(:,3) + Btmp(:,4);
%%%%% C08
Btime(:,3) = Btime(:,2) + Btmp(:,5) + Btmp(:,6);
%%%%% C10
Btime(:,4) = Btime(:,3) + Btmp(:,7) + Btmp(:,8);
%%%%% C12
Btime(:,5) = Btime(:,4) + Btmp(:,9) + Btmp(:,10);
Btime;
%%%%%%%%%%%%%%%%%%%%%%%%%%%%%%%%%%%%%%%%%%%%%%%%%%%%%%%%%%%%%%%%%%%%%%%%
%%%%% Calculate all travel time w/ all wave possibilities
% Make transpose since the direction of calculation of SUM, MEAN, STD
% is vertical not horizontal !

% Mean dist, arrival time
% Dist, Tc, Tt, Tf16 8, 4, 2, 1, .5, .25, .125
Tmean=mean(Ttmp(:,3:10)');
%%%%% Possibility of traveling waves
% 1: compressional, 2: torsional, 3: flexural
% B05 C06 (6 x 2)
C06= [1 1;
1 2;
1 3;
2 2;
2 3;
3 3];
% B05 C06 B07 C08 (15 x 4)
C08= [1 1 1 1;
1 1 1 2;
1 1 1 3;
1 1 2 2;
1 1 2 3;
1 1 3 3;
1 2 2 2;
1 2 2 3;
1 2 3 3;
1 3 3 3;
2 2 2 2;
2 2 2 3;
2 2 3 3;
2 3 3 3;
3 3 3 3];
% B05 C06 B07 C08 B09 C10 (28 x 6)
C10= [1 1 1 1 1 1;
1 1 1 1 1 2;
1 1 1 1 1 3;
1 1 1 1 2 2;
1 1 1 1 2 3;
1 1 1 1 3 3;
1 1 1 2 2 2;
1 1 1 2 2 3;
1 1 1 2 3 3;
1 1 1 3 3 3;
1 1 2 2 2 2;
1 1 2 2 2 3;
1 1 2 2 3 3;
1 1 2 3 3 3;
1 1 2 3 3 3];

```

```

1 1 3 3 3 3;
1 2 2 2 2 2;
1 2 2 2 2 3;
1 2 2 2 3 3;
1 2 2 3 3 3;
1 2 3 3 3 3;
1 3 3 3 3 3;
2 2 2 2 2 2;
2 2 2 2 2 3;
2 2 2 2 3 3;
2 2 2 3 3 3;
2 2 3 3 3 3;
2 3 3 3 3 3;
3 3 3 3 3 3];
% B05 C06 B07 C08 B09 C10 B11 C12 (45 x 8)
C12= [1 1 1 1 1 1 1 1;
1 1 1 1 1 1 1 2;
1 1 1 1 1 1 1 3;
1 1 1 1 1 1 2 2;
1 1 1 1 1 1 2 3;
1 1 1 1 1 1 3 3;
1 1 1 1 1 2 2 2;
1 1 1 1 1 2 2 3;
1 1 1 1 1 2 3 3;
1 1 1 1 1 3 3 3;
1 1 1 1 2 2 2 2;
1 1 1 1 2 2 2 3;
1 1 1 1 2 2 3 3;
1 1 1 1 2 3 3 3;
1 1 1 1 3 3 3 3;
1 1 1 2 2 2 2 2;
1 1 1 2 2 2 2 3;
1 1 1 2 2 2 3 3;
1 1 1 2 2 3 3 3;
1 1 1 2 3 3 3 3;
1 1 1 3 3 3 3 3;
1 1 2 2 2 2 2 2;
1 1 2 2 2 2 2 3;
1 1 2 2 2 2 3 3;
1 1 2 2 2 3 3 3;
1 1 2 2 3 3 3 3;
1 2 2 2 2 2 2 2;
1 2 2 2 2 2 2 3;
1 2 2 2 2 3 3 3;
1 2 2 2 3 3 3 3;
1 2 2 3 3 3 3 3;
1 2 3 3 3 3 3 3;
1 3 3 3 3 3 3 3;
2 2 2 2 2 2 2 2;
2 2 2 2 2 2 2 3;
2 2 2 2 2 2 3 3;
2 2 2 2 2 3 3 3;
2 2 2 2 3 3 3 3;
2 2 2 3 3 3 3 3;
2 2 3 3 3 3 3 3;
2 3 3 3 3 3 3 3;
3 3 3 3 3 3 3 3];
%%%% calculate
%%%% set Travel-time matrix [comp, tors, flex]
%%%%%%%%%%%%%%%%%%%%%%%%%%%%%%%%%%%%%%%%%%%%%%%%%%%%%%%%%%%%%%%%%%%%%%%%
%%%% freq 16 8 4 2 1 .5 .25 .125
%%%% Flexf 4 5 6 7 8 9 10 11
Flexf=7;
Traveltime=[Tmean(2:3) Tmean(Flexf)];
position=C12;

```

```

[M,N]=size(position);
time=zeros(M,1);
for i=1:M,
    for j=1:N,
        if position(i,j) == 1 % compressional
            time(i) = time(i) + Traveltime(1);
        elseif position(i,j) == 2 % torsional
            time(i) = time(i) + Traveltime(2);
        else % flexural
            time(i) = time(i) + Traveltime(3);
        end
    end
end
%%%%% Final time including Comp, Tors, Flex at A4
Ftime(:,1)=time + ones(M,1).*Ttmp(2,2);
Ftime(:,2)=time + ones(M,1).*Ttmp(3,2);
%%%%%%%%%%%%%%%%%%%%%%%%%%%%%%%%%%%%%%%%%%%%%%%%%%%%%%%%%%%%%%%%%%%%%%%%%%%%%%
% Flex time location 16 8 4 ... -> Ttmp(4:11,2)
Ftime(:,3)=time + ones(M,1).*Ttmp(Flexf,2);
%%%%% Result      Comp Tors Flex at A04
Result=[position round(Ftime.*100)./100]
%%%%%%%%%%%%%%%%%%%%%%%%%%%%%%%%%%%%%%%%%%%%%%%%%%%%%%%%%%%%%%%%%%%%%%%%%%%%%%
%%%%%%%%%%%%%%%%%%%%%%%%%%%%%%%%%%%%%%%%%%%%%%%%%%%%%%%%%%%%%%%%%%%%%%%%%%%%%%
%%%%% C04
%%%%% direct arrival time can be found from Ttime
%%%%% freq 16 8 4 2 1 .5 .25 .125
%%%%% Flexf 4 5 6 7 8 9 10 11
Flexf=7;
% reflect from a04 to c04
C04_1 = [1 1;
         1 2;
         1 3;
         2 2;
         2 3;
         3 3];
% travel path src -> c04 -> a04 -> c04
C04_2 = [1 1 1;
         1 1 2;
         1 1 3;
         1 2 2;
         1 2 3;
         1 3 3;
         2 2 2;
         2 2 3;
         2 3 3;
         3 3 3];
a4c4=Ttmp(2:11,1)+Ttmp(2:11,2);
Ftime1=zeros(6,1);
for i = 1:6,
    if C04_1(i,1) == 1
        Ftime1(i)=Ttmp(2,1);
    elseif C04_1(i,1) == 2
        Ftime1(i)=Ttmp(3,1);
    else
        Ftime1(i)=Ttmp(Flexf,1);
    end
end
for i = 1:6,
    if C04_1(i,2) == 1
        Ftime1(i)=Ftime1(i) + a4c4(2,1);
    elseif C04_1(i,2) == 2
        Ftime1(i)=Ftime1(i) + a4c4(3,1);
    else
        Ftime1(i)=Ftime1(i) + a4c4(Flexf,1);
    end
end
Ftime2=zeros(10,1);
for i = 1:10,

```







```

isrc=ifft(cvsrc);
ic04=ifft(cvc04);
ic06=ifft(cvc06);
ic08=ifft(cvc08);
ic10=ifft(cvc10);
ic12=ifft(cvc12);
%%%%%%%%%%%%%%%%%%%%%%%%%%%%%%%%%%%%%%%%%%%%%%%%%%%%%%%%%%%%%%%%%%%%%%%%
%b=remez(n,f,m);
%y=filtfilt(b,a,x); %a=1 for FIR
%%%%%%%%%%%%%%%%%%%%%%%%%%%%%%%%%%%%%%%%%%%%%%%%%%%%%%%%%%%%%%%%%%%%%%%%
%%25.6kHz LOWPASS
nf= [0 0.8084 0.9094 1];
m = [1 1 0 0];
n=40
b=remez(n,nf,m)*.9906;
%%%%%%%%%%%%%%%%%%%%%%%%%%%%%%%%%%%%%%%%%%%%%%%%%%%%%%%%%%%%%%%%%%%%%%%%
%%FREQUENCY RESPONSE
[H,ff]=freqz(b,1,Fs/2,Fs);
%%%%%%%%%%%%%%%%%%%%%%%%%%%%%%%%%%%%%%%%%%%%%%%%%%%%%%%%%%%%%%%%%%%%%%%%
%%filter
%%%%%%%%%%%%%%%%%%%%%%%%%%%%%%%%%%%%%%%%%%%%%%%%%%%%%%%%%%%%%%%%%%%%%%%%
ftsrc=filtfilt(b,1,isrc);
ftc04=filtfilt(b,1,ic04);
ftc06=filtfilt(b,1,ic06);
ftc08=filtfilt(b,1,ic08);
ftc10=filtfilt(b,1,ic10);
ftc12=filtfilt(b,1,ic12);
ftsrc=ftsrc-mean(ftsrc);
ftc04=ftc04-mean(ftc04);
ftc06=ftc06-mean(ftc06);
ftc08=ftc08-mean(ftc08);
ftc10=ftc10-mean(ftc10);
ftc12=ftc12-mean(ftc12);
%%%%%%%%%%%%%%%%%%%%%%%%%%%%%%%%%%%%%%%%%%%%%%%%%%%%%%%%%%%%%%%%%%%%%%%%
%%'msec' index of time vector
%%%%%%%%%%%%%%%%%%%%%%%%%%%%%%%%%%%%%%%%%%%%%%%%%%%%%%%%%%%%%%%%%%%%%%%%
t1 =length(t)/256+6;
t2 =length(t)/128+5;
t4 =length(t)/64+8; % 4.0131 msec
t5 =length(t)/64+73; % 5.0049 msec
t8 =length(t)/32+14; % 8.0109
t10=length(t)/32+145; %10.0097
t12=length(t)/32+length(t)/64+20; %12.0087
t15=length(t)/16-39; %15.0146
t16=length(t)/16+26; %16.0065
t20=length(t)/16+288; %20.0042
t24=length(t)/16+550; %24.0020
t32=length(t)/8+51; %32.0129
t40=length(t)/8+575; %40.0085
%%%%%%%%%%%%%%%%%%%%%%%%%%%%%%%%%%%%%%%%%%%%%%%%%%%%%%%%%%%%%%%%%%%%%%%%
figure(1)
orient tall
subplot(211)
plot(t(1:F1).*1e3,src)
title('Input Signal in Time Domain')
ylabel('acceleration (m/s^2)')
xlabel('Time in msec')
axis([0,t(t10).*1e3,-300,300])
subplot(212)
plot(f/1000,20*log10(fsrc))
title('Input Signal in Frequency Domain')
ylabel('acceleration dB re m/s^2/Hz')
xlabel('Frequency in kHz')
axis([0,Fs/2000,0,80])
%%%%%%%%%%%%%%%%%%%%%%%%%%%%%%%%%%%%%%%%%%%%%%%%%%%%%%%%%%%%%%%%%%%%%%%%
%%rectangular lowpass filter
nf= [0 0.8084 0.8085 0.9094 1];
m= [1 1 0 0 0];
%%%%%%%%%%%%%%%%%%%%%%%%%%%%%%%%%%%%%%%%%%%%%%%%%%%%%%%%%%%%%%%%%%%%%%%%
figure(2)

```

```

orient portrait
plot(ff/1e3, 20*log10(abs(H)), nf/1e3*(Fs/2), [0 0 -50 -50 -50], '--')
axis([0 Fs/2/1e3 -45 5])
title('Frequency Response of FIR Filter with fc=25.6kHz')
ylabel('20log(H)')
xlabel('Frequency in kHz')
%%%%%%%%%%%%%%%%%%%%%%%%%%%%%%%%%%%%%%%%%%%%%%%%%%%%%%%%%%%%%%%%%%%%%%%%
figure(3)
orient tall
subplot(611)
plot(t, 20*log10(abs(ftsrc)))
title('Magnitude of Lowpass Filtered Impulse Response Function with fc=25.6kHz, dB')
ylabel('SRC')
axis([0, 125e-3, -40, 0])
subplot(612)
plot(t, 20*log10(abs(ftc04)))
ylabel('c04')
axis([0, 125e-3, -65, -25])
subplot(613)
plot(t, 20*log10(abs(ftc06)))
ylabel('c06')
axis([0, 125e-3, -80, -40])
subplot(614)
plot(t, 20*log10(abs(ftc08)))
ylabel('c08')
axis([0, 125e-3, -80, -40])
subplot(615)
plot(t, 20*log10(abs(ftc10)))
ylabel('c10')
axis([0, 125e-3, -80, -40])
subplot(616)
plot(t, 20*log10(abs(ftc12)))
ylabel('c12')
axis([0, 125e-3, -85, -45])
xlabel('Time in sec')
%%%%%%%%%%%%%%%%%%%%%%%%%%%%%%%%%%%%%%%%%%%%%%%%%%%%%%%%%%%%%%%%%%%%%%%%
figure(4)
orient tall
subplot(611)
plot(t.*1e3, 20*log10(abs(ftsrc)))
title('Magnitude of Lowpass Filtered Impulse Response Function with fc=25.6kHz, dB')
ylabel('SRC')
axis([0, 5, -40, 0])
subplot(612)
plot(t.*1e3, 20*log10(abs(ftc04)))
ylabel('c04')
axis([0, 5, -65, -25])
subplot(613)
plot(t.*1e3, 20*log10(abs(ftc06)))
ylabel('c06')
axis([0, 5, -80, -40])
subplot(614)
plot(t.*1e3, 20*log10(abs(ftc08)))
ylabel('c08')
axis([0, 5, -80, -40])
subplot(615)
plot(t.*1e3, 20*log10(abs(ftc10)))
ylabel('c10')
axis([0, 5, -80, -40])
subplot(616)
plot(t.*1e3, 20*log10(abs(ftc12)))
ylabel('c12')
axis([0, 5, -90, -50])
xlabel('Time in msec')
%%%%%%%%%%%%%%%%%%%%%%%%%%%%%%%%%%%%%%%%%%%%%%%%%%%%%%%%%%%%%%%%%%%%%%%%
return
%%%%%%%%%%%%%%%%%%%%%%%%%%%%%%%%%%%%%%%%%%%%%%%%%%%%%%%%%%%%%%%%%%%%%%%%

```

```

%%%%%%%%%%%%%%%%%%%%%%%%%%%%%%%%%%%%%%%%%%%%%%%%%%%%%%%%%%%%%%%%%%%%%%%%
%%
%% Gaussian Bandpass Filtered Output Signal
%%
%%%%%%%%%%%%%%%%%%%%%%%%%%%%%%%%%%%%%%%%%%%%%%%%%%%%%%%%%%%%%%%%%%%%%%%%
%INPUT Trigger freq: 1Hz Trigger:      every frame
% Freq span: 22kHz Level:      10%
% spectral line: 3201 Slope: positive
% Max freq:      25600Hz
% Frame size:    8192 Pretrigger
% delta t:      1.52588e-5 samples:    100
% Frame length: 0.125sec time:      0.00152588
% Sampling freq: 65536.0Hz percentage: 1.2207
Fs=65536;
Fl=8192;
t=[0:16383]/Fs;
f=[0:16383]/(Fl*2)*Fs;
%[data,q1,q2,q3,q4,q5,q6,q7]=ReadUniversal('Bpulse.unv');
load /arctici/jhpark/truss/Oct30/Bpulse
src = real(data(:,24).');
c04 = real(data(:,7).');
c06 = real(data(:,11).');
c08 = real(data(:,15).');
c10 = real(data(:,19).');
c12 = real(data(:,23).');
src = src - mean(src);
c04 = c04 - mean(c04);
c06 = c06 - mean(c06);
c08 = c08 - mean(c08);
c10 = c10 - mean(c10);
c12 = c12 - mean(c12);
%% FFT
fsrc=fft(src,Fl*2);
fc04=fft(c04,Fl*2);
fc06=fft(c06,Fl*2);
fc08=fft(c08,Fl*2);
fo10=fft(c10,Fl*2);
fo12=fft(c12,Fl*2);
%clear src c04 c06 c08 c10 c12
%% transfer function
H(1,:)=fsrc./fsrc; % src
H(2,:)=fo04./fsrc; % c04
H(3,:)=fo06./fsrc; % c06
H(4,:)=fo08./fsrc; % c08
H(5,:)=fo10./fsrc; % c10
H(6,:)=fo12./fsrc; % c12
%clear fsrc fo04 fo06 fo08 fo10 fo12
%% for complex envelope
for i=1:6,
H(i,8193:16384)=zeros(1,8192);
H(i,:)=2*H(i,:);
end
%%%%%%%%%%%%%%%%%%%%%%%%%%%%%%%%%%%%%%%%%%%%%%%%%%%%%%%%%%%%%%%%%%%%%%%%
%% Gaussian Filter G(w)=exp(-(f0-f)^2/(2*fbw^2));
%% The mean and std parameters used to create the filter
%% such that the 6dB down points are located at the band edges.
%% Bandwidth is approximately equivalent to that of an octave band
%% fbw=sqrt((fo-f1)^2/(2*6.906e-1))
f0=16e3;
for i=1:8,
fo(i)=f0/2^(i-1);
f1(i)=fo(i)/sqrt(2);
fbw(i)=sqrt((fo(i)-f1(i))^2/(2*6.906e-1));
%% index for fo
%idx=floor(Fl*fo(i)/f(Fl))+1;
%
end
for i=1:8,

```

```

for j=1:F1,
gaussfilter(i,j)=exp(-(fo(i)-f(j))^2/(2*fbw(i)^2));
gaussfilter(i,F1*2-(j-1))=gaussfilter(i,j);
end
end
%%%%%%%%%%%%%%%%%%%%%%%%%%%%%%%%%%%%%%%%%%%%%%%%%%%%%%%%%%%%%%%%%%%%%%%%%%%%%%
%%%%% TIME vs LOG Impulse response with a specific Gaussian BP Filter
%%%%%%%%%%%%%%%%%%%%%%%%%%%%%%%%%%%%%%%%%%%%%%%%%%%%%%%%%%%%%%%%%%%%%%%%%%%%%%
%%%%% gaussfilter(1:8,:)= [16 8 4 2 1 0.5 0.25 0.125] kHz
%%%%%%%%%%%%%%%%%%%%%%%%%%%%%%%%%%%%%%%%%%%%%%%%%%%%%%%%%%%%%%%%%%%%%%%%%%%%%%
%%%%% fo=16kHz
for i=1:6,
    h(i,:)=ifft(H(i,:).*gaussfilter(1,:));
end
%%%%%%%%%%%%%%%%%%%%%%%%%%%%%%%%%%%%%%%%%%%%%%%%%%%%%%%%%%%%%%%%%%%%%%%%%%%%%%
figure(1)
orient tall
subplot(611)
plot(t,20*log10(h(1,:)))
title('Magnitude of Gaussian Octave Bandpass Filtered Impulse Response Function with fo=16kHz, dB')
ylabel('SRC')
axis([0 125e-3 -50 -10])
subplot(612)
plot(t,20*log10(h(2,:)))
ylabel('c04')
axis([0 125e-3 -83 -43])
subplot(613)
plot(t,20*log10(h(3,:)))
ylabel('c06')
axis([0 125e-3 -97 -57])
subplot(614)
plot(t,20*log10(h(4,:)))
ylabel('c08')
axis([0 125e-3 -97 -57])
subplot(615)
plot(t,20*log10(h(5,:)))
ylabel('c10')
axis([0 125e-3 -110 -70])
subplot(616)
plot(t,20*log10(h(6,:)))
ylabel('c12')
xlabel('Time in sec')
axis([0 125e-3 -105 -65])
%%%%%%%%%%%%%%%%%%%%%%%%%%%%%%%%%%%%%%%%%%%%%%%%%%%%%%%%%%%%%%%%%%%%%%%%%%%%%%
figure(2)
orient tall
subplot(611)
plot(t.*1e3,20*log10(h(1,:)))
title('Magnitude of Gaussian Octave Bandpass Filtered Impulse Response Function with fo=16kHz, dB')
ylabel('SRC')
axis([0 5 -50 -10])
subplot(612)
plot(t.*1e3,20*log10(h(2,:)))
ylabel('c04')
axis([0 5 -83 -43])
subplot(613)
plot(t.*1e3,20*log10(h(3,:)))
ylabel('c06')
axis([0 5 -97 -57])
subplot(614)
plot(t.*1e3,20*log10(h(4,:)))
ylabel('c08')
axis([0 5 -97 -57])
subplot(615)
plot(t.*1e3,20*log10(h(5,:)))
ylabel('c10')
axis([0 5 -110 -70])

```

```

subplot(616)
plot(t.*1e3,20*log10(h(6,:)))
ylabel('c12')
xlabel('Time in msec')
axis([0 5 -105 -65])
%%%%%%%%%%%%%%%%%%%%%%%%%%%%%%%%%%%%%%%%%%%%%%%%%%%%%%%%%%%%%%%%%%%%%%%%
%%% Plot the Estimated Arrival Time of Elastic Waves
%%% with Center Frequency of fo=16kHz
%%%%%%%%%%%%%%%%%%%%%%%%%%%%%%%%%%%%%%%%%%%%%%%%%%%%%%%%%%%%%%%%%%%%%%%%
dT=.25/16384
arvT4=[.18 .26 .34 .44 .52 .72 .80].*1e-3
idx4=ceil(arvT4./dT+ones(length(arvT4),1)')
T4=t(idx4).*1e3
H4=20*log10(h(2,idx4))
arvT6=[.39].*1e-3
idx6=ceil(arvT6./dT+ones(length(arvT6),1)')
T6=t(idx6).*1e3
H6=20*log10(h(3,idx6))
arvT8=[.68 .79 .92].*1e-3
idx8=floor(arvT8./dT+ones(length(arvT8),1)')
T8=t(idx8).*1e3
H8=20*log10(h(4,idx8))
arvT10=[.95 1.01 1.08 1.22 1.33 1.44].*1e-3
idx10=floor(arvT10./dT+ones(length(arvT10),1)')
T10=t(idx10).*1e3
H10=20*log10(h(5,idx10))
arvT12=[1.16 1.36 1.47 1.54 1.64 1.76 1.86].*1e-3
idx12=floor(arvT12./dT+ones(length(arvT12),1)')
T12=t(idx12).*1e3
H12=20*log10(h(6,idx12))
%%%%%%%%%%%%%%%%%%%%%%%%%%%%%%%%%%%%%%%%%%%%%%%%%%%%%%%%%%%%%%%%%%%%%%%%
figure(2)
subplot(612)
hold
plot(T4,H4,'o')
hold
subplot(613)
hold
plot(T6,H6,'o')
hold
subplot(614)
hold
plot(T8,H8,'o')
hold
subplot(615)
hold
plot(T10,H10,'o')
hold
subplot(616)
hold
plot(T12,H12,'o')
hold
%%%%%%%%%%%%%%%%%%%%%%%%%%%%%%%%%%%%%%%%%%%%%%%%%%%%%%%%%%%%%%%%%%%%%%%%
return
%%%%%%%%%%%%%%%%%%%%%%%%%%%%%%%%%%%%%%%%%%%%%%%%%%%%%%%%%%%%%%%%%%%%%%%%

%%%%%%%%%%%%%%%%%%%%%%%%%%%%%%%%%%%%%%%%%%%%%%%%%%%%%%%%%%%%%%%%%%%%%%%%
%%%
%%% Find Index for Decay Constant Calculation
%%% run after gaus_arr.m
%%% gausfilter(1:8,:)= [16 8 4 2 1 0.5 0.25 0.125] kHz
%%%
%%%%%%%%%%%%%%%%%%%%%%%%%%%%%%%%%%%%%%%%%%%%%%%%%%%%%%%%%%%%%%%%%%%%%%%%
for i=2:6,
    h(i,:)=ifft(H(i,:).*gausfilter(1,:));
end
hC04=20*log10(abs(h(2,:)));

```

```

hC06=20*log10(abs(h(3,:)));
hC08=20*log10(abs(h(4,:)));
hC10=20*log10(abs(h(5,:)));
hC12=20*log10(abs(h(6,:)));
maxC04=max(hC04)
I04=find(hC04>maxC04-1)
hC04(I04)
t(I04)
maxC06=max(hC06)
I06=find(hC06>maxC06-1)
hC06(I06)
t(I06)
maxC08=max(hC08)
I08=find(hC08>maxC08-1)
hC08(I08)
t(I08)
maxC10=max(hC10)
I10=find(hC10>maxC10-1)
hC10(I10)
t(I10)
maxC12=max(hC12)
I12=find(hC12>maxC12-1)
hC12(I12)
t(I12)
%%%%%%%%%%%%%%%%%%%%%%%%%%%%%%%%%%%%%%%%%%%%%%%%%%%%%%%%%%%%%%%%%%%%%%%%
return
%%%%%%%%%%%%%%%%%%%%%%%%%%%%%%%%%%%%%%%%%%%%%%%%%%%%%%%%%%%%%%%%%%%%%%%%

%%%%%%%%%%%%%%%%%%%%%%%%%%%%%%%%%%%%%%%%%%%%%%%%%%%%%%%%%%%%%%%%%%%%%%%%
%%%%%
%%%%% Find & Plot Double Decay Rate
%%%%%
%%%%%%%%%%%%%%%%%%%%%%%%%%%%%%%%%%%%%%%%%%%%%%%%%%%%%%%%%%%%%%%%%%%%%%%%
%%%%%%%%%%%%%%%%%%%%%%%%%%%%%%%%%%%%%%%%%%%%%%%%%%%%%%%%%%%%%%%%%%%%%%%%
%%%%%%%%%%%%%%%%%%%%%%%%%%%%%%%%%%%%%%%%%%%%%%%%%%%%%%%%%%%%%%%%%%%%%%%%
%%%%% Polynomial Curve Fitting (LINEAR SCHEME)
%%%%% run after gauss_arr.m
%%%%% gaussfilter(1:8,:)= [16 8 4 2 1 0.5 0.25 0.125] kHz
%%%%%
%
% Energy Increase Rate is difficult (impossible) to find least square curve
% since the peak of energy arrival is rounded.
% Can't pick the highest point for linear scheme
%%%%%%%%%%%%%%%%%%%%%%%%%%%%%%%%%%%%%%%%%%%%%%%%%%%%%%%%%%%%%%%%%%%%%%%%
Fs=65536;
Fl=8192;
%%%%% fc=16kHz
for i=2:6,
    h(i,:)=ifft(H(i,:).*gaussfilter(1,:));
end
%%%%%%%%%%%%%%%%%%%%%%%%%%%%%%%%%%%%%%%%%%%%%%%%%%%%%%%%%%%%%%%%%%%%%%%%
%%%%% FROM DIRECT OBSERVATION
%%%%% .5493 3.3 4.4 7.6 6.7 45 50 45 50 45 msec
last=7865 %%%% 120msec
idx= [ 37 219 289 497 441 2949 3276 2949 3276 2949 last];
%%%%%%%%%%%%%%%%%%%%%%%%%%%%%%%%%%%%%%%%%%%%%%%%%%%%%%%%%%%%%%%%%%%%%%%%
%%%%%% DECAF 1
% C04
[p04d,S04d]=polyfit(t(idx(1):idx(6)),20*log10(abs(h(2,idx(1):idx(6))))),1);
[y04d,delta04d]=polyval(p04d,t(idx(1):idx(6)),S04d);
% C06
[p06d,S06d]=polyfit(t(idx(2):idx(7)),20*log10(abs(h(3,idx(2):idx(7))))),1);
[y06d,delta06d]=polyval(p06d,t(idx(2):idx(7)),S06d);
% C08
[p08d,S08d]=polyfit(t(idx(3):idx(8)),20*log10(abs(h(4,idx(3):idx(8))))),1);
[y08d,delta08d]=polyval(p08d,t(idx(3):idx(8)),S08d);
% C10
[p10d,S10d]=polyfit(t(idx(4):idx(9)),20*log10(abs(h(5,idx(4):idx(9))))),1);

```

```

[y10d,delta10d]=polyval(p10d,t(idx(4):idx(9)),S10d);
% C12
[p12d,S12d]=polyfit(t(idx(5):idx(10)),20*log10(abs(h(6,idx(5):idx(10))))),1);
[y12d,delta12d]=polyval(p12d,t(idx(5):idx(10)),S12d);
pd=[p04d; p06d; p08d; p10d; p12d];
%%%%%% DECAY 2
% C04
[p04d2,S04d2]=polyfit(t(idx(6):idx(11)),20*log10(abs(h(2,idx(6):idx(11))))),1);
[y04d2,delta04d2]=polyval(p04d2,t(idx(6):last),S04d2);
% C06
[p06d2,S06d2]=polyfit(t(idx(7):idx(11)),20*log10(abs(h(3,idx(7):idx(11))))),1);
[y06d2,delta06d2]=polyval(p06d2,t(idx(7):last),S06d2);
% C08
[p08d2,S08d2]=polyfit(t(idx(8):idx(11)),20*log10(abs(h(4,idx(8):idx(11))))),1);
[y08d2,delta08d2]=polyval(p08d2,t(idx(8):last),S08d2);
% C10
[p10d2,S10d2]=polyfit(t(idx(9):idx(11)),20*log10(abs(h(5,idx(9):idx(11))))),1);
[y10d2,delta10d2]=polyval(p10d2,t(idx(9):last),S10d2);
% C12
[p12d2,S12d2]=polyfit(t(idx(10):idx(11)),20*log10(abs(h(6,idx(10):idx(11))))),1);
[y12d2,delta12d2]=polyval(p12d2,t(idx(10):last),S12d2);
pd2=[p04d2; p06d2; p08d2; p10d2; p12d2];
%%%%%% slope (dB/10msec)
lgd='fc=16kHz'
DecayRate1=round(pd(:,1)/10)/10
DecayRate2=round(pd2(:,1)/10)/10
%%%%%%%%%%%%%%%%%%%%%%%%%%%%%%%%%%%%%%%%%%%%%%%%%%%%%%%%%%%%%%%%%%%%%%%%
%%%%%% Let's make smooth transition from decay 1 to decay 2
y04c =y04d(length( y04d))- y04d(1);
y04d2=y04d2+ones(size(y04d2)).*y04c;
y06c =y06d(length( y06d))- y06d(1);
y06d2=y06d2+ones(size(y06d2)).*y06c;
y08c =y08d(length( y08d))- y08d(1);
y08d2=y08d2+ones(size(y08d2)).*y08c;
y10c =y10d(length( y10d))- y10d(1);
y10d2=y10d2+ones(size(y10d2)).*y10c;
y12c =y12d(length( y12d))- y12d(1);
y12d2=y12d2+ones(size(y12d2)).*y12c;
%%%%%%%%%%%%%%%%%%%%%%%%%%%%%%%%%%%%%%%%%%%%%%%%%%%%%%%%%%%%%%%%%%%%%%%%
figure(1)
orient tall
subplot(521)
plot(t,20*log10(h(2,:)))
%%%%%% fc=16kHz
ylabel('h(c04) dB')
subplot(523)
plot(t,20*log10(h(3,:)))
ylabel('h(c06) dB')
subplot(525)
plot(t,20*log10(h(4,:)))
ylabel('h(c08) dB')
subplot(527)
plot(t,20*log10(h(5,:)))
ylabel('h(c10) dB')
subplot(529)
plot(t,20*log10(h(6,:)))
ylabel('h(c12) dB')
xlabel('Time in sec')
%%%%%% Plot regression data
subplot(522)
plot(t(idx(1):idx(6)), y04d, t(idx(6):idx(11)), y04d2)
subplot(524)
plot(t(idx(2):idx(7)), y06d, t(idx(7):idx(11)), y06d2)
subplot(526)
plot(t(idx(3):idx(8)), y08d, t(idx(8):idx(11)), y08d2)
subplot(528)
plot(t(idx(4):idx(9)), y10d, t(idx(9):idx(11)), y10d2)
subplot(5,2,10)

```

```

plot(t(idx(5):idx(10)),y12d,t(idx(10):idx(11)), y12d2)
xlabel('Time in sec')
%%% AXIS SCALING
figure(1)
for i=0:1
subplot(5,2,1+i)
axis([0 120e-3 -120 -30])
subplot(5,2,3+i)
axis([0 120e-3 -120 -30])
subplot(5,2,5+i)
axis([0 120e-3 -120 -30])
subplot(5,2,7+i)
axis([0 120e-3 -120 -30])
subplot(5,2,9+i)
axis([0 120e-3 -120 -30])
end
%%%%%%%%%%%%%%%%%%%%%%%%%%%%%%%%%%%%%%%%%%%%%%%%%%%%%%%%%%%%%%%%%%%%%%%%
return
%%%%%%%%%%%%%%%%%%%%%%%%%%%%%%%%%%%%%%%%%%%%%%%%%%%%%%%%%%%%%%%%%%%%%%%%

%%%%%%%%%%%%%%%%%%%%%%%%%%%%%%%%%%%%%%%%%%%%%%%%%%%%%%%%%%%%%%%%%%%%%%%%
%% Early Arrival Trend of Total Elastic Wave Field
%%
%%%%%%%%%%%%%%%%%%%%%%%%%%%%%%%%%%%%%%%%%%%%%%%%%%%%%%%%%%%%%%%%%%%%%%%%
% Corresponds to joints
%   c04      c06      c08      c10      c12
l = [.545    1.125    2.090    3.061    4.031];
lx = [0      4.7/6    4.7/6*2  4.7/6*3  4.7/6*4];
f16= [.18   .39   .68   .945  1.16 ;
      .26 NaN  .79   1.013 1.363;
      .34 NaN  .92   1.08  1.47;
      .44 NaN NaN  1.22  1.543;
      .52 NaN NaN  1.33  1.64;
      .72 NaN NaN  1.44  1.76;
      .80 NaN NaN  NaN   1.86];
f8=  [.18   .43   .68   .981  .81;
      .51 NaN  .917  1.237 1.245;
      .93 NaN  1.16  1.43  1.535;
      NaN NaN NaN  1.60  1.72;
      NaN NaN NaN  NaN   1.93;
      NaN NaN NaN  NaN   2.16];
f4=  [.34   .50   .51   1.70 1.125;
      .42 NaN  1.04  1.76 1.585;
      .44 NaN  1.18  2.06 2.01;
      .72 NaN  1.51 NaN  2.79;
      .84 NaN NaN NaN  NaN];
fx16=f16;
fx8=f8;
fx4=f4;
X=linspace(0,4.5);
[p,S]=polyfit([0 l],[0 f16(1,:)],1);
[Y16,delta]=polyval([p(1) 0],X,S);
f16_speed=1000/p(1)
[p,S]=polyfit([0 l(1:4)],[0 f8(1,1:4)],1);
[Y8,delta]=polyval([p(1) 0],X,S);
f8_speed=1000/p(1)
[p,S]=polyfit([0 l(1) l(2) l(3) l(5)],[0 f4(1,1) f4(1,2) f4(1,3) f4(1,5)],1);
[p,S]=polyfit([0 l],[0 f4(1,:)],1);
[Y4,delta]=polyval([p(1) 0],X,S);
f4_speed=1000/p(1)
AX=linspace(0,3.5);
[p,S]=polyfit(lx,fx16(1,:),1);
[AY16,delta]=polyval([p(1) fx16(1,1)],AX,S);
f16_Aspeed=1000/p(1)
[p,S]=polyfit(lx(1:4),fx8(1,1:4),1);
[AY8,delta]=polyval([p(1) fx8(1,1)],AX,S);

```



```

f8_Aspeed=1000/p(1)
[p,S]=polyfit([lx(1) lx(2) lx(3) lx(5)],[fx4(1,1) fx4(1,2) fx4(1,3) fx4(1,5)],1);
[p,S]=polyfit(lx,fx4(1,:),1);
[AY4,delta]=polyval([p(1) fx4(1,1)],AX,S);
f4_Aspeed=1000/p(1)
%%%%%%%%%%%%%%%%%%%%%%%%%%%%%%%%%%%%%%%%%%%%%%%%%%%%%%%%%%%%%%%%%%%%%%%%
figure(1)
clg
orient portrait
axes('position',[.1 .1 .8/3 .8])
plot(l,f16(1,:), 'o',l,f16(2,:), '+' ,l,f16(3,:), 'x',l,f16(4,:), '*' , ...
      l,f16(5,:), '+' ,l,f16(6,:), 'x',l,f16(7,:), '*' ,...
      l,f16(5,:), 'o',l,f16(6,:), 'o',l,f16(7,:), 'o',X,Y16, ':')
legend('1st arriv', '2nd', '3rd', '4th', ...
       '5th', '6th', '7th')
title('fo=16kHz')
xlabel('Shortest Path in m')
ylabel('Time in msec')
axis([0 4.5 0 3])
axes('position',[.1+.8/3*1 .1 .8/3 .8])
plot(l,f8(1,:), 'o',l,f8(2,:), '+' ,l,f8(3,:), 'x',l,f8(4,:), '*' , ...
      l,f8(5,:), '+' ,l,f8(6,:), 'x',l,f8(5,:), 'o',l,f8(6,:), 'o',X,Y8, ':')
set(gca, 'YTickLabels', '')
title('fo=8kHz')
xlabel('Shortest Path in m')
axis([0 4.5 0 3])
axes('position',[.1+.8/3*2 .1 .8/3 .8])
plot(l,f4(1,:), 'o',l,f4(2,:), '+' ,l,f4(3,:), 'x',l,f4(4,:), '*' , ...
      l,f4(5,:), '+' ,l,f4(5,:), 'o',X,Y4, ':')
set(gca, 'YTickLabels', '')
title('fo=4kHz')
xlabel('Shortest Path in m')
axis([0 4.5 0 3])
%%%%%%%%%%%%%%%%%%%%%%%%%%%%%%%%%%%%%%%%%%%%%%%%%%%%%%%%%%%%%%%%%%%%%%%%
figure(2)
clg
orient portrait
axes('position',[.1 .1 .8/3 .8])
plot(lx,fx16(1,:), 'o',lx,fx16(2,:), '+' ,lx,fx16(3,:), 'x',lx,fx16(4,:), '*' , ...
      lx,fx16(5,:), '+' ,lx,fx16(6,:), 'x',lx,fx16(7,:), '*' ,...
      lx,fx16(5,:), 'o',lx,fx16(6,:), 'o',lx,fx16(7,:), 'o',AX,AY16, ':')
legend('1st arriv', '2nd', '3rd', '4th', ...
       '5th', '6th', '7th')
title('fo=16kHz')
xlabel('Axial Distance in m')
ylabel('Time in msec')
axis([- .5 3.5 0 3])
axes('position',[.1+.8/3*1 .1 .8/3 .8])
plot(lx,fx8(1,:), 'o',lx,fx8(2,:), '+' ,lx,fx8(3,:), 'x',lx,fx8(4,:), '*' , ...
      lx,fx8(5,:), '+' ,lx,fx8(6,:), 'x',lx,fx8(5,:), 'o',lx,fx8(6,:), 'o',...
      AX,AY8, ':')
set(gca, 'YTickLabels', '')
title('fo=8kHz')
xlabel('Axial Distance in m')
axis([- .5 3.5 0 3])
axes('position',[.1+.8/3*2 .1 .8/3 .8])
plot(lx,fx4(1,:), 'o',lx,fx4(2,:), '+' ,lx,fx4(3,:), 'x',lx,fx4(4,:), '*' , ...
      lx,fx4(5,:), '+' ,lx,fx4(5,:), 'o',AX,AY4, ':')
set(gca, 'YTickLabels', '')
title('fo=4kHz')
xlabel('Axial Distance in m')
axis([- .5 3.5 0 3])
%%%%%%%%%%%%%%%%%%%%%%%%%%%%%%%%%%%%%%%%%%%%%%%%%%%%%%%%%%%%%%%%%%%%%%%%
figure(3)
df16=[8.4 6.5 5.9 4.6 4.9];
df8 =[6.8 5.1 5.0 3.7 5.2];
df4 =[4.4 3.8 3.2 3.1 3.4];
d2f16=[0.8 0.2 0.0 0.4 0.0];

```

```

d2f8 =[0.6 0.4 0.1 0.9 0.1];
d2f4 =[2.0 0.8 1.9 0.7 0.7];
orient tall
subplot(211)
plot(l,df16,'-',l,df8,'--',l,df4,'-.',l,df16,'o',l,df8,'o',l,df4,'o')
title('Eta_0 Decay Rate')
xlabel('Shortest Path in m')
ylabel('dB/10msec')
axis([0 4.5 0 10])
set(gca,'YTick',[0:1:10])
legend('fo=16kHz','fo=8kHz','fo=4kHz')
grid
subplot(212)
plot(l,d2f16,'-',l,d2f8,'--',l,d2f4,'-.',l,d2f16,'o',l,d2f8,'o',l,d2f4,'o')
title('Eta_1 Decay Rate')
xlabel('Shortest Path in m')
ylabel('dB/10msec')
axis([0 4.5 -5 5])
set(gca,'YTick',[-5:1:5])
grid
%%%%%%%%%%%%%%%%%%%%%%%%%%%%%%%%%%%%%%%%%%%%%%%%%%%%%%%%%%%%%%%%%%%%%%%%
return
%%%%%%%%%%%%%%%%%%%%%%%%%%%%%%%%%%%%%%%%%%%%%%%%%%%%%%%%%%%%%%%%%%%%%%%%

```

## Appendix A

```

%%%%%%%%%%%%%%%%%%%%%%%%%%%%%%%%%%%%%%%%%%%%%%%%%%%%%%%%%%%%%%%%%%%%%%%%
%%%%%%
%%%%%% Dispersion Relation of Timoshenko Beam
%%%%%%
%%%%%%%%%%%%%%%%%%%%%%%%%%%%%%%%%%%%%%%%%%%%%%%%%%%%%%%%%%%%%%%%%%%%%%%%
rho=2700; % density of Al6061
E=70e9; % Young's modulus
G=26e9; % Shear modulus
K=3.950e-3; % radius of gyration
f=[0:10:25e3];
w=f.*(2*pi);
Cl=sqrt(E/rho); % longitudinal wave speed
Ct=sqrt(G/rho); % torsional wave speed
%%%%%%%%%%%%%%%%%%%%%%%%%%%%%%%%%%%%%%%%%%%%%%%%%%%%%%%%%%%%%%%%%%%%%%%%
Timoshenko Beam
tc=0.545; % Timoshenko shear coeff. for thin-walled pipe 0.5~0.545
A=(rho/E+rho/(tc*G));
B=(rho/E/K^2);
C=(rho^2/(E*tc*G));
kT= sqrt(w.^2*A + sqrt(w.^4*(A^2-4*C)+w.^2*B*4).*2).*0.5;
CTp=w./kT;
CTg= ((sqrt(w.^2*A*2 + sqrt(w.^4*(A^2-4*C)+w.^2*B*4).*2)) ./ ...
      (w.*A*4+(w.^3*(A^2*4-16*C)+w.*B*8)./sqrt(w.^4*(A^2-4*C)+w.^2*B*4))).*4;
%%%%%%%%%%%%%%%%%%%%%%%%%%%%%%%%%%%%%%%%%%%%%%%%%%%%%%%%%%%%%%%%%%%%%%%%
Euler Bernoulli Beam
kB=sqrt(w).*(rho/E/K^2)^(1/4);
CBp=sqrt(w).*(E*K^2/rho)^(1/4);
CBg=sqrt(w).*2.*(E*K^2/rho)^(1/4);
%%%%%%%%%%%%%%%%%%%%%%%%%%%%%%%%%%%%%%%%%%%%%%%%%%%%%%%%%%%%%%%%%%%%%%%%
figure(1)
plot(f/1e3,CTp,'-',f/1e3,CBp,'-.',f/1e3,CTg,'--',f/1e3,CBg,':')
title('Wave Speed of Timoshenko and Euler-Bernoulli Beam')
ylabel('Wave Speed (m/s)')
xlabel('Frequency in kHz')
%legend('C_phase(Timoshenko Beam)', 'C_phase(Euler-Bernoulli Beam)', ...
% 'C_group(Timoshenko Beam)', 'C_group(Euler-Bernoulli Beam)')
%%%%%%%%%%%%%%%%%%%%%%%%%%%%%%%%%%%%%%%%%%%%%%%%%%%%%%%%%%%%%%%%%%%%%%%%
figure(2)
plot(f/1e3,kT,'-',f/1e3,kB,'--')
title('Dispersion Relation of Timoshenko and Euler-Bernoulli Beam')
xlabel('Frequency in kHz')
ylabel('Wave Number (1/m)')
%legend('Timoshenko Beam', 'Euler-Bernoulli Beam')
%%%%%%%%%%%%%%%%%%%%%%%%%%%%%%%%%%%%%%%%%%%%%%%%%%%%%%%%%%%%%%%%%%%%%%%%
f1=[125 250 500 1e3 2e3 4e3 8e3 16e3]
w1=f1.*2*pi
CBp1=sqrt(w1).*(E*K^2/rho)^(1/4);
CBg1=sqrt(w1).*2.*(E*K^2/rho)^(1/4);
kT1= sqrt(w1.^2*A + sqrt(w1.^4*(A^2-4*C)+w1.^2*B*4).*2).*0.5;
CTp1=w1./kT1;
CTg1= ((sqrt(w1.^2*A*2 + sqrt(w1.^4*(A^2-4*C)+w1.^2*B*4).*2)) ./ ...
      (w1.*A*4+(w1.^3*(A^2*4-16*C)+w1.*B*8)./sqrt(w1.^4*(A^2-4*C)+w1.^2*B*4))).*4;
Cl
Ct
idx='f CBp CBg CTp CTg'
result=[f1' CBp1' CBg1' CTp1' CTg1']
%%%%%%%%%%%%%%%%%%%%%%%%%%%%%%%%%%%%%%%%%%%%%%%%%%%%%%%%%%%%%%%%%%%%%%%%
return
%%%%%%%%%%%%%%%%%%%%%%%%%%%%%%%%%%%%%%%%%%%%%%%%%%%%%%%%%%%%%%%%%%%%%%%%

```

# Bibliography

- [1] M.R.A. Heath, "Dynamic Behavior of a Three Dimensional Aluminum Truss in Free Space," S.M. Thesis (MIT, Cambridge, MA, 1994).
- [2] D. Branthonne, "Influence of Dynamic Absorbers on a Three Dimensional Truss," S.M. Thesis (MIT, Cambridge, MA, 1994).
- [3] K.U. Machens and I. Dyer, "Energy Partitioning in a Truss Structure," *Acustica*, **81**, 587-594 (1995).
- [4] R.L. Frink, "Dynamic Behavior of Multi-legged Pinned and Rigid Structural Joints," S.M. Thesis (MIT, Cambridge, MA, 1995)
- [5] L.E. Chiasson, "Radiated Noise From a Three Dimensional Truss," S.M. Thesis (MIT, Cambridge, MA, 1995).
- [6] Y.P. Guo, "Wave Propagation in Truss Structures," *J. Acoust. Soc. Am.*, **96**, 3291 (A) (1994).
- [7] L. Brillouin, *Wave propagation in Periodic Structures* (Dover Publications, Inc. New York, NY, 1946).
- [8] L. Cremer, M. Heckl and E.E. Ungar, *Structure-Borne Sound* 2nd ed. (Springer-Verlag, Berlin, 1988).
- [9] D.J. Mead, "A General Theory of Harmonic Wave Propagation in Linear Periodic Systems with Multiple Coupling," *J. Sound. Vib.*, **27**, 235-260 (1973).
- [10] D.J. Mead and S. Markus, "Coupled Flexural-longitudinal Wave Motion in a Periodic Beam," *J. Sound. Vib.*, **90**, 1-24 (1983).
- [11] Y. Yong and Y.K. Lin, "Dynamic Response Analysis of Truss-type Structural Networks: a Propagation Approach," *J. Sound. Vib.*, **156**(1), 27-45 (1992).
- [12] A.H. von Flotow, "Disturbance Propagation in Structural Networks," *J. Sound. Vib.*, **106**, 433-450 (1986).
- [13] R.A. Mills, "Natural Vibrations of Beam-like Trusses," S.M. Thesis (MIT, Cambridge, MA, 1985).
- [14] J. Sinorelli, "Wave Propagation in Periodic Truss Structures," S.M. Thesis (MIT, Cambridge, MA, 1987).

- [15] D. Branthonne, "Mode Shape of a Cradle Structure," MIT Internal Report (MIT, Cambridge, MA, 1994).
- [16] J.S. Bendat and A.G. Piersol, *Engineering Applications of Correlation and Spectral Analysis* (John Wiley & Sons, New York, NY, 1980).
- [17] D.H. Johnson and D.E. Dudgeon, *Array Signal Processing* (Prentice Hall, Englewood Cliffs, NJ, 1993).
- [18] W.K. Blake and R.V. Waterhouse, "The Use of Cross-Spectral Density Measurements in Partially Reverberant Sound Fields," *J. Sound. Vib.*, **54**(4), 589-599 (1977).
- [19] Private communication with Professor Ira Dyer at MIT, 1996.
- [20] Private communication with Dr. Joseph Bondaryk at MIT, 1996.
- [21] C.N. Corrado, "Mid-Frequency Acoustic Backscattering from Finite Cylindrical Shells and the Influence of Helical Membrane Waves," Ph.D. Thesis (MIT, Cambridge, MA, 1993).
- [22] W. Siebert, *Circuits, Signals, and Systems* (McGraw Hill, New York, NY, 1986).
- [23] S. Rao, *Mechanical Vibrations* 3rd ed. (Addison Wesley, New York, NY, 1995).
- [24] J.M. Gere and S.P. Timoshenko, *Mechanics of Materials* (PWS-Kent, Boston, MA, 1990).
- [25] G.R. Cowper, "The Shear Coefficient in Timoshenko's Beam Theory," *J. Appl. Mech.*, **33**, 335-340 (1966).
- [26] A.D. Pierce, *Acoustics* (Acoustical Society of America, Woodbury, NY, 1989).
- [27] F. Fahy, *Sound and Structural Vibration - Radiation, Transmission and Response* (Academic Press, London, 1985).
- [28] M.C. Junger and D. Feit, *Sound Structures and Their Interactions* 2nd ed. (MIT Press, Cambridge, MA, 1986).
- [29] P.M. Morse, *Vibration and Sound* (McGraw Hill, New York, NY, 1948).
- [30] J.P. Den Hartog, *Mechanical Vibrations* (McGraw Hill, New York, NY, 1956).
- [31] M.P. Norton, *Fundamental of Noise and Vibration Analysis for Engineers* (Cambridge University Press, Cambridge, 1989).
- [32] A.V. Oppenheim and R.W. Schaffer, *Discrete-Time Signal Processing* (Prentice Hall, Englewood Cliffs, NJ, 1989).
- [33] P.H. Wirsching, T.L. Paez, and K. Ortiz, *Random Vibration* (John Wiley & Sons, New York, NY, 1995).